1985

Enthalpies of formation in the systems tantalum-sulfur and tantalum-aluminum

Stephen R. Schmidt
Iowa State University

Schmidt, Stephen R.

ENTHALPIES OF FORMATION IN THE SYSTEMS TANTALUM-SULFUR AND TANTALUM-ALUMINUM

Iowa State University PH.D. 1985

PLEASE NOTE:

In all cases this material has been filmed in the best possible way from the available copy. Problems encountered with this document have been identified here with a check mark __√__.

1. Glossy photographs or pages _____
2. Colored illustrations, paper or print _____
3. Photographs with dark background _____
4. Illustrations are poor copy _____
5. Pages with black marks, not original copy _____
6. Print shows through as there is text on both sides of page _____
7. Indistinct, broken or small print on several pages __✓__
8. Print exceeds margin requirements _____
9. Tightly bound copy with print lost in spine _____
10. Computer printout pages with indistinct print _____
11. Page(s) _____ lacking when material received, and not available from school or author.
12. Page(s) _____ seem to be missing in numbering only as text follows.
13. Two pages numbered _____. Text follows.
14. Curling and wrinkled pages _____
15. Dissertation contains pages with print at a slant, filmed as received _____
16. Other _____

_____

_____

Enthalpies of formation in the systems tantalum-sulfur and tantalum-aluminum

by

Stephen R. Schmidt

A Dissertation Submitted to the
Graduate Faculty in Partial Fulfillment of the
Requirements for the Degree of
DOCTOR OF PHILOSOPHY

Department: Chemistry
Major: Physical Chemistry

Approved:

Signature was redacted for privacy.

In Charge of Major Work

Signature was redacted for privacy.

For the Major Department

Signature was redacted for privacy.

For the Graduate College

Iowa State University
Ames, Iowa

1985

TABLE OF CONTENTS

I. INTRODUCTION

A. Purpose of Thermochemistry in General

The determination of changes in thermodynamic properties such as the enthalpy and Gibbs free energy during chemical reactions is of considerable interest and utility for physical scientists. When dealing with reactions involving crystalline compounds, the practitioners of thermochemistry often ultimately seek accurate heats of formation, which may be related to facts and speculations about crystal structures, type and extent of chemical bonding, and variability of stoichiometry. Very comprehensive catalogues of thermodynamic measurements of this sort, or of the sort from which this information may be derived, exist in compendia such as the JANAF tables[1] or the volume on thermodynamic properties of alloys by Hultgren et al.[2] Depending on the degrees of commonness, accessibility, and perceived significance of a series of compounds one has chosen to study, information useful for comparison to one's results may range in quantity from copious to nearly nonexistent. In the latter case, of which the two interrelated studies in this dissertation are examples, one may choose to make comparisons with properties of analogous compounds or with model-based predictions, and may regard the effort as only a beginning step toward the compilation of a network of knowledge which may facilitate interpretation of subsequent findings.

B. Format

Because the methods, data analyses and interpretations of results for the tantalum-sulfur and tantalum-aluminum experiments reported herein

differ significantly, they will be detailed in separate sections, following some additional introductory comments and a description of the experimental technique in general.

C. Methods Used in Thermochemical Measurements

The Knudsen effusion method, or indeed the measurement of vapor pressures over condensed phases by any means, is but one of many ways in which thermodynamic behavior of solids can be observed. Other methods include: emf measurements, calorimetry involving direct reactions of components of a compound, measurement of equilibrium constants of reactions between the condensed phases and an introduced gas, the method of distribution coefficients, and C_p° determinations by low temperature calorimetry. Perhaps only calorimetry rivals vaporization techniques in terms of breadth of applicability and the variety of types of information obtainable.

As has been nicely stated by Gilles[3] in an introductory level article on vaporization studies, the Knudsen effusion method is particularly powerful when coupled to mass spectrometric techniques, through which vapor species may be identified and in some instances gas phase equilibria may be measured. Among the characteristics common to all vaporization studies are (i) the necessity of establishing equilibrium between condensed and gaseous phases and (ii) the requirement of some method for determination of the partial pressures of one or more species which allow the calculation of an equilibrium constant for a known reaction at a given temperature. Each of these considerations can be quite

complicated in its full implications for a given experiment, but they do comprise the essence of any vaporization study.

II. GENERAL DESCRIPTION OF EXPERIMENTS

A. Implementation of the Knudsen Effusion Technique

The power and versatility of the combined mass loss-mass spectrometric equipment utilized in these measurements have previously been demonstrated in a handful of studies, of which a few[4,5,6,7] are particularly relevant because the types of compound and their mode of vaporization resemble those in the Ta-Al and Ta-S systems.

The apparatus is best described in reference 4 and in reference 7, the latter augmenting the former with an explanation of the recent addition of computerized experimental control and data collection. Only the essentials are detailed here.

The polycrystalline sample to be vaporized is contained in one or more thin semi-toroidal containers made of tungsten, which are in turn stacked in the sturdier tungsten Knudsen cell of approximate dimensions: diameter = 1.2 cm, height = 2.0 cm. The Knudsen cells employed have bevelled, or "knife-edge" orifices such that the channel length to cross sectional area ratio is small and thus the Clausing factor (accounting for the deviation from equilibrium pressure as shown by Cater[8]) is effectively unity. The other significant assumption related to crucible design is that of negligible top-to-bottom temperature gradients. This is important because most effusing particles make their final collision with the top wall before escaping via the orifice on the other end, and the effective and actual locations of the sample should be at the same temperature so that the equilibrium $A_{sample} \sim A_{wall}$ holds (A

being the effusing species). The semi-toroids are placed such that their 'donut-holes' are approximately coaxial with the orifice in the Knudsen cell floor, to allow relatively large volumes of material to be contained without blocking the orifice. A tightly fitting lid, also of tungsten, sits atop the cell. To ensure that the orifice is the only path for effusion from the cell, the contact surfaces of both the crucible top and lid are ground to smoothness.

The sample-bearing cell is encased in a tungsten wire bucket and suspended into the core of a (resistive type) tungsten mesh furnace. At any constant temperature provided by this furnace, some of the sample is vaporized and an equilibrium partial pressure, it is hoped, results. Actually, only in the absence of an orifice could a true state of rest be obtained even in principle. However, given a sufficiently small orifice, the rate at which vapor escapes is slow enough that, barring serious kinetic hindrance (to be discussed later) a steady state pressure is obtained and chemical equilibrium between the condensed and gaseous phases is closely approximated, with the overall composition of the system changing negligibly on the time scale required for a measurement.

The kinetic-molecular theory of gases provides the Knudsen equation, relating the rate R_i of mass loss from the cell to the equilibrium vapor pressure P_i of species i with molecular weight M_i:

$$P_i = \frac{C}{A} \cdot R_i \sqrt{T/M_i} \qquad (1)$$

in which A is the orifice area, T the absolute temperature, and numerical constants are combined as $C = 3.76 \times 10^{-7}$. The measurement of the total

rate $\sum_i R_i$ is accomplished by recording the timed output of a Cahn electrobalance from which the cell just described is suspended.

Because this mass loss is recorded as a line on a strip chart and ~0.5 mg or more of vapor must effuse to allow a reliable slope to be determined, it is desirable, and for some chemical systems a must, to possess a more sensitive method of determining vapor pressures which can make many more measurements in a given time interval and corresponding composition range. This sensitivity is provided by quadrupole mass spectrometry, to the extent that measurement of the ion current I_i^+ of a species i requires less than two minutes even when allowing for signal averaging. The UTI quadrupole mass spectrometer employed is positioned below the Knudsen cell and an intervening shutter which is automatically controlled by a stepping motor. Schematic diagrams of the apparatus and the MINC-11 microcomputer to which it is interfaced are shown in Figures 1 and 2, respectively. Automation of the temperature measurement and control, opening and closing of the shutter, scanning of a mass spectrum, measurement of voltages output by the microbalance and their conversion to mass values, and the recording of all these observations in floppy disk format is accomplished by this computer. A pressure measurement is made by scanning a user-specified AMU range before and after opening the shutter and finding the difference between the spectra.

To use the ion currents so obtained in calculating partial pressures one must calibrate the mass spectrometer during data collection to determine its sensitivity to each species whose I_i^+ is measured. Regarding the temperature-dependent Knudsen equation pressures $P_i(T)$ as the

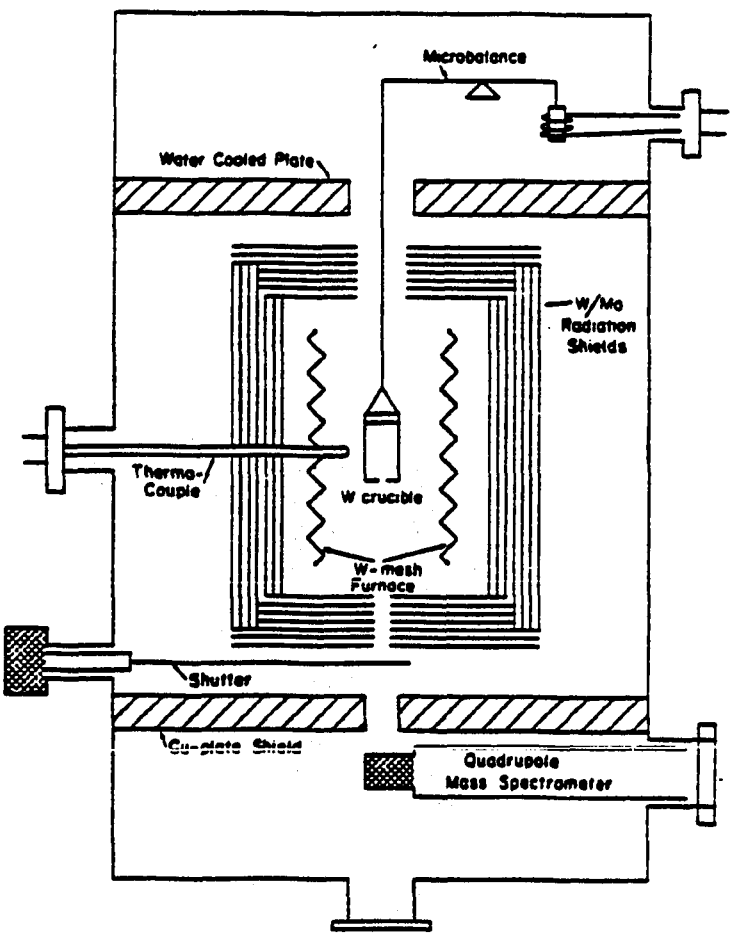

Figure 1. Essential components within the mass loss-mass spectrometer vacuum chamber

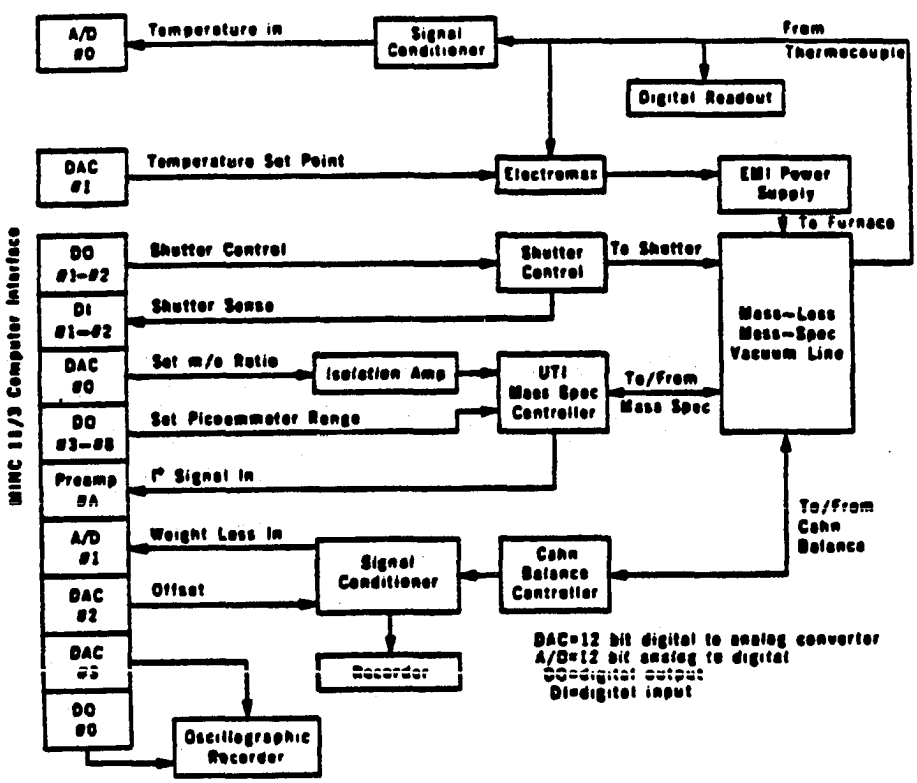

Figure 2. Interface between MINC-11 minicomputer and ML-MS apparatus

standard, simultaneously observed I_i^+ values are related to them in the form

$$P_i = k_i I_i^+ T \qquad (2)$$

in which k_i depends on the instrument's sensitivity to species i but not on the condensed phase from which that species vaporizes. Thus, once k_i is found as the average of P_i/I_i^+T for a small number of discrete temperatures spanning the experimental range, the more numerous I_i^+ readings at intermediate temperatures are converted to P_i.

The third major type of measurement required in thermodynamic studies (overall composition from the observed total mass loss and partial pressures from the ion currents and/or rate of mass loss are the other two) is that of the temperature, which is achieved by positioning the junction of a tantalum sheathed W/W-26% Re thermocouple a few millimeters from the side of the suspended Knudsen cell. Actual contact with the cell, or ideally with the sample itself, would ordinarily be desirable, but for the instrumental design employed here this would hinder the free movement of the cell and prevent accurate observation by the balance of very slow changes in mass.

Because temperature gradients along the direction normal to the axis of the crucible are suspected to exist within the heating zone, calibration of the thermocouple actually used for experimental measurements is done beforehand by comparing its readings over a large temperature range to those from a comparable thermocouple junction, positioned within an

empty but otherwise duplicate Knudsen cell. Corrections of up to 50°C were found to be necessary by this method.

B. The Phase Rule and Implications

In the event that the system studied vaporizes incongruently, i.e., the vapor and condensed phases differ in composition, the system's overall composition varies monotonically with time. The equilibrium being measured may thereby change repeatedly as different regions of the T-X diagram are entered. It is therefore useful to know beforehand the number of condensed phases to be encountered in the T-X regions to be measured and at least their approximate compositional ranges of existence. Armed with this knowledge and the Gibbs phase rule, one can predict whether the observed isothermal pressure should change or remain constant with time and thus judge the validity of pressure measurements at a given known composition. Specifically, for two component systems such as Ta-S and Ta-Al, one expects invariant isothermal pressure as composition moves through a region where two solid phases coexist in equilibrium with the vapor phase ($f = c-p+2 = 2-3+2 = 1$) and continuously varying pressure as an isotherm crosses a one-condensed-phase region ($f = c-p+2 = 2-2+2 = 2$). If the locations of phase boundaries are not established prior to the vapor pressure measurements, it becomes more important to establish what equilibria are being measured by identifying the condensed phase(s) present at a series of compositions. This is often done by quenching a sample of known composition from high temperature

during a vaporization experiment and then removing a portion for X-ray powder diffraction.

The very feature of some systems which makes possible the traversal of several phase regions using a single sample, namely incongruent vaporization, can lead to kinetic barriers to equilibration and thus to ambiguity if the independent phase identification is not performed. It is presumed that this barrier occurs when depletion of the more volatile component from the outside of granules of the material results in the trapping of one phase within a layer of another, or in a concentration gradient if only one phase is present. Avoidance of this nonequilibrium situation is attempted by intermittently restoring concentration homogeneity through annealing the sample at a relatively low temperature. That this annealing usually succeeds in raising the observed vapor pressure with time suggests that there is a narrow range of temperature within which the rates of (i) atomic diffusion through the bulk sample and (ii) evaporation from the sample surface are compatible. Below that range neither rate is large enough to change local or overall composition at a useful speed, and above that range evaporation depletes the surface concentration more quickly than bulk diffusion can restore homogeneity. As noted by Shilo et al.[5] and Shilo and Franzen[6] the keys to success in measuring meaningful, i.e., equilibrium vapor pressures can be (i) the discovery of the necessary temperatures and times for annealing and (ii) the minimizing of time spent at much higher temperatures.

III. TANTALUM-SULFUR SYSTEM

A. Introduction and Background

The tantalum sulfur system exhibits a number of intermediate crystalline compounds ranging in stoichiometry from TaS_3 to Ta_6S. Of these compounds only TaS_3[9,10] and TaS_2[11] have previously been the subject of thermodynamic measurements, while the others, $Ta_{1+x}S_2$, Ta_2S and Ta_6S were mainly characterized structurally. It is the metal-rich phases Ta_2S and Ta_6S which are of interest here because of their unusual stoichiometry and refractory behavior at high temperature, both of which are consistent with a substantial amount of intermetallic bonding character. The refractory behavior is observable during the synthesis of the compounds, i.e., they do not melt, decompose quickly, or show evidence of rapid solid state diffusion when annealed at $\gtrsim$ 1500°C, while the bonding character can be seen in the crystal structures determined by Smeggil.[12] Both structures (Figure 3) possess the same essential feature, a column consisting mostly of Ta atoms in pentagonal rings staggered relative to one another, with a chain of Ta atoms at its center.

Two expectations existed regarding the vaporization of Ta_2S and Ta_6S existed prior to performing the experiments: (i) incongruent vaporization with S being the more volatile component and (ii) atomization enthalpies resembling that of metallic tantalum more than those of the sulfur-rich Ta-S phases. Precedents for incongruent vaporization are to be found in the related systems Sc-S[13] and Lu-S[14] (although both systems also exhibit congruent vaporization at a certain composition), while the high

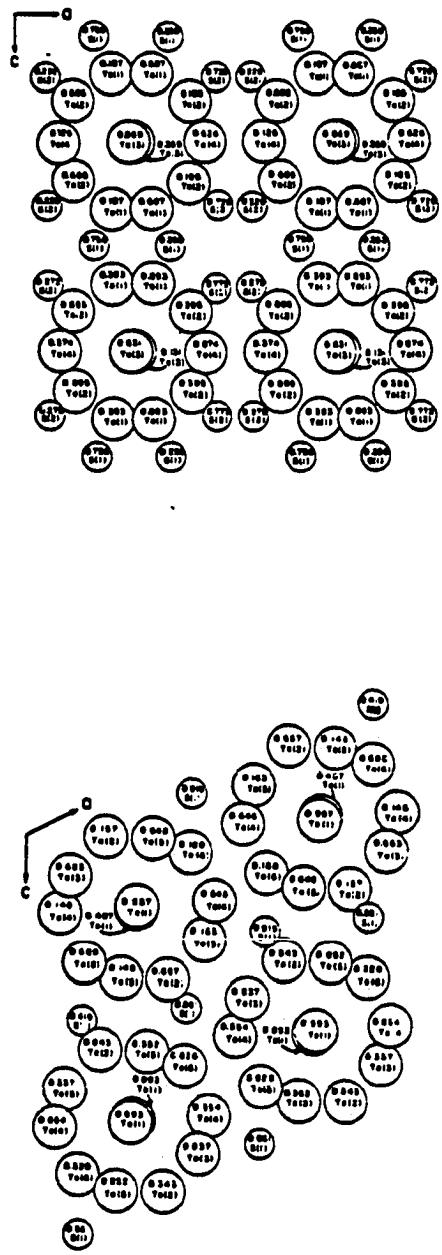

Figure 3. Projection of structures of Ta_2S (top) and Ta_6S

atomization enthalpies are predictable from other transition metal sulfides (see Discussion, this thesis) and the metal-like bulk physical properties of Ta_2S and Ta_6S. The incongruent nature of the vaporization, as verified in preliminary observations during this study, makes these compounds ideal candidates for study by ML-MS Knudsen effusion because their vapor pressures are measurable by either the combined ML-MS method or by mass loss alone.

B. Experimental Methods

1. Synthesis and characterization

Synthesis and identification of crystalline Ta/S phases was accomplished by B. U. Harbrecht (Ames Laboratory Postdoctoral Fellow) using standard techniques of solid state chemistry, summarized as follows: in variable starting ratios near the stoichiometries of desired phases, granular tantalum (Alpha Products, 60 mesh, 99.98%) and lump sulfur (Alpha Products 99.9999%) were combined in evacuated quartz glass ampules and heated to above 850°C for 3-5 days. As previous experience suggested the reactions would be incomplete at this stage, the intermediate products usually were not analyzed but were compressed into small pellets and then heated in a tungsten crucible by rf induction. The temperature range required for homogenization of the sulfides in this manner increases with decreasing sulfur content, and for Ta_2S was $\leq$ 1550°C. The maximum temperature was approached gradually to avoid melting or rapid change in composition and was maintained for 6 to 10 hours. All phase analyses were performed by comparing d (or 2Θ) values from Guinier

powder films to published patterns (see Table 1). The samples actually used in the vaporization experiments appeared to contain only Ta_2S. Two-phase mixtures obtained from Ta/S starting ratios other than 2:1 showed that (i) Ta_2S coexists with $Ta_{1.35}S_2$ to the sulfur-rich side or with Ta_6S to the tantalum-rich side of 2:1 stoichiometry with no detectable change in unit cell dimensions and similarly (ii) Ta_6S has the same lattice constants whether in Ta_2S/Ta_6S or Ta_6S/Ta mixtures. This suggested negligible phase width for each compound and thus the scope of the study was restricted to measuring vapor pressures in equilibrium with each of the mixtures Ta_2S/Ta_6S and Ta_6S/Ta without concern for determination of phase boundaries.

2. Vapor pressure measurements

Preliminary measurements using both the ML and MS techniques as explained in the general introduction revealed two significant limitations. The first was that S and S_2 were the only vapor species detected using the mass spectrometer. This allowed the assumption, employed in the data analysis section, that a single vapor pressure measurement would suffice in determining both P_S and P_{S_2} since the two are related by an equilibrium constant. The second observation was that, while steady rates of mass loss could be monitored with the electrobalance at any fixed temperature and a composition corresponding to a mixture of two solid phases, the mass spectrometer could not be used to simultaneously measure significant or reproducible ion currents at either 32 AMU or 64 AMU. Specifically, the readings at those AMU settings were not

Table 1. Comparison of lattice parameters determined by Guinier powder method with those in literature

Phase	Lattice type	Lattice parameters (Å) This study	Literature	Ref. no.
Ta	bcc	3.307(1)	3.303	15
Ta_6S	monoclinic	a = 14.141(2)	14.158(4)	12
		b = 5.286(1)	5.284(1)	
		c = 14.807(2)	14.789(5)	
		β =117.96(1)°	118.01(2)°	
Ta_2S	orthorhombic	a = 7.3775(5)	7.381(2)	12
		b = 5.5740(4)	5.574(1)	
		c = 15.199(3)	15.195(3)	
$Ta_{1.35}S_2$	hexagonal	a = 3.286(4)	3.29	16
		c = 12.651(2)	12.65	

significantly greater with the shutter to the mass spectrometer open than with it closed, probably because too great a background of S and S_2 remained in the system from previous experiments. With the sulfur vapor thus adjudged "unshutterable", all P vs T data were measured in the form of rates of mass loss, monitored on a calibrated variable-speed recording chart receiving the output from the balance. Each sample of Ta_2S used in a series of measurements was of about 400 mg in mass, thus containing ca.

32 mg S, and an average of no more than 0.5 mg of mass loss was used to determine a single P vs T point. This rather slow method of data collection, which is due to the limited sensitivity of the Knudsen effusion method (already alluded to in the general methods section IIA), resulted in no more than 35 measurements in a given two-phase region of a single sample. However, attempts to replicate the measurements using Knudsen cells with a gradation of orifice size resulted in additional useful data. The raw data from the three runs performed are listed in Table A1.

Because incongruent vaporization often results in nonequilibrium pressures due to surface depletion of the volatile component, the chosen sequence in which pressures were measured alternated between temperatures higher and lower in the overall range. This was combined with overnight (10 hr or longer) annealings at usually no greater than 1000°C to restore sample homogeneity. Reproducibility of pressures measured upon returning to a given temperature after such annealings verified the effectiveness of this sequence. As will be seen, total elimination of the surface depletion effects was not that easily achieved; a small range in observed pressure at any single temperature resulted from varying the orifice size. This is expected when surface depletion occurs because, relative to a given true equilibrium pressure, the deviation in the observed pressure is more serious as the rate of evaporation increases, and rate of evaporation at any fixed temperature increases with orifice size. The method of accounting for this deviation is explained in the data analysis section (IIIC).

When the mole fraction of sulfur remaining in a sample approached zero (pure tantalum), no gradual decrease in isothermal pressure could be observed. Instead, the decrease was rather abrupt, after which no appreciable mass loss occurred even at ~1630°C. This suggests negligible solubility of S in Ta, which is consistent with the agreement of the lattice parameter of Ta in Ta_6S/Ta mixtures with that of pure Ta.

C. Data Analysis and Results

1. Derivation of P_S

Having measured the net rate at which mass in the form of S(g) and S_2(g) is lost from two different solid-phase mixtures, it is possible to write these corresponding chemical reactions:

$$\frac{3}{2}\,Ta_2S(s) \rightleftharpoons \frac{1}{2}\,Ta_6S(s) + S(g) \qquad (3)$$

$$Ta_6S(s) \rightleftharpoons 6Ta(s) + S(g) \qquad (4)$$

and to then determine thermodynamic properties from the temperature dependence of the equilibrium constant, which is simply P_S in each case. Initially, it was asserted that S and S_2 are in equilibrium in the gas phase; since reactions 3 and 4 could have been written with S_2(g) as the vapor species, this assertion actually follows from the assumption of condensed phase/vapor phase equilibrium. At the pressures involved, mean free paths of vapor species are much too long (~ 1 m at 5×10^{-7} atm) for S/S_2 equilibrium to be achieved through vapor phase collisions and so

the equilibration mechanism must involve the condensed sample's surface, i.e., equilibrated S and S_2 evaporate from the solid, or from the inner surface of the cell. The equilibrium constant for the reaction $S_2(g) = 2S(g)$ was interpolated from tables in reference 1 and used in determining P_S (T) as follows:

$$P_{S_2} = P_S^2 / K_{p,vap}. \tag{5}$$

The rate $\left(\frac{\Delta m_{total}}{\Delta t} \right)$ which is actually measured, is $\frac{\Delta m_S}{\Delta t} + \frac{\Delta m_{S_2}}{\Delta t}$

or
$$AP_S \left(\frac{M_S}{2\pi RT} \right)^{1/2} + AP_{S_2} \left(\frac{M_{S_2}}{2\pi RT} \right)^{1/2} = \frac{\Delta m_{total}}{\Delta t} \tag{6}$$

from the rearranged Knudsen equation (Equation 1).

Substituting (5) and $M_{S_2} = 2M_S$ into (6) yields

$$\frac{\Delta m_{total}}{\Delta t} = A \left(\frac{M_S}{2\pi RT} \right)^{1/2} P_{eff} \tag{7a}$$

where
$$P_{eff} = P_S + \frac{\sqrt{2} P_S^2}{K_{p,vap}} \tag{7b}$$

Solving 7b, a quadratic equation in P_S, yields:

$$P_S = \frac{K_{p,vap}}{2\sqrt{2}} \left[\left(1 + \left(\frac{4\sqrt{2}}{K_{p,vap}} \right) \left(\frac{\Delta m_{total}}{\Delta t} \right) \left(\frac{2\pi RT/M_S}{A} \right)^{1/2} \right) - 1 \right] \tag{8}$$

Thus, from each measured $\frac{\Delta m_{total}}{\Delta t}$ (T), P_{eff}(T) and P_S(T) were calculated.

The deviation of P_S(T) (observed) from true equilibrium pressure,

dependent on orifice cross sectional area A as noted earlier, ranged between factors of about 1.3 and 3. In the absence of any other systematic errors, the true $P_S(T)$ should be obtained for A = 0, so the correction of $P_S(T)_{obs}$ was done by extrapolation to A = 0 in this manner: the assumed orifice (and hence, effusion rate) dependence of this error was approximated as the truncated form of a series expansion of

$$P_S(T)_{obs} = P_S(T)_{equil} - \alpha \frac{\Delta m}{\Delta t} \qquad (9)$$

with α an unknown coefficient. Substitution of Equation 7a yielded

$$P_S(T)_{obs} = P_S(T)_{equil} - \alpha' A \cdot P_{eff}(T) \qquad (10)$$

in which $\alpha' = \alpha(2\pi RT/M_S)^{-1/2}$. Five equally-spaced temperatures spanning the experimental range for reaction (3) were chosen; another five spanning the range for reaction (4) were also chosen. α' was found at each such T by linear least-squares fit of equation (10) to the $A \cdot P_{eff}(T)$, $P_{S(obs)}$ pairs corresponding to the three orifices used. Then $\alpha'(T)$ was parameterized by the five-point least-squares fit of $\alpha'(T)$ vs $T^{-1/2}$. (Linear $T^{1/2}$ dependence was observed.) The results were:

reaction (3) : $\alpha'(T) = -7.4(1) \times 10^7 \cdot T^{-1/2} + 1.51(3) \times 10^6$

reaction (4) : $\alpha'(T) = -5.51(6) \times 10^7 \cdot T^{-1/2} + 8.8(1) \times 10^5$

Pressures were then corrected by applying these values for $\alpha'(T)$ to the $P_S(T)_{obs}$ as in Equation (10); the adjustments can be seen in

comparing the last two columns of Table A1. The significance of these corrections in terms of the resulting enthalpies of reaction is shown in the next section.

2. Calculation of ΔH°_{rxn} by 2nd law and 3rd law methods

From knowledge of the temperature dependence of the equilibrium constant (in this case $P_S(T)$) one may calculate the enthalpy change for the reaction, or ΔH°_{rxn}, in two ways. If one fits a straight line to the points ($x = 1/T$, $y = -R \ln K_p$) there results a slope of $\Delta H^\circ_{T_{med}}$ and an intercept of $-\Delta S^\circ_{T_{med}}$. The T_{med} here signifies the median temperature in the experimental range, so chosen because the 'line' determined by the experimental points has a slight (but usually unmeasurable) curvature owing to the dependence of ΔH°_{rxn} on T and the slope of the tangent to this curve at $1/T_{med}$ represents an average of ΔH°_T over the whole temperature range. What is more frequently done is a linear least squares fit to ($x = 1/T$, $y = -R \ln K_p - \Delta fef$) in which Δfef is the change (for a reaction) in the 'free energy function', $(\Delta G^\circ_T - \Delta H^\circ_{T_{ref}})/T$. Because of the following relationships

$$\Delta G^\circ_T = -RT \ln K_p \tag{11}$$

$$-R \ln K_p - \Delta fef = \Delta H^\circ_{T_{ref}}/T \tag{12}$$

such a fit results in a zero-intercept line with a slope of $\Delta H^\circ_{T_{ref}}$ if the choice of Δfef has closely approximated ΔS°. As tabulated in the JANAF tables[1], T_{ref} is 298 K. With or without the

use of free energy functions, a linear fit vs 1/T, which is essentially an application of the van't Hoff equation, is called a 'second law method' despite a common misconception that the form including Δfef should be termed a 'third law method' because fefs are evaluated using the third law of thermodynamics. However, this slope determination (equation 12) involves a $\Delta(\Delta fef)$ which cancels the dependence upon the third law.

'Third law method' will here refer to the single point determination of $\Delta H^{\circ}_{T_{ref}}$ by multiplying Equation 12 by T. In this method the correct measurement of absolute values of K_p is required because the zero points in ΔC°_p and ΔS° are fixed by the use of the third law-based fefs. In contrast, the 2nd law method actually depends only on relative changes in K_p with 1/T, as the zero-intercept (the distinguishing characteristic of 2nd vs 3rd law method) is not required. Used without corroboration, the 2nd law method (with fefs) has only goodness-of-fit and nearness of the resulting intercept to zero as criteria for evaluating accuracy. It is somewhat less susceptible to erroneous results due to pressure measurements, because ΔH°_{298} is not strongly sensitive to the correct measurement of K_p in absolute numerical terms, but more susceptible to systematic nonconstant errors in temperature measurement. On the other hand, the 3rd law method is quite dependent on both correctly scaled (not merely internally consistent) K_p determinations and judicious choices of Δfef. An intercomparison of ΔH°_{298} K determined by each method, therefore, provides a test of the combined

effects of accuracy in measuring T and K_p and in the choice of Δfef for the reaction in question.

The 2nd law results at T_{med} do not involve any input besides measured data and thus represent the temperature dependence of P_S, probably subject only to temperature measurement errors (orifice dependence of P_S has already been adjusted for):

$$Ta_2S/Ta_6S \quad \ln P_S = \frac{-51.7(3) \times 10^3}{T} + 16.0(1) \qquad (13)$$

$$Ta_6S/Ta \quad \ln P_S = \frac{-57.4 \times 10^3}{T} + 18.3(3) \qquad (14)$$

Initially, application of the 2nd law (298 K) and 3rd law methods to reactions (3) and (4) was attempted by assigning Δfefs (according to reference 1) as follows:

$$3/2Ta_2S(s) \rightarrow 1/2Ta_6S(s) + S(g) \quad \Delta fef = fef(S(g))-fef(S(s))$$

$$Ta_6S(s) \rightarrow 6Ta(s) + S(g) \quad \Delta fef = fef(S(g))-fef(S(s)).$$

This follows from assuming the Neumann-Kopp additivity rule for heat capacities holds.

The results for ΔH°_{298} using the Δfef assumptions were:
reaction (3): 104.9(6) kcal by 2nd law vs 99.6(3) kcal by 3rd law,
reaction (4): 115.9(9) kcal by 2nd law vs 101.1(4) kcal by 3rd law.

The discrepancies between the reaction enthalpies as determined by the two methods were too large to be due to nonequilibrium P_S values; the extrapolation described earlier resulted in a correction of ~3 kcal or less in ΔH°_{298}. Another possibility considered was systematic error

in temperature measurement, to which 2nd law calculations are much more sensitive than are 3rd law calculations. However, no temperature error could account for such disparate results for the two reactions; a temperature correction of any size would still leave a large 2nd law-3rd law disagreement for at least one of the reactions because although the range of temperature measurement was nearly the same for both, $\Delta H^{\circ}_{rxn,298}$ adjustments differing by about a factor of three are required.

The only likely explanation remaining was an inappropriate choice of fef values for the compounds $Ta_2S(s)$ and $Ta_6S(s)$. Assuming the high-temperature 2nd law (without Δfef) P_S-T relationships as measured (Equations 13 and 14) to be basically correct, adjusted fef's were derived thusly: expressions for 2nd- and 3rd law T-dependence of ΔG° were written and then equated:

$$\Delta G^{\circ}_{T,2nd} = H^{\circ}_{T_{med}} - T\Delta S^{\circ}_{T_{med}} \tag{15}$$

$$= \Delta G^{\circ}_{T,3rd} = \Delta H^{\circ}_{T_{ref}} + T\Delta fef_T \tag{16}$$

but with $T_{ref} = 298$ K and $\Delta H^{\circ}_{T_{ref}} = \Delta H^{\circ}_{T_{med}} + \int_{T_{med}}^{T_{ref}} \Delta C^{\circ}_p \, dT$

this became

$$-T\Delta S^{\circ}_{T_{med}} = \int_{T_{med}}^{T_{ref}} \Delta C^{\circ}_p \, dT + T\Delta fef_T \tag{17}$$

or $$\Delta fef_T = \frac{1}{T}\left[\int_{T_{ref}}^{T_{med}} \Delta C^{\circ}_p \, dT \right] - \Delta S^{\circ}_{T_{med}} . \tag{18}$$

By assuming ΔC_p° to be well-approximated by C_p° (S(g)) - C_p° (Ta(s)) and performing a graphical integration using tabulated[1,17] values the quantity 1.54 kcal was found for the integral term in equation (17). When the unknowns fef(Ta in cpd) and fef(S in cpd) were replaced by x and y, respectively, the following equations corresponding to reactions (3) and (4) resulted:

$$\Delta fef_3 = fef(S(g)) - y \qquad (19)$$

$$\Delta fef_4 = 6[fef(Ta(s)) - x] + fef(S(g)) - y. \qquad (20)$$

Substituting the Δfef_{rxn} values calculated from equation (18) for the appropriate reaction into Equation (19) and Equation (20) at each temperature spanning 1400 K to 2000 K in 100 K increments yielded pairs of equations. These were solved simultaneously to give the adjusted fef's, which are compared with tabulated values in Table 2.

With these derived fefs the 2nd and 3rd law $\Delta H^\circ_{rxn,298}$ calculations agree (of course). The final adjusted values are listed in the last column of Table 3 along with those from the individual experiments done with varying orifice area A. Corresponding to the 2nd law quantities are the series of plots in Figures 4 to 7 which depict the ln K_p vs 1/T behavior for both equilibria, comparing points with orifice dependence to the line of extrapolated points.

Table 2. Comparison of derived (der) and tabulated (tab) values for fef_{Ta}/R and fef_S/R in the solids. $\Delta fef/R$ for reactions (3) and (4) employed for the derivation are also listed

T in K	$-fef_{Ta}/R$ (der)	$-fef_{Ta}/R$ (tab)	$-fef_S/R$ (der)	$-fef_S/R$ (tab)	$-\Delta fef_3/R$	$-\Delta fef_4/R$
1400	7.02	7.403	5.68	6.723	16.56	18.87
1500	7.20	7.583	5.87	6.984	16.52	18.83
1600	7.37	7.754	6.03	7.241	16.49	18.80
1700	7.53	7.918	6.19	7.494	16.46	18.77
1800	7.69	8.076	6.35	7.744	16.43	18.75
1900	7.84	8.225	6.49	7.991	16.41	18.73
2000	7.99	8.374	6.62	8.235	16.39	18.70

Table 3. Results of 2nd and 3rd law calculations of $\Delta H°_{vap,298}/R$ using derived fef values

Reaction, Method	10^7 x A in m^2 12.5	7.5	1.53	0.00
$3/2\ Ta_2S\ (s) = 1/2\ Ta_6S\ (s) + S\ (g)$				
2nd	54.9 (0.3)	55.7 (0.3)	53.9 (0.5)	53.0 (0.3)
3rd	54.5 (0.1)	54.2 (0.1)	53.4 (0.1)	
$Ta_6S\ (s) = 6Ta\ (s) + S\ (g)$				
2nd	58.2 (0.3)	58.1 (0.5)	58.2 (1.0)	58.1 (0.4)
3rd	59.7 (0.1)	59.4 (0.1)	58.6 (0.3)	

A = area of orifice.
Numbers in parentheses are std. deviations

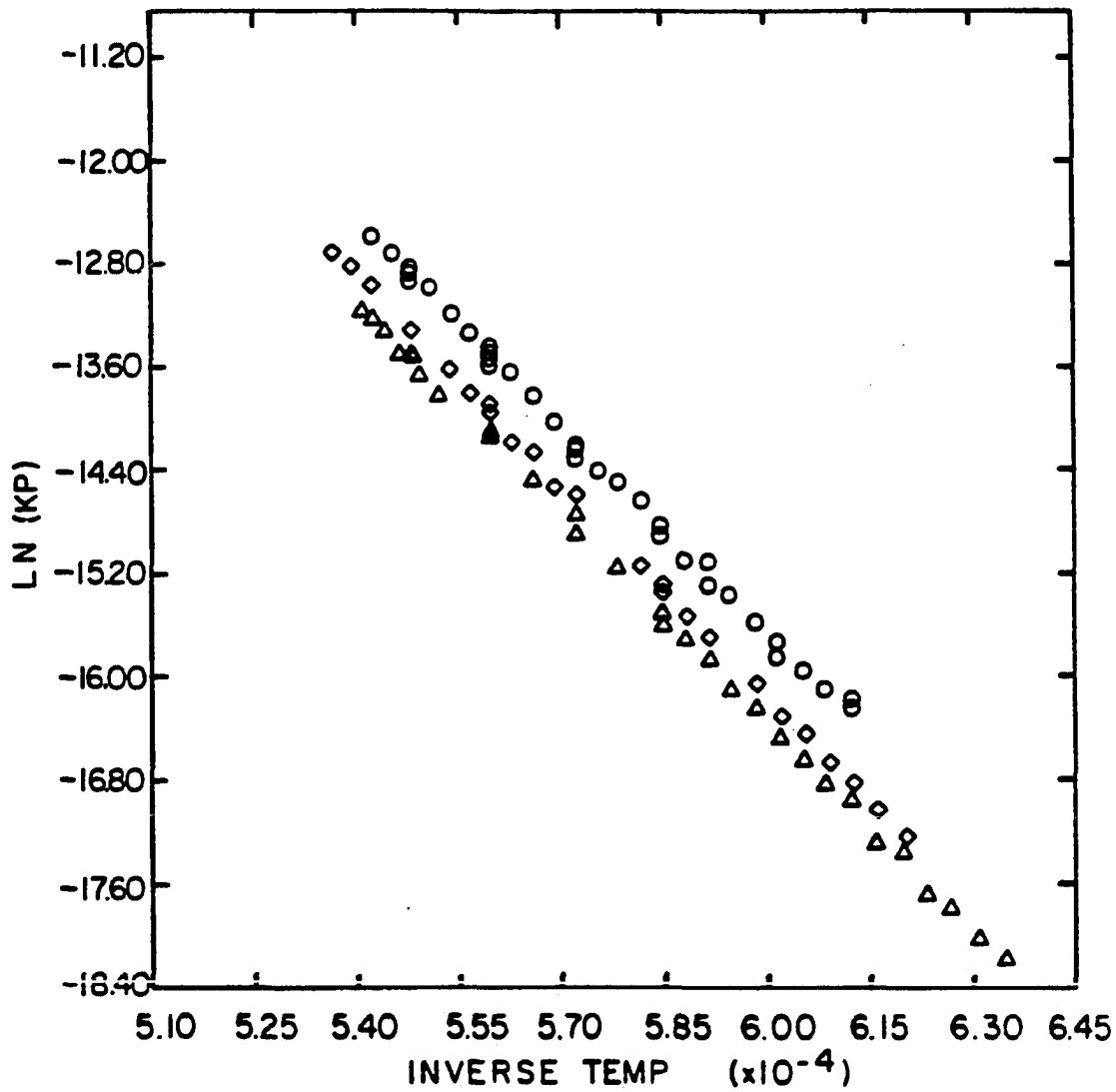

Figure 4. $\ln K_p$ vs 1/T plots of the reaction 3/2 $Ta_2S(s)$ = 1/2 $Ta_6S(s)$+ S(g) for three different Knudsen cell orifice sizes

Key:

Symbol (Figs. 1a,1b)	Expt. No. (cf. Table A1)	Orifice Area (in 10^{-7} m^2)
○	1	1.53
△	2	12.5
◇	3	7.50

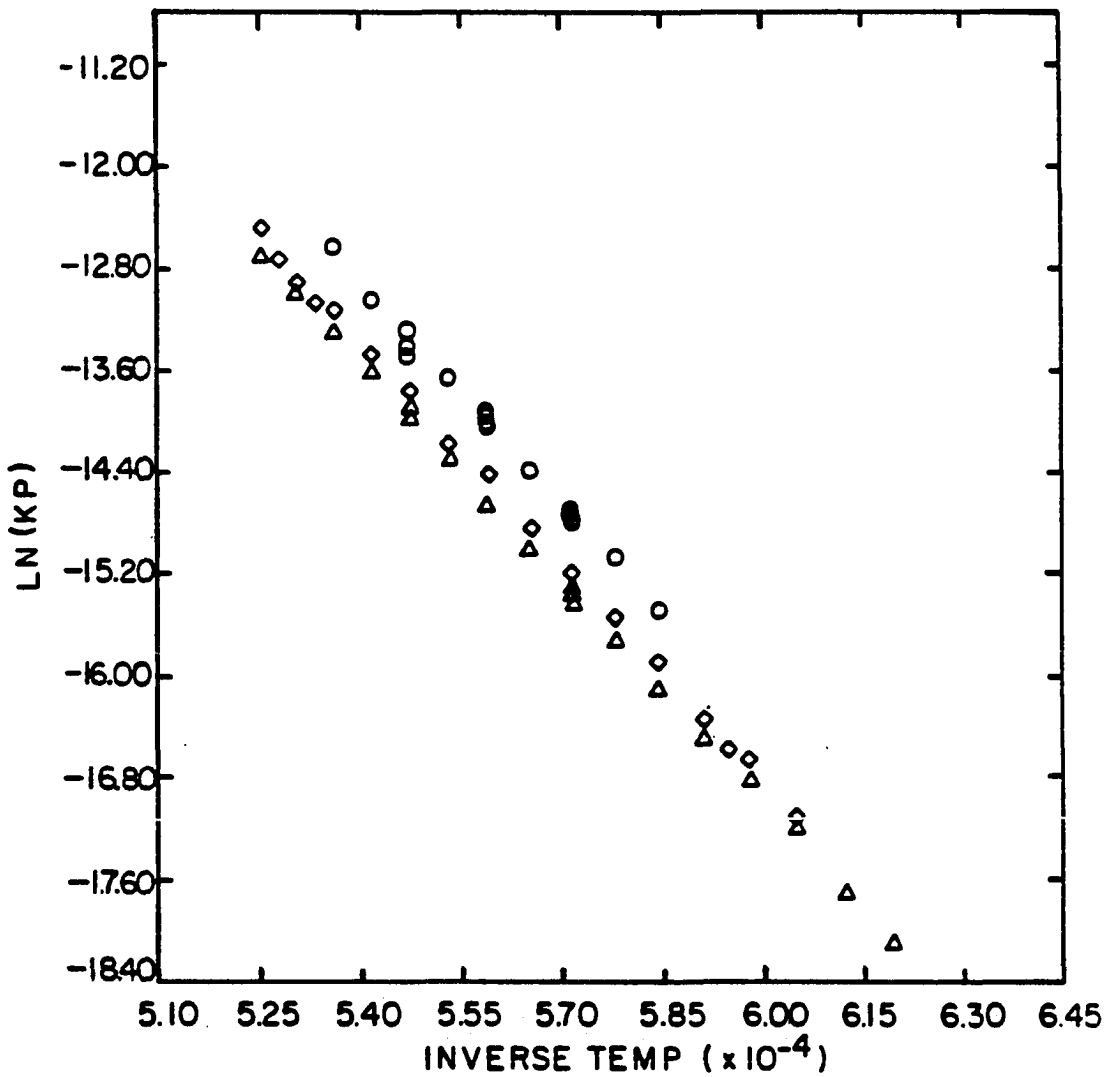

Figure 5. $\ln K_p$ vs 1/T plots of the reaction $Ta_6S(s) = 6\ Ta(s) + S(g)$ for three different Knudsen cell orifice sizes

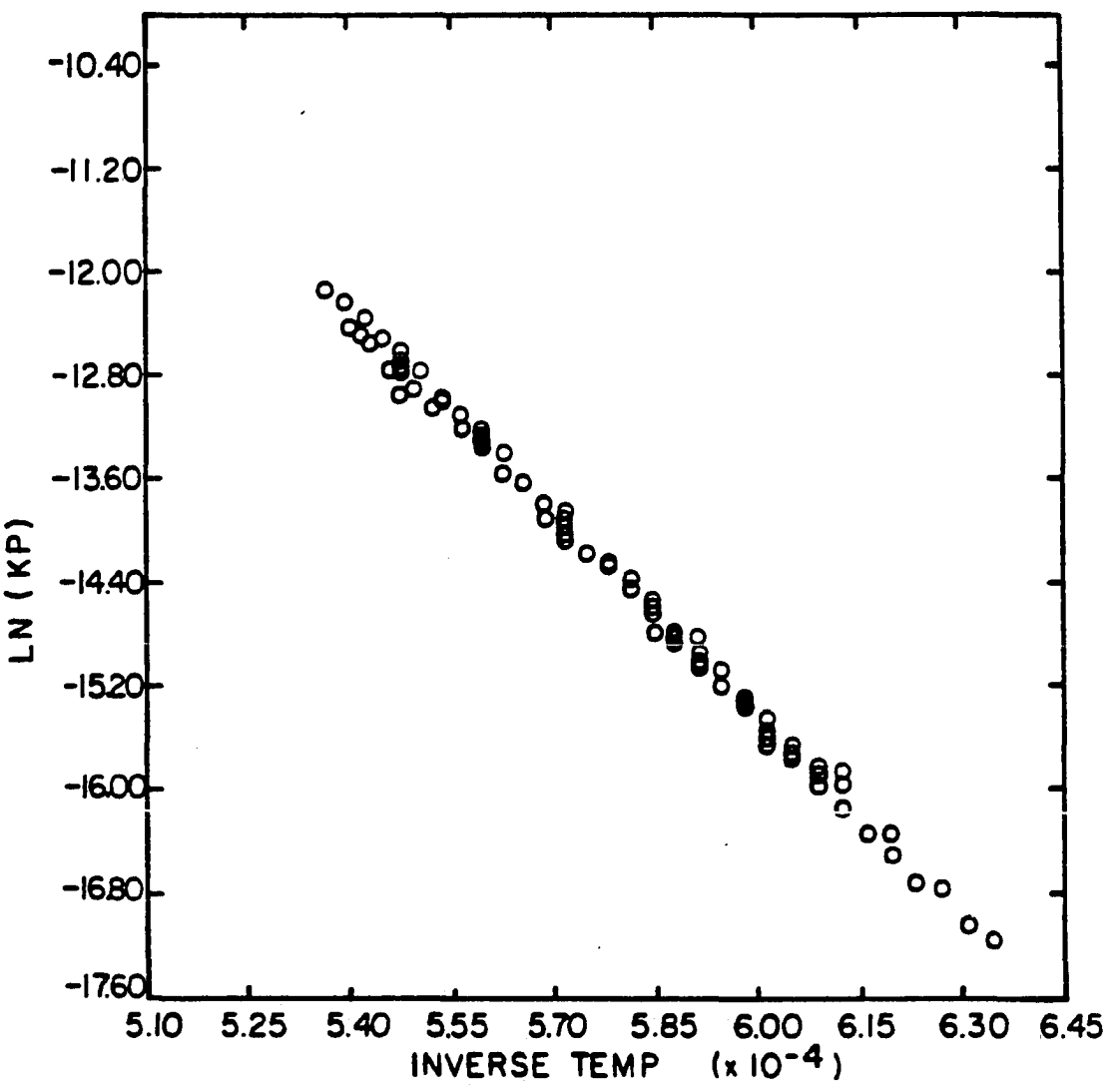

Figure 6. Results of adjusting data of Fig. 4 by extrapolating to equilibrium pressures

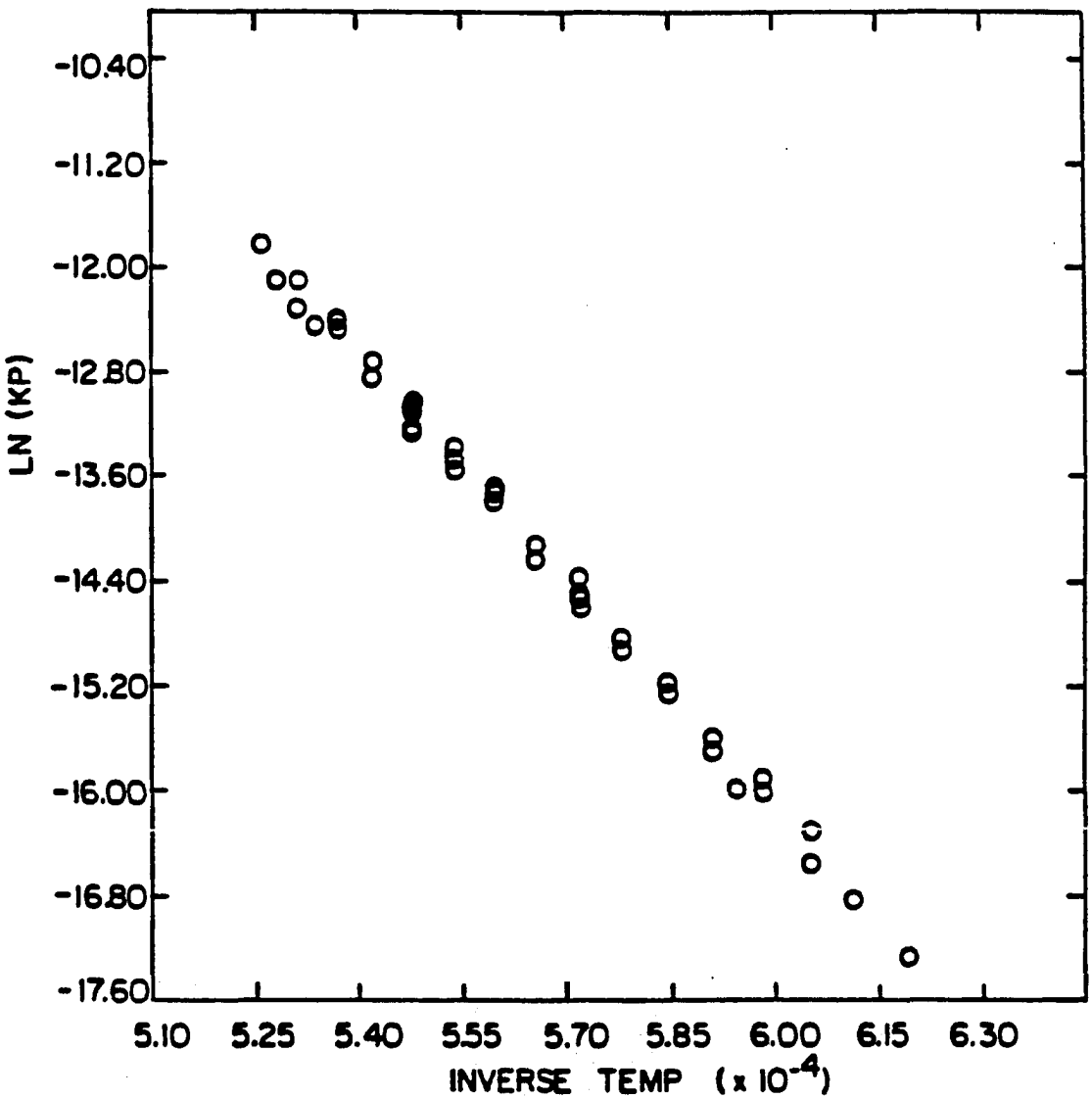

Figure 7. Results of adjusting data of Fig. 5 by extrapolating to equilibrium pressures

3. Enthalpies of formation and atomization

Because standardized tables of enthalpy measurements are often in terms of $\Delta H^{\circ}_{f,298}$ and because comparisons to other chemical systems are desirable, $\Delta H^{\circ}_{rxn,298}$ calculated as just described were in turn used to derive other properties:

$$\Delta H^{\circ}_{f,298K}\ (Ta_6S) = 2\cdot\left(\frac{3}{2}\Delta H^{\circ}_{f,298}\ (Ta_2S) - \Delta H^{\circ}_{f,298}(S(g)) + \Delta H^{\circ}_{rxn\ 3,298}\right) \tag{21}$$

$$\Delta H^{\circ}_{f,298K}\ (Ta_6S) = \Delta H^{\circ}_{f,298}\ (S(g)) - \Delta H^{\circ}_{rxn\ 4,298} \tag{22}$$

$$\Delta H^{\circ}_{at,298}\ (Ta_6S) = \Delta H^{\circ}_{rxn\ 4,298} + 6\Delta H^{\circ}_{f,298}\ (Ta(g)) \tag{23}$$

$$\Delta H^{\circ}_{at,298}(Ta_2S) = -\Delta H^{\circ}_{f,298}(Ta_2S) + 2\Delta H^{\circ}_{f,298}\ (Ta(g)) + \Delta H^{\circ}_{f,298}(S(g)). \tag{24}$$

Using the tabulated values $\Delta H^{\circ}_{f,298}(S(g))$ = 66.68 kcal/mole[1] and $\Delta H^{\circ}_{f,298}(Ta(g))$ = 186.8 kcal/mole[17] these equations yielded (in kcal/mol):

Phase	$\Delta H^\circ_{f,298}$	$\Delta H^\circ_{at,298}$
Ta_6S	-48.6(1.0)	1235.1(0.6)
Ta_2S	-41.8(0.6)	482.0(0.4)

To facilitate comparisons both within and outside of the Ta-S system, two further adjustments have been made: enthalpies of atomization were divided by the number of moles of atoms in a formula unit (e.g., by 7 for Ta_6S), and all enthalpies were divided by R; the reported results are in terms of 10^3 K and can be quickly converted to any desired energy unit via multiplication by the appropriate R. Enthalpies of atomization/mole of atoms are compared to those of related systems in Table 4, while intrasystem comparisons of both $\Delta H^\circ_{at,298}$ and $\Delta H^\circ_{f,298}$ are seen in Table 5 and Figure 8.

D. Discussion

Assessment of the results reported here will attempt to deal with two concerns: 'how reliable are the numerical quantities?' and 'what is their chemical significance?'

As already mentioned at various points, enthalpies of reaction as determined by the Knudsen mass loss method are subject to errors from a small number of potentially serious sources: nonequilibrium pressure measurements, erroneous temperature determination, and incorrect choice of fefs in the data analysis. The deviation of observed vapor pressure from that at true equilibrium was probably minimized by the frequent

Table 4. Enthalpies of atomization/mole atoms, $\Delta H^{\circ}_{at,298}/R$ in 10^3 K for Ta_2S, Ta_6S and related compounds

Solid phase	$\Delta H^{\circ}_{at,298}/R/(x+y)$	References
Pd_4S	44.9(5)	18
Rh_2S	59(5)	11
ScS	64.3(7)	19
TiS	61.0(7)	20
VS	64.9	21
Ta_2S	80.9(2)	this study
Ta_6S	88.9(3)	this study

Table 5. Enthalpies of formation (f) and atomization (at); $\Delta H^{\circ}_{298}/R/(x+y)$ in 10^3 K

phase (solid)	$\Delta H^{\circ}_{f,298}/R$ in 10^3 K	$\Delta H^{\circ}_{at,298}/R$ in 10^3 K	References
S	0	33.6 (0.3)	1
TaS_3	-45.3 (2.5)	60.0 (0.7)	9
	-43.3 (5.0)	59.5 (1.3)	10
TaS_2 (2nd)	-36.7 (3.0)	66.0 (1.0)	11
(3rd)	-42.6 (2.0)	67.9 (0.7)	
$Ta_{1+x}S_2$			
x = 0.2	-48.8 (3.8)	71.5 (1.2)	estim.
x = 0.35	-50.5 (4.0)	73.0 (1.2)	estim.
Ta_2S (2nd)	-21.0 (0.3)	80.9 (0.2)	this work
Ta_6S (2nd)	-24.5 (0.5)	88.9 (0.3)	this work
Ta	0	94.0 (0.3)	17

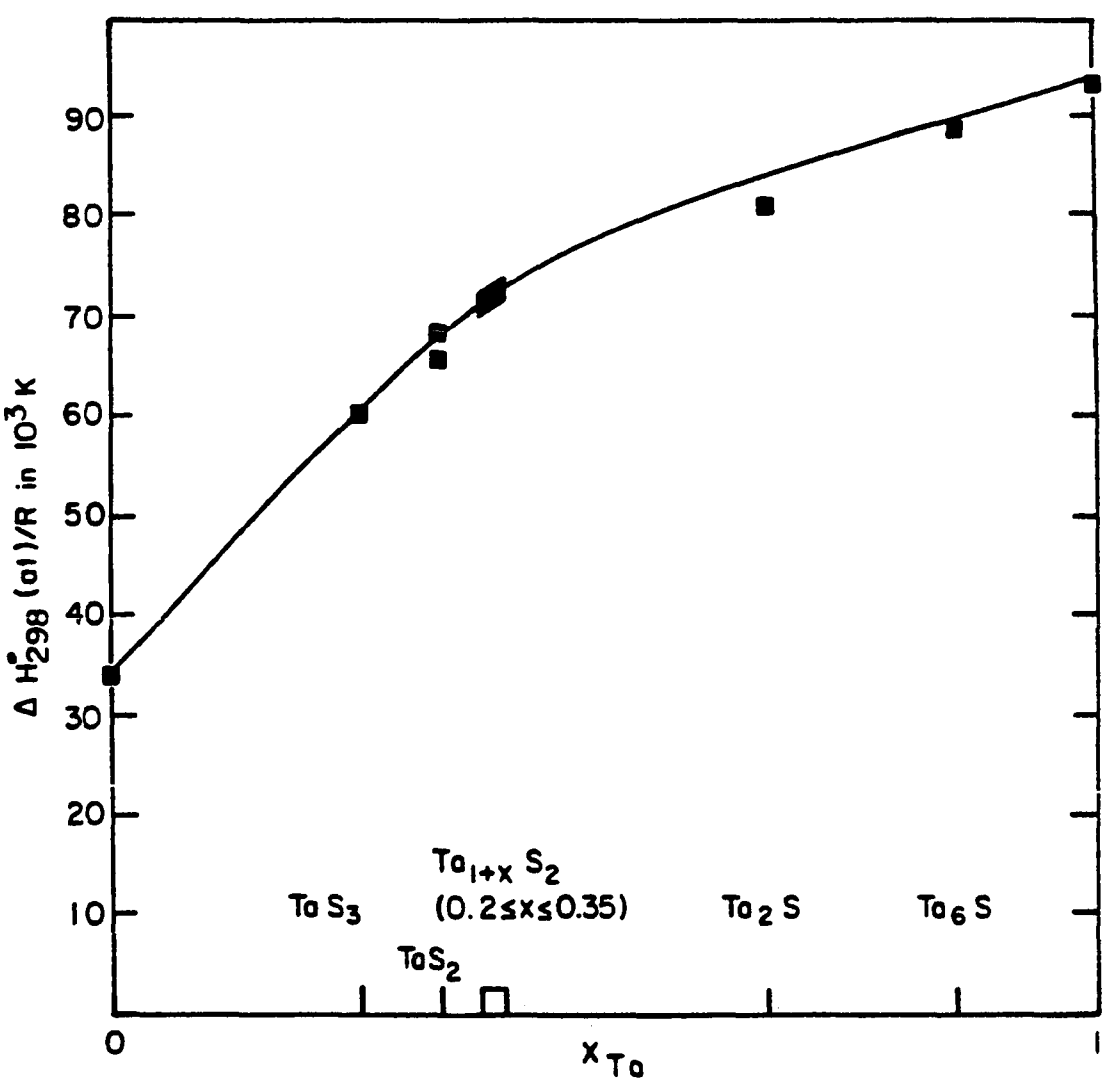

Figure 8. The trend in enthalpy of atomization for Ta-S phases

annealings at low temperature; the extent to which the problem remained was accounted for in the extrapolation to A = 0 and seen not to be a serious problem. The measurement of temperature was a less tractable problem due to the impossibility of contact between the thermocouple and the tungsten crucible; the two-thermocouple calibration described in the general methods section is the best corrective measure available presently. However, as previously explained, a serious error in temperature measurement could not account for the initially large discrepancy in the 2nd law/3rd law comparison which is generally the ultimate criterion for evaluation of calculated ΔH°_{298}. Admittedly, the agreement or disagreement between the results calculated by each method is only the net effect of all error sources combined. The approach of determining new fef values for the compounds $Ta_6S(s)$ and $Ta_2S(s)$ implicitly attributes errors in ΔH°_{298} to assignment of fefs, consistent with the above dismissal of P and T errors. Yet it is still possible that this masks the true sources of error and thus the credibility of the new fef values becomes the criterion of judgment; an unreasonable value of fef(Ta) and/or fef(S) could suggest undetected systematic problems.

Referring again to Table 2 one can see that the newly determined fef values are in fact quite reasonable. At each temperature, the normalized (by R) derived |fef| of Ta is smaller than the tabulated value by about 0.4 K. This is nearly the same as the entropy difference between the hcp (low temperature) and bcc (high temperature) forms of metals such as Ti, Hf, and Ca. Tantalum exhibits only the bcc form, but perhaps the intermetallic bonding and consequent heat capacity contributions in the Ta_2S

and Ta_6S structures are more similar to those of a hypothetical hcp arrangement of Ta than to those of bcc Ta. (ΔH_f°(Ta(hcp)) = 6 kcal/mol according to Brewer). In any event, the discrepancy is not significantly large. The somewhat larger difference of $(|fef|_{tab}(S)-|fef|_{der}(S))/R \approx 1$ is apparently the more important difference between the behavior of metal-rich Ta_2S or Ta_6S and compounds of more conventional stoichiometry for which the Neumann-Kopp rule is appropriate. This fef adjustment is at least in the right direction, as one would expect S in Ta_6S or Ta_2S to be more vibrationally rigid than in $S_8(s)$. For assessing the correctness of the absolute size of $fef_{der}(S)$, low temperature heat capacity measurements on the metal rich tantalum sulfides to directly determine fefs would be needed.

This method of calculating new fefs relies on the accuracy of $\Delta H^\circ_{T_{med}}$ found by the second law fits. $\Delta H^\circ_{T_{med}}$ showed good reproducibility from one experiment to the next and small statistical scatter within a given experiment, with the combined result of standard deviations of ~1 kcal or less for both reactions. It can therefore be fairly concluded that the enthalpies reported herein are reliable numerically, although their estimated accuracy of 0.7 kcal/mol atoms (see p. 67) is worse than suggested by the quoted standard deviations, which are indicative only of precision in the calculated means or least-squares slopes.

Discussing the chemical significance of the results is at best semi-quantitative due to the lack of a well-established model for predicting ΔH_f° for compounds such as these and to the paucity of thermodynamic

measurements on metal-rich compounds in general. The intent of Table 4 is to suggest the qualitative reasonableness of the $\Delta H^{\circ}_{atm,298}/R$ for Ta_2S and Ta_6S by listing them along with the few reduced transition metal sulfides for which such data are published; a high temperature vaporization study was involved in each case. That the listings for the Ta compounds are the highest is not surprising, because their stoichiometry and known structures obviously mean that many metal-metal bonds are broken in an atomization process. The average Ta-Ta distance is 3.03 Å in both Ta_2S and Ta_6S are 3.03 Å and 3.03 Å, respectively (cf 2.69 in Ta, 3.38 in TaS_3), so one expects bonding enthalpy intermediate between that of the pure metal and that of sulfur-rich compounds.

In Figure 8 is depicted the intra-system variation in $\Delta H^{\circ}_{at,298}$ for Ta/S phases; the value for $Ta_{1.35}S_2$ is estimated assuming that it is not metastable. A straight line connecting points at $X_{Ta} = 0.0$ (pure S) and $X_{Ta} = 1.0$ (pure Ta) would signify the atomization enthalpy of x mole of Ta(s) and y mole of S(s) such that $x + y = 1.0$. Thus, the length of the vertical segment from a known compound's point on the curve to the straight line represents $\Delta H^{\circ}_{f,298}/R$ on a mole-of-atoms basis. Ta_2S and Ta_6S can be readily seen to be less stable relative to the solid elements than are the less metal-rich sulfides. This illustrates that $\Delta H^{\circ}_{f,298}$ of a compound is a property of both the compound and the standard state elements; Ta_6S and Ta_2S are more difficult to vaporize than the other Ta-S phases (also apparent from the curve) but are composed mostly of Ta which is nearly as refractory.

The other facts denoted by this graph are the metastability of Ta_2S and Ta_6S. Each falls below the concave-downward curve through the phases and each is thereby expected to disproportionate; Ta_2S into $Ta_{1.35}S_2$ + Ta and Ta_6S into Ta_2S + Ta (and therefore into $Ta_{1.35}S_2$ + Ta). Supplementary experiments by B. Harbrecht using I_2 as a transport agent succeeded in converting Ta_6S into $Ta_{1.35}S_2$ and Ta at 1220 K after 2 days, but Ta_2S could not be converted at 1270 K after 3 days. One can attempt to calculate the transition temperature for the disproportionation as follows. Using $\Delta G_T = 0 = \Delta H_T - T\Delta S_T$ as the criterion for the transformation via $2Ta_6S(s) \rightarrow Ta_{1.35}S_2(s) + 10.65\ Ta(s)$ and approximating ΔS_T by $-12\cdot[fef(Ta)-fef(Ta\ in\ Ta_6S)] - 2[fef(S)-fef(S\ in\ Ta_6S)]$ or 13.6 cal/K and ΔH_T by $\Delta H^{\circ}_{f,298}(Ta_{1.35}S_2) - 2\Delta H^{\circ}_{f,298}(Ta_6S)$ or - 3.0 kcal yields a negative value for T_t, i.e., the disproportionation is energetically feasible at all temperatures. However, the large uncertainty (~8 kcal) in the estimated $\Delta H^{\circ}_{f,298}(Ta_{1.35}S_2)$ makes the test inconclusive. It could either be the case that ΔG for the reaction is <0 for all temperatures and the metastability of Ta_6S (and similarly of Ta_2S) at room temperature is due to lack of an easy reaction path, or that ΔH is in fact >0 and Ta_6S exists at equilibrium only below $T_t \leq 1220$ K, above which $T\Delta S$ outweighs ΔH and the disproportionation occurs. Only with more precisely determined values for $\Delta H_f(Ta_{1.35}S_2)$ and for ΔC_p° for the reaction in question can more quantitative conclusions be made. It must suffice at present to say that Ta_6S and Ta_2S both appear to be nearly unstable with respect to disproportionation at room temperature. If the disproportionation has occurred near the

experimental temperature range and the equilibrium being measured differs from that assumed, the enthalpy derived will still be nearly indistinguishable from that of the assumed reaction, since at nearby T_t all three solid phases will coexist at one point.

In addition to the low-temperature heat capacity measurements already suggested, a worthwhile future study would be determination of $\Delta H^\circ_{f,298}$ for $Ta_{1.35}S_2$ to further the knowledge of relative stabilities in this system. There was also the indication of a structural modification of Ta_6S slightly different from that originally reported; elucidation of that structure could also prove interesting.

IV. TANTALUM-ALUMINUM SYSTEM

A. Introduction

Intermetallic compounds have a shorter and more rapidly developed history than do more familiar metal-nonmetal compounds. It was not recognized that true intermetallic compounds, with properties (e.g., hardness and melting point) significantly different from those of the component elements, occurred at certain stoichiometries until the early 19th century, with β-brass (CuZn) being the protype discovery.[22] The availability of X-ray powder diffraction methods for phase identification, which remains to this day the most frequently used technique, was the real catalyst for the accelerated rate of discovery after 1921. The measurement of thermodynamic properties of intermetallics has a correspondingly brief legacy, but examples have not proliferated at anything like the rate of discovery of the compounds themselves. Since the first thermochemical measurements on the CuZn system in 1901,[23] so few attempts to systematize existing data have been made that it is still a fair assessment to say that there is no well-established model of bonding and resultant stability of intermetallics. Broad and mostly qualitative arguments relating trends in enthalpies of formation to differences in size, valence or electronegativity of the components are the common features of most attempts to model the existing phenomena.

It is clear that in most known cases the $\Delta H^{\circ}_{f,298}$ per mole of atoms are not large (-8 kcal to -3 kcal), and combined with usually small entropy differences between elements and compounds this suggests that

intermetallics are often not markedly stable relative to pure metals. Exceptions to this, referred to as "superalloys" are rationalized by Brewer and Wengert[24] in terms of availability of empty d orbitals for bonding likened to Lewis acid-base behavior, which may contribute to $\Delta H^{\circ}_{f,298}$ as large as -80 kcal/mole.

In general, models like that of Kubaschewski[25] deal with binary compounds in which the components may belong to any metallic group. The newer model due to Miedema et al.[26] whose predictions (as will be seen later) still often miss the mark, at least improves on earlier attempts in considering separately instances of transition metal-main group intermetallics. (Data on such compounds were employed in empirically deriving Miedema's model.)

In providing a conceptual and historical background for the Ta-Al system which is the subject of this study, it is most relevant to consider t-Al systems (t being a transition metal). Restricting the scope to the most similar cases, the following background exists: vapor pressure measurements have been employed in arriving at $\Delta H^{\circ}_{f,298}$ in the systems Mo-Al,[5] Nb-Al[6] and Zr-Al[7] through methods very similar to those in this study. With direct reaction calorimetric methods, enthalpies of formation for compounds in the systems Ti-Al,[27], V-Al[28] and Cr-Al[29] have also been determined. In each of these six systems the values for $\Delta H^{\circ}_{f,298}$ per mole of atoms fall in the range -3 kcal to -11 kcal, indicating that previously studied aluminides are typical intermetallics (as referred to above) with respect to stability.

B. Historical Background

Tantalum-aluminum alloys have their most important occurrence and application in the microelectronics industry, where their reliability as thin film resistors and the ease of producing them via cosputtering techniques has made them quite popular[30]. Some physical measurements on Ta-Al compounds have focussed on thin film properties relevant to this sort of use, e.g., resistivity and Hall effect. However, the only bulk phase also occurring as a thin film is $TaAl_3$.

Measurements of bulk phase properties have included those of density,[31] hardness,[32] Young's modulus,[33] and electrical and thermal conductivity among others. The current study is unprecedented; it is the first attempt to determine thermal stabilities of Ta-Al compounds.

The remaining (and most significant) reports of previous work on the Ta-Al system have been attempts to identify and classify the intermediate compounds. These results have been a basis for phase identification in this work. With varying degrees of completeness the following phases had been observed and characterized prior to this study: $TaAl_3$, Ta_2Al_3, $Ta_{17}Al_{12}$, and a "σ" phase of compositional range Ta_2Al to Ta_4Al.

The historical progress leading to this accumulated knowledge can be summarized as follows: $TaAl_3$, the existence of which had been predicted in 1868 by Marignac[34] was identified by Brauer[35] in 1939 and was said to be isotypic with $TiAl_3$ (space group I_4/mmm) (see Figure 9). In 1960, Edshammar and Holmberg[36] prepared the σ-phase (sg $P4_2/mnm$) at approximate composition Ta_2Al (near the Al-rich extreme) and noticed the similarity

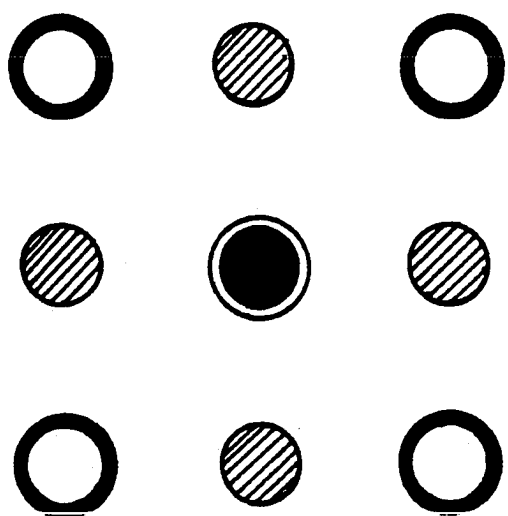

Figure 9. The structure of $TaAl_3$ in projection along the c axis. Large circles are Ta atoms; smaller are Al; solid: z = 0; empty: z = $^1/_2$; shaded: z = $^1/_4$,$^3/_4$

of its X-ray powder diffraction pattern to that of σ-NiV, thereby assigning the atomic positions depicted in Figure 10. Variable stoichiometry is achieved by (disordered) mixed occupancy of the positions labeled A and D. They also mention the analogous σ-Nb_2Al compound observed by McKinsey and Faulring one year earlier.[37] Nearly simultaneous findings by Nowotny et al.[38] added to knowledge of this region of the phase diagram in claiming that the Al-rich and Ta-rich boundaries of the σ-phase were ~$Ta_{1.8}Al$ and ~Ta_4Al, respectively and suggesting that a compound of approximate stoichiometry $TaAl_2$ coexisted with the former. In still another contemporary study, Wilhelm and Witte[39] state (without including numerical evidence) that $TaAl_3$ as well as "Ta_2Al" (σ-phase) has a compositional range. They also examined melting behavior and observed that $TaAl_3$ and "Ta_2Al" both melt peritectically, beginning at temperatures of 1500 ± 50°C and 2100 ± 50°C, respectively. Other solid-liquid phase diagram features include the peritectic melting of the solid solution of Ta in Al (up to 0.037 at % Ta) observed by Glazov et al.[40], an eutectic of $TaAl_3$-Al (95.7 at % Al) melting at 615°C according to Spengler[41], and another eutectic claimed by Wilhelm and Cowgill[42] to occur near 90 at % Ta in the σ + Ta(ss) region.

Gupta[43] also observed the σ-phase and reported an unknown phase at near 40 at % Al. Schubert[44] and Raman[45] both identified this unknown phase as $Ta_{17}Al_{12}$, with a disordered bcc structure of α-Mn type, a_o = 9.88 Å, in analogy to $Nb_{17}Al_{12}$. Both also stated that $Ta_{17}Al_{12}$ is a high-temperature phase, Raman claiming that the minimum temperature at

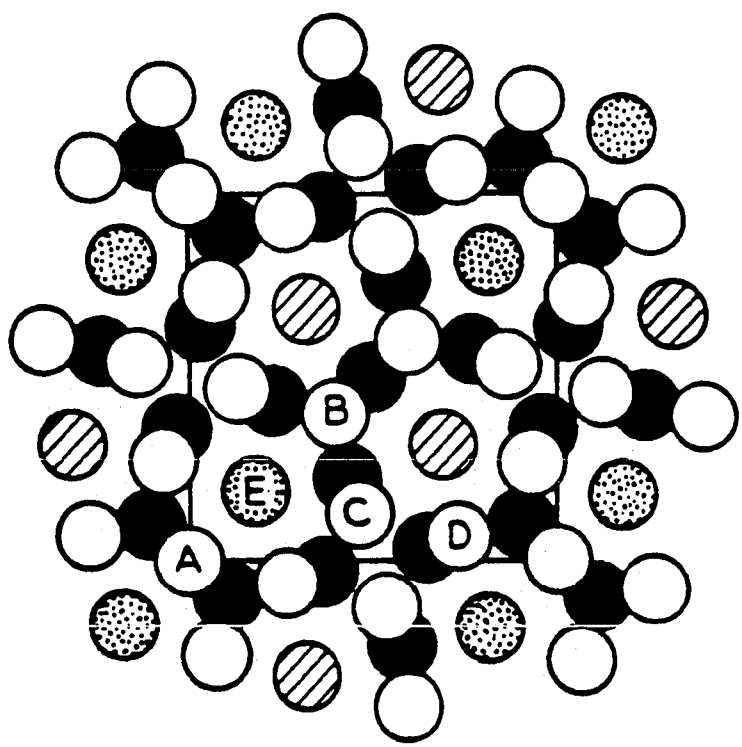

Figure 10 Projection along c-axis of "Ta_2Al" (sigma phase) structure. Approximate z coordinates: empty circles, 0; filled circles, 1/2; others, 1/4 and 3/4. Ta atoms reside in position types B, C, and E; Al atoms in A and D

which it is stable is ~1300°C. Raman's other significant contribution was to claim that the compound $Ta_{12}Al_{17}$ existed and was indexable as fcc, a_0 = 19.315. This was likely the phase "$TaAl_2$" seen earlier by Magneli et al.[46] and Nowotny et al.[38] A more internally-consistent indexing was later provided by Girgis and Harnik[47] with a hexagonal cell of a_0 = 12.776(5) Å and c_0 = 27.04(4) Å and they labeled the compound Ta_2Al_3. The structure of Ta_2Al_3 is undetermined to date. A summary of updated phase information will follow the sections on synthesis and phase relationships at which time a comparison with findings from the current study will be made.

No quantitative phase diagram exists; there is only the fragmentary information on the Al(ss) region, the claim by Nowotny that Ta dissolves "very little" Al (according to lattice parameters), and the above-mentioned melting point behavior, most of which is not useful in the present study due to the composition and temperature ranges involved.

C. Experimental Methods

1. Synthesis

A series of single- and two-phase Ta-Al materials of varying overall composition was made, both for the purpose of verification of the previously reported phase relationships and for use in the vaporization experiments. The essence of the synthetic technique was a two step process. First, powdered Ta (60 mesh, Alfa Ventron) and granular Al (Alfa Ventron, 99.98% m or Baker, no quoted purity) were pressed into small pellets using 12000 lb/sq. in. hydraulic pressure on a 1/2 in. diam.

stainless steel die. These pellets, which were far from homogeneous at this stage because of the difficulty of mixing particles of such different sizes, were then arc melted under a continuously flowing dry Ar atmosphere for three minutes or longer, pausing periodically to invert the pellet to encourage further mixing. Much of the aluminum originally present was often lost in this step because of the much higher vapor pressure of Al relative to Ta. By trial and error the minimum excess of Al required for arriving at a desired composition was found to be rather larger for the $TaAl_3/Ta_2Al_3$ range than for Ta_2Al_3/σ or σ/Ta. Neither phase identification nor quantitative analysis was attempted at this intermediate point after early efforts showed the mixtures to be inhomogeneous.

In the subsequent step, annealing of the alloys in tungsten containers by inductive heating resulted in further (but much slower) vaporization of Al but also in homogenizing of the samples, often first indicated by the relative ease with which they could be pulverized after cooling to room temperature. Preliminary Knudsen effusion experiments provided information useful in choosing optimum annealing temperatures for this step: ca. 950 ± 50°C for mixtures more Al-rich than "Ta_2Al" and $\gtrsim$1100°C for more Ta-rich mixtures.

2. Phase relationships

Phase identification was accomplished by X-ray powder diffraction using Cu-Kα radiation (λ = 1.5406 A) and a Guinier camera. With the exception of the high-temperature compound $Ta_{17}Al_{12}$, all previously

reported phases were observed, with no significant deviation from the unit cell dimensions ("lattice parameters") expected. No evidence of significant nonstoichiometry of $TaAl_3$ (as had been suggested by Wilhelm and Witte) was obtained. Two phase mixtures of Ta_2Al_3 with $TaAl_3$ or with the σ-phase indicated very similar lattice parameters and thus very small phase width for Ta_2Al_3. Lattice parameter determinations both within and to either side of the σ-phase showed reasonable agreement with the range previously reported. Only in the subsequent Knudsen effusion experiments were any efforts made to establish phase boundaries, which efforts were less than conclusive for reasons to be described later. Interruptions of vaporization experiments on three different samples at various overall compositions provided additional qualitative (identification of phases present) and quantitative (lattice parameters) data. A summary of all lattice parameter data obtained is presented in Table 6 with comparisons to literature values.

In several Guinier X-ray films, there were unidentifiable lines attributed to contaminants. The Ta reagent powder itself gave several such lines of diffuse quality but quite strong intensity. These lines were not present in Ta powder which had been heated in a vacuum at 1300°C for several hours, indicating relatively high volatility of the contaminant, nor did they ever appear along with lines due to Ta-Al phases in either synthesized samples or residue from interrupted vaporization experiments. Other extraneous phases, believed to be due to oxidation or contact with container surfaces during preparation, were indicated by

Table 6. Lattice parameters of phases in the Ta-Al system

Phase	Crystal system	Lattice parameters (A)	
Ta	cubic	a = 3.303	
		3.3104(8)	
		3.3106(8)	
		3.3006(4)	
		3.304(2)	
Ta_4Al ("σ" phase)	tetragonal	a = 9.98	c = 5.16
		9.875(1)	5.210(1)
		9.901(1)	5.2019(8)
Ta_2Al ("σ" phase)		a = 9.825	c = 5.232
		9.828	5.232
		9.823(4)	5.234(3)
		9.824(2)	5.233(2)
Ta_2Al_3	hexagonal	a = 12.776(5)	c = 27.04(4)
		12.76(1)	27.14(8)
		12.81(1)	27.04(3)
$TaAl_3$	tetragonal	a = 3.842	c = 8.553
		3.840	8.537
		3.839	8.535
		3.844(1)	8.552(1)
		3.8429(3)	8.546(1)

Comments
Ref. 15
starting material.
heated in vacuo,
1300°C, 3 hr.
residue, run 7;
with σ phase.
residue, run 8;
with σ phase.
Ref. 38
residue, run 7;
with Ta.
residue, run 8;
with Ta.
Ref. 38
Ref. 36
interrupt run 3;
with Ta_2Al_3.
sample 11a; before
run 8.
Ref. 47
interrupt run 3;
with Ta_2Al
sample 2av; with
$TaAl_3$.
Ref. 35
Ref. 38
Ref. 45
sample 2av; with
Ta_2Al_3.
with Al

lines that were quite weak in intensity and few in number. None of the samples actually used in Knudsen experiments had indications of any unknown phases in the form of X-ray diffraction lines, but because of the recognized limited sensitivity of X-ray diffraction in qualitative analysis, further analyses were performed on both starting materials and synthesized compounds using other methods. Tests for metallic impurities were performed by Clarence Ness and Robert Conzemius of the Ames Laboratory using spark source mass spectrometry. Carbon was analyzed by a combustion/chromatographic method by Robert Bachman of Ames Laboratory Analytical Services, and dissolved H, O, and N were detected with vacuum fusion analysis by Nile Beymer. Results are summarized in Table 7. The most significant metallic impurity was potassium in the Ta reagent powder, indicated to be roughly 3-4 at %. This was presumed due to the method of industrial preparation of the powder from bulk tantalum, about which no claims of purity were made by the manufacturer, Alfa Ventron Corp. The greatly reduced value of K concentration in an arc-melted sample analyzed in the same manner and the aforementioned disappearance of contaminant lines after heating of the Ta powder or synthesis of compounds suggest that the contaminant was an easily removed potassium-containing species, although comparison with available powder data on likely phases did not identify it as such.

Further examination of Table 7 reveals that the contamination by dissolved gases varied during each stage of the thermal history of a sample.

Table 7. Impurities of phases in Ta-Al system in atomic ppm; dashes entered indicate analysis not performed

Sample, history	Greatest metallic impurities				Greatest nonmetal impurities				
	K	B	Na	Si	H	C	N	O	F
Ta, starting material	40,000	200	200	100	1000	64	57	2400	800
	Fe	Si	Ga	Ca					
Al, starting material	700	60	43	36	520	1277	120	5900	10
	Fe	Si							
Alloy sample, arc-melted	180	50			17	500	860	1600	<20
Sample 2av, before run #6					25	-	30	800	-
Sample 2av, after run #6					0	-	32	400	-

Sample 2av, which is representative of all samples actually employed in ML-MS runs, contained a tolerable amount of dissolved oxygen which decreased further during run #6. This corresponds to the observation that the Al_2O (M = 70) MS signal always decreased with time, from ~1/200 to ~1/5000 the size of I_{27}^+. The degree of oxygen contamination still present after arc-melting suggests that the subsequent inductive annealing under vacuum is necessary not only for homogenization of the samples but purification as well. It is both surprising and reassuring that no detectable Cu was present in the arc-melted sample despite melting it on a copper surface.

3. Mass spectrometry and mass loss

The general methods have already been described. (Please refer to section IIA and Figures 1 and 2.) As in the Ta-S system, incongruent vaporization occurs, in this instance to Al(g) which was the only significant entity detected in the vapor. Mass spectrometry proved useful in measuring vapor pressures; reproducible ion current readings I_i^+ could be obtained at 27 amu at temperatures as low as ~1000°C through the use of signal averaging techniques. The standard technique was to perform 5 sweeps, each of 10 seconds duration, across a 0.5 amu range centered on the peak of interest. This 0.5 amu range was divided into 10 channels, at each of which ~1064 observations of I_i^+ were made during each sweep. The accumulated I_i^+ after all sweeps were completed were averaged on a per-channel basis and the entire procedure was done both with the shutter open and then closed. The I_{27}^+ value used in further

calculations was the difference in the two peak centers thus obtained; this value was always observed to be a nearly constant fraction of the open-closed difference in peak area owing to the constancy of the Al peak shape: a broad, nearly featureless shoulder on the much larger signal at ~28 amu due to CO and N_2. The standard deviation in I_{27}^+, calculated as the average scatter in the readings at a given channel, was approximately 3×10^{-12} giving a signal-to-noise ratio of ~3:1 in the case of the weakest signals used. Kematick[48] has stated that the signal-averaging method may lower the minimum temperature at which meaningful I_{27}^+ measurements are obtainable by ~100°C. That this is desirable was learned in repeated Ta-Al experimental sequences which suggested reduced kinetic hindrance to equilibrium at a range of ~1050°C to 1250°C for $X_{Al} \geq 0.33$ ("Ta_2Al") and approximately 100°C higher for $X_{Al} \lesssim 0.20$ ("Ta_4Al"). The optimum temperature range is apparently the lowest at which reproducible P_{Al} measurements are obtainable.

Calibration of the mass spectrometer with reference to the P_{Al} determined by mass loss was based on measurements at as many as 20 temperature-points in two-phase regions during a given experimental run. The constant $K = P/I_{27}^+ \cdot T$ ranged from 1.35(8) to 2.2(2) in these determinations. A least-squares fit for one such calibration is depicted in Figure 11.

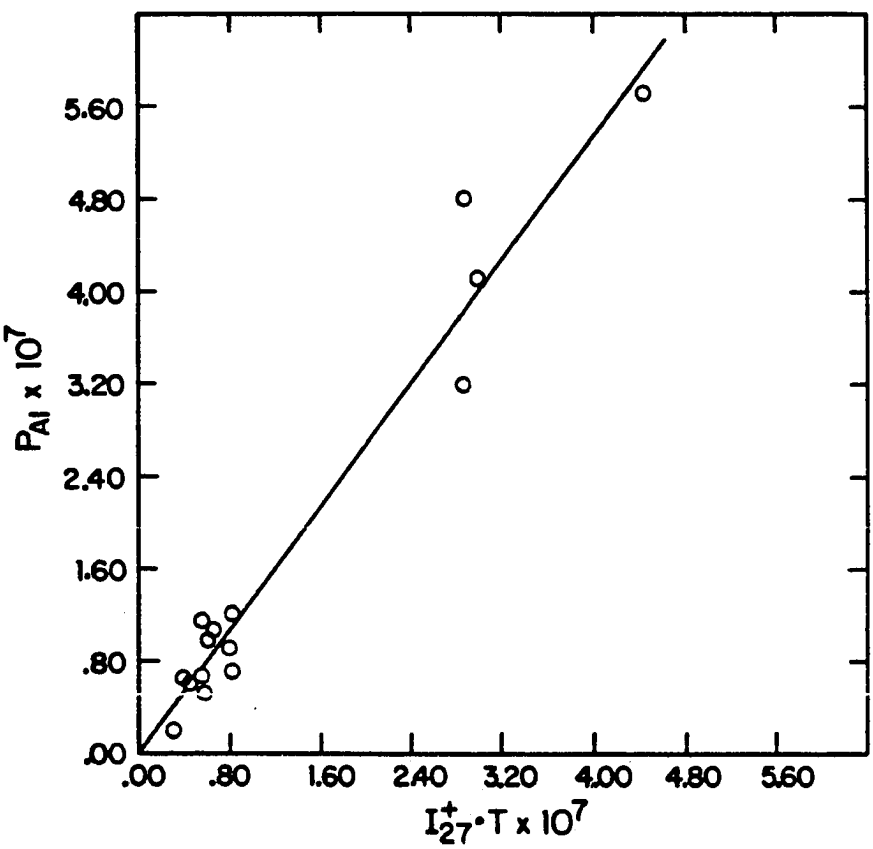

Figure 11. Least-squares fit to P_{Al} (in atm) vs MS current-T product (in Amp•K)

The previously described surface depletion syndrome plagued the first few experimental runs quite severely; of the 10 samples vaporized in all, only 3 of the last 4 provided data which were ultimately used. The criteria for accepting P_{Al} (T) measured in a given two-phase region included more than just internal consistency because it was noted that higher pressures could be achieved by longer annealings and by performing measurements in optimum temperature ranges, the latter determined mainly by trial-and-error. As a result, repetition of pressure measurements in the same compositional range with identical samples in the same crucible sometimes differed by as much as a factor of 4. Fortunately, there is a basis for making the correct choice among discrepant P_{Al} determinations, in that the highest value obtained at a given (T,X) point supersedes all lower values. There is effectively a lower boundary to the equilibrium pressure (for incongruently vaporizing systems) based on the understanding that the only likely source of systematic error will be manifested as an erroneously low pressure. One conceivable exception to this is a leakage of effusing vapor at the crucible/lid contact surface, which would result in a faulty calibration due to mass/loss not "seen" by the mass spectrometer. This was ruled out by a check of each crucible for leakage by vaporizing Pb from the cell while surrounded by an evacuated glass enclosure. Effusing Pb which recondensed on the glass surfaces gave no indication of significant effusion from other than the orifice. Data presented and evaluated hereafter represent the highest pressures measured over each T-X range studied.

Table 8 summarizes the experiments producing useful P_{Al} vs T data, and/or phase identification. The previously described method of verifying which equilibria were being measured by interrupting an experiment for sampling and Guinier powder diffraction showed that the expected solid compounds were present in all cases. Based on earlier reports of solid regions of the phase diagram and continuous monitoring of the overall sample composition using the mass balance, these interruptions were performed after anticipated solid-solid phase boundaries were crossed. More accurate determination of these boundaries by MS observations of isothermal pressure changes was attempted but not accomplished, due to the inability to distinguish diffusion-related effects from equilibrium effects.

In run 6, during which the equilibria involving first $TaAl_3$ with Ta_2Al_3 and then Ta_2Al_3 with "Ta_2Al" (the Al-rich extreme of the σ-phase region) were measured, there was no observable variation in P_{Al} as $X_{Al} = 0.60$ (corresponding to Ta_2Al_3) was crossed. As will be demonstrated in the upcoming data analysis and results section, this has implications about the relative stability of Ta_2Al_3 and neighboring phases. It also means that the assumption that Ta_2Al_3 is effectively a 'line compound' at $X_{Al} = 0.60$, which is indicated by determinations of unit cell size, must be employed in the absence of additional evidence of phase boundary locations. Similarly, it was not possible to pinpoint the boundaries of the single-phase region ("σ") occurring from approximately $X_{Al} = 0.33$ to $X_{Al} = 0.25$, in this case because the variation in P_{Al} across this relatively wide phase is small and quite

Table 8. Summary of selected mass-loss mass spectrometry runs
$A = 6.0 \times 10^{-7}$ m^2

Run No.	Sample No.	Initial, Final X_{Al}(at.)		Comments
3	2av	0.696	0.593	Identified Ta_2Al_3/Ta_2Al mixture in residue
6	2av	0.696	0.574	Data on $TaAl_3/Ta_2Al_3$ and Ta_2Al_3/Ta_2Al regions
7	4aiv	0.226	0.097	Data on Ta_4Al/Ta region, superseded by run 8. Lattice parameters of Ta_4Al from residue
8	11aii	0.406	0.158	Data on Ta_2Al_3/Ta_2Al, σ, and Ta_4Al/Ta. Ta(ss) region not reached due to kinetic hindrance.

gradual. Again, the assumption of phase boundaries consistent with previous reports as corroborated by near agreement of lattice parameters was made, i.e., Ta_2Al and Ta_4Al are the assumed boundaries. The final boundary of interest was the Al-rich limit of the Ta solid solution, expected to be very near $X_{Al} = 0.0$ due to previous claims[36] of negligible solubility of Al in Ta and the similarity of the unit cell dimension (cf. 3.303 Å to 3.304(2) Å) of Ta determined from pure Ta and from Ta(ss) in equilibrium with Ta_4Al, respectively. Kinetic hindrance and the resultant drop in P_{Al} occurred well before the Ta(ss) region was reached and made this boundary indeterminable also. The assumption of this boundary location and its effects on subsequent calculations were assessed as reasonable and not contributing to serious uncertainty (see Data Analysis and Results).

Isothermal trends in P_{Al} at T = 1548 K and 1625 K spanning the (overall) compositional ranges accessible to equilibrium measurements are shown in Figure 12. Measurements of P_{Al} using two orifice areas differing by a factor of 2.1 showed no significant systematic difference and thus orifice dependence was not further examined. The total temperature ranges were 1386 K - 1713 K for $TaAl_3/Ta_2Al_3$ and Ta_2Al_3/Ta_2Al measurements, 1321 K - 1628 K for the σ region, and 1321 K - 1626 K for the Ta_4Al/Ta region.

In all regions the I_{27}^+ measurements by mass spectrometry were programmed to occur at equally spaced temperature intervals in a cyclic fashion, first moving from minimum to maximum and then in the opposite direction. In the two phase regions, the temperature interval between

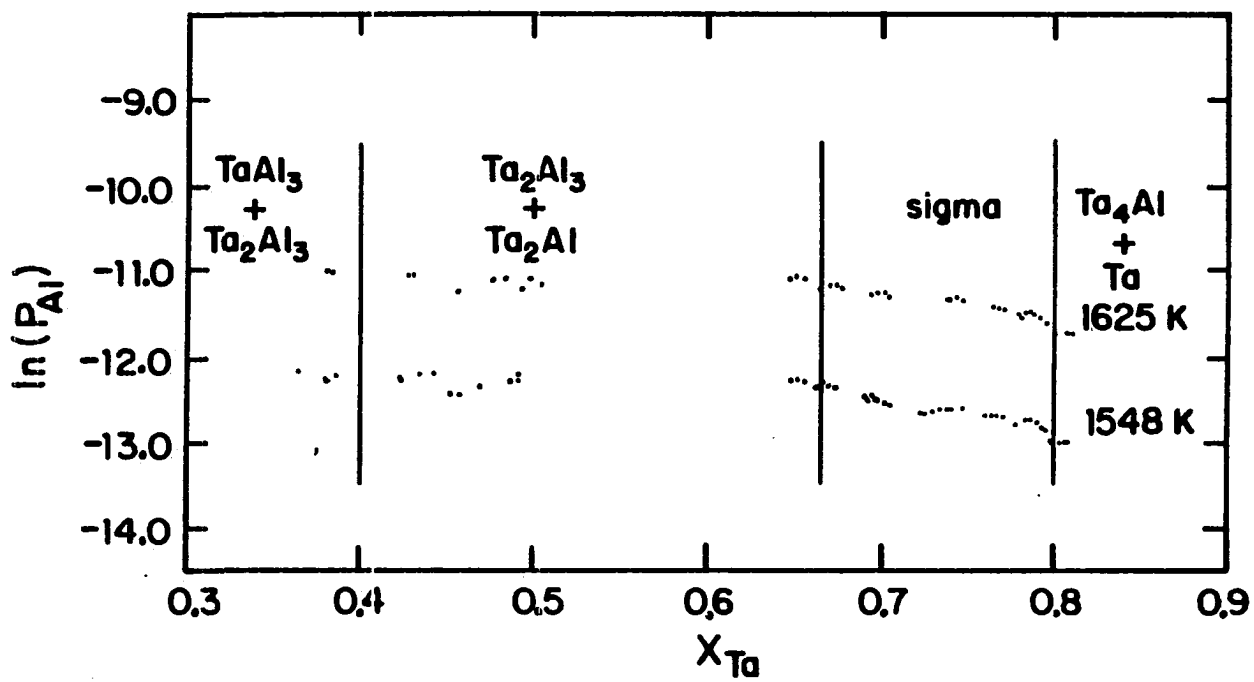

Figure 12. Variation in isothermal P_{Al} (at 1548 K and 1625 K) with overall composition in the Ta-Al system

successive measurements was no smaller than 10 K, while in the σ single phase region the measurements were aimed only at providing a small number of isotherms and were separated by ~80 K. It was frequently observed that I_{27}^{+} measurements made during the increasing half of the temperature cycle were 5 to 10% smaller than those at the same temperatures during the decreasing half-cycle. A dwell time of 3 minutes was employed at each new temperature before a MS measurement was made, in an effort to minimize the temperature direction dependence and allow sufficient equilibration at each point. Raw data from the successful Ta-Al experiments are presented in Tables A3 to A6.

D. Data Analysis and Results

P_{Al} vs T data obtained in two-solid-phase regions during runs 6 and 8 correspond to equilibria expressed in the following chemical reactions:

$$\frac{2}{3}TaAl_3(s) \rightleftarrows \frac{1}{3}Ta_2Al_3(s) + Al(g) \qquad (25)$$

$$\frac{1}{2}Ta_2Al_3(s) \rightleftarrows \frac{1}{2}Ta_2Al(s) + Al(g) \qquad (26)$$

$$Ta_4Al(s) \rightleftarrows 4Ta(s) + Al(g) \qquad (27)$$

Using $\Delta fef = fef(Al(g)) - fef(Al(s))$ from reference 1 the 2nd and 3rd law methods are applied to the above-mentioned data to calculate $\Delta H^{\circ}_{rxn,298}$ for reactions 25 to 27. Figures 13 to 15 show the 2nd law

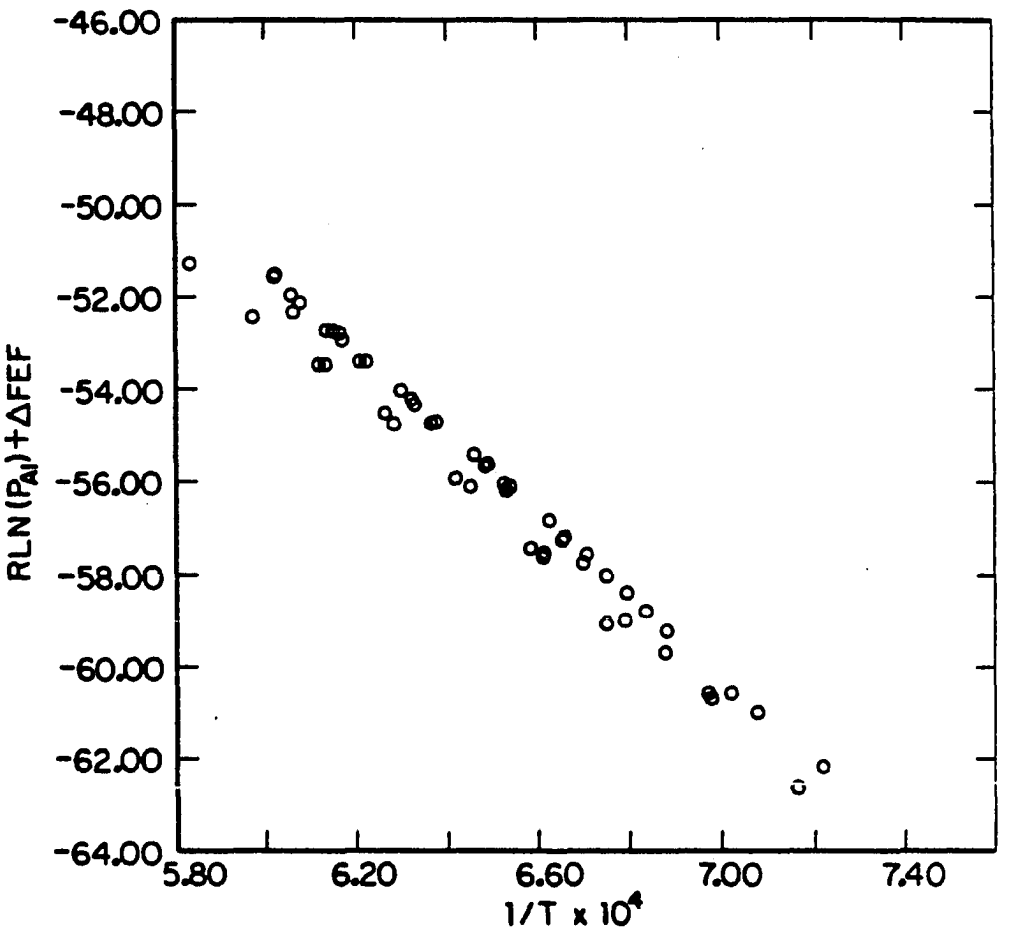

Figure 13. 2nd law (298 K) plot for the reaction

$$\frac{2}{3}\,TaAl_3(s) \rightleftharpoons \frac{1}{3}\,Ta_2Al_3(s) + Al(g)$$

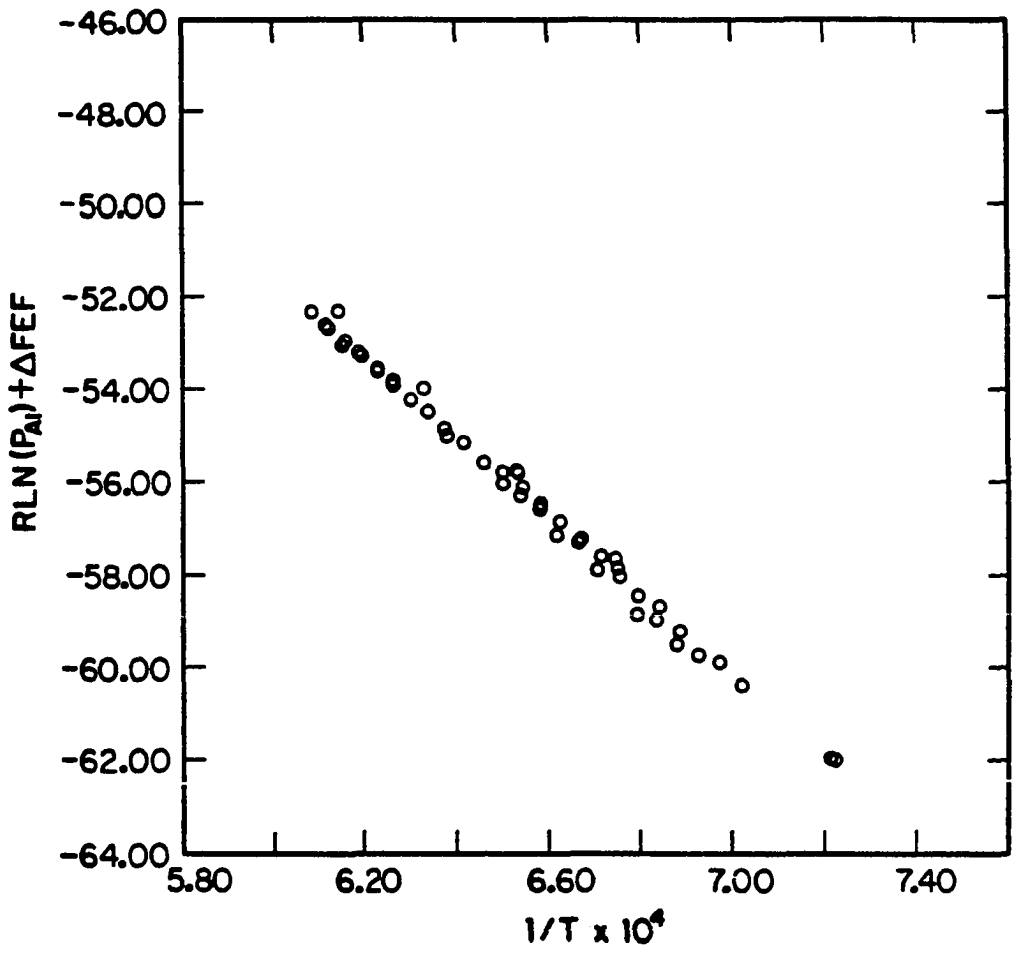

Figure 14. 2nd law (298 K) plot for the reaction
$\frac{1}{2}\,Ta_2Al_3(s) \rightleftharpoons \frac{1}{2}\,Ta_2Al(s) + Al(g)$

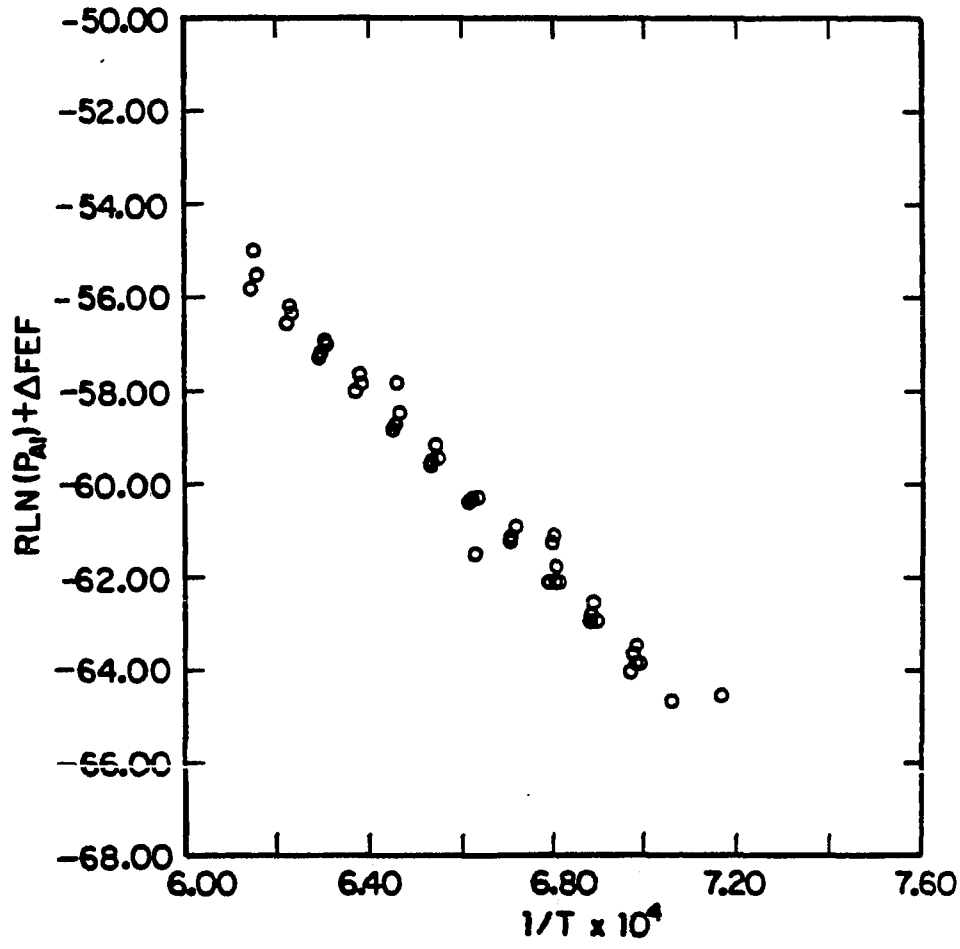

Figure 15. 2nd law (298 K) plot for the reaction $Ta_4Al(s) \rightleftarrows 4Ta(s) + Al(g)$

(298) fits corresponding to these reactions. Only in the case of reaction (27) is it possible to immediately proceed with determination of $\Delta H^{\circ}_{f,298}$ for any Ta-Al intermetallic compound. The $\Delta H^{\circ}_{f,298}$ of Ta_2Al, required for calculation of $\Delta H^{\circ}_{f,298}$ of more Al-rich phases, corresponds to a chosen composition at one limit of a broad single phase (σ), and was determined using a different method.

By applying the Gibbs-Duhem equation it is possible to find the variation in the chemical potential (and therefore, partial pressure) of one component of a binary system if the composition dependence of μ of the other component is known at some fixed temperature. In this system P_{Ta} is immeasurably small ($\sim 10^{-19}$ atm or lower) but is determined by knowledge of P_{Ta} at some overall composition X_1 through:

$$\Delta \ln P_{Ta} = \int_{X_1}^{X_2} \frac{X_{Al}}{X_{Ta}} \, d \ln P_{Al} \, . \qquad (28)$$

The composition X_1 is taken as $X_{Al} = 0.20$ (Ta_4Al), the Ta-rich boundary of the σ phase, at which P_{Ta} is equal to its value at the Al-rich boundary of the Ta solid solution. Assuming $X_{Ta} = 0.99$ at the SS boundary and Raoult's law behavior for P_{Ta} (linear dependence on X_{Ta}, which is bolstered by observation of Raoult's law behavior in the Nb-Al and Mo-Al systems) P_{Ta} at X_1 or $X_{Al} = 0.20$ becomes $0.99 \cdot P^{\circ}_{Ta}$ or 1.73×10^{-18} atm at 1625 K: $P_{Ta} = 9.75 \times 10^{-20}$ atm at 1548 K. Plots of X_{Al}/X_{Ta} vs $\ln P_{Al}$ as measured in run #8 were graphically integrated between the limits $X_{Al} = 0.20$ and $X_{Al} = 0.33$ to yield:

$$T = 1625\ K: \quad P_{Ta} = 1.52 \times 10^{-18}\ atm$$

$$T = 1548\ K: \quad P_{Ta} = 8.24 \times 10^{-20}$$

The ΔH°_{298} for the atomization reaction

$$Ta_2Al(s) \rightleftarrows 2Ta(g) + Al(g) \tag{29}$$

for which

$$\Delta G^\circ_T = -RT \ln (P^2_{Ta} \cdot P_{Al}) \tag{30}$$

was then found by combining P_{Al} as measured with P_{Ta} determined as just described, again using Δfef prescribed as usual according to the Neumann-Kopp assumption. $\Delta H^\circ_{f,298}$ of Ta_2Al is then found from

$$\Delta H^\circ_{f,298}(Ta_2Al) = -\Delta H^\circ_{rxn\ 29,298} + 2 \cdot \Delta H^\circ_{at,298}(Ta) + \Delta H^\circ_{at,298}(Al). \tag{31}$$

The uncertainty in $\Delta H^\circ_{f,298}$ for Ta_2Al contributes to the uncertainty in $\Delta H^\circ_{f,298}$ for all other phases except Ta_4Al; the means of estimating this error should be briefly described. The determination of $\Delta H^\circ_{f,298}(Ta_2Al)$ is subject to errors in Δfef, T, P_{Ta}, and P_{Al}. The estimation of ±1 eu in Δfef, ±15 K in T, and relative errors of ±0.15 in P_{Al} and P_{Ta} yielded an error estimate of ±2.2 kcal in $\Delta H^\circ_{f,298}(Ta_2Al)$ in a standard propagation-of-errors treatment. Therefore, all phases more Al-rich than Ta_2Al should be considered to have $\Delta H^\circ_{f,298}/(x+y)$ determined to an accuracy of no better than ±0.7 kcal.

Determination of $\Delta H^{\circ}_{f,298}$ for $TaAl_3$ and Ta_2Al_3 involves combination of $\Delta H^{\circ}_{f,298}$ from the neighboring phase with $\Delta H^{\circ}_{rxn,298}$ for vaporization of the phase in question, as in, e.g.,:

$$\Delta H^{\circ}_{f,298}\ (Ta_2Al_3) = 2\cdot\left(\frac{1}{2}\Delta H^{\circ}_{f,298}(Ta_2Al) + \Delta H^{\circ}_{at,298}(Al) - \Delta H^{\circ}_{rxn\ 26,298}\right) \quad (32)$$

Tables 9 and 10 list the reaction enthalpies and enthalpies of formation, respectively, calculated as explained above. The values of $\Delta H^{\circ}_{rxn,298}$ and $\Delta H^{\circ}_{f,298}$ for "Ta_3Al" were found by Gibbs-Duhem integration as for Ta_2Al (with different limits of integration); the uncertainty in $\Delta H^{\circ}_{f,298}(Ta_3Al)$ and $\Delta H^{\circ}_{f,298}(Ta_4Al)$ were estimated in the same manner as that of $\Delta H^{\circ}_{f,298}(Ta_2Al)$.

E. Discussion

Figure 16 depicts the variation with composition of the normalized values for $\Delta H^{\circ}_{f,298}$ in the Ta-Al system and visually compares them with values for compounds in the similar systems V-Al, Mo-Al, and Nb-Al. The similarity in both the trends and average magnitude from one system to another is evident. In this context, the otherwise surprisingly small $\Delta H^{\circ}_{f,298}$ of Ta-Al phases may be viewed as quite reasonable. Further discussion of these quantities and the underlying reasons for their magnitudes will follow in section V.

It can also be observed that Ta_2Al_3 appears to be nearly unstable with respect to disproportionation into $TaAl_3$ and Ta_2Al. This is

Table 9. Enthalpies of vaporization reactions at 298 K, Ta-Al system; $\Delta H^{\circ}_{298}/R$ in 10^3 K

Reaction	2nd Law	3rd Law
$\frac{2}{3}TaAl_3(s) \rightleftarrows \frac{1}{3}Ta_2Al_3(s) + Al(g)$	44.5(7)	43.4(4)
$\frac{1}{2}Ta_2Al_3(s) \rightleftarrows \frac{1}{2}Ta_2Al(s) + Al(g)$	43.9(4)	43.2(3)
$Ta_2Al(s) \rightleftarrows 2Ta(g) + Al(g)$	-	232(2)
$Ta_3Al(s) \rightleftarrows 3Ta(g) + Al(g)$	-	326(2)
$Ta_4Al(s) \rightleftarrows 4Ta(s) + Al(g)$	46.4(1)	44.8(4)

Table 10. Enthalpies of formation[a] and atomization of Ta_xAl_y and related phases; $\Delta H^\circ_{298}/(x+y)/R$ in 10^3 K

Phase	Formation	Atomization	Atomization, related phases	
$TaAl_3$	-2.86	56.1	VAl_3	48.5
			$NbAl_3$	55.3
			Mo_3Al_8	55.1
Ta_2Al_3	-2.27	63.6	V_5Al_8	60.1
Ta_2Al	-1.37	77.2	Nb_2Al	74.0
Ta_3Al	-1.12	81.5	Nb_3Al	77.3
			Mo_3Al	72.6
Ta_4Al	-1.05	84.2		
Ta	0	92.5	V	61.9
			Nb	87.1
			Mo	79.2

[a]Uncertainty in $\Delta H^\circ_{f,298}(x+y)/R$ estimated (see p.67) to be $\pm 0.3 \times 10^3$ K.

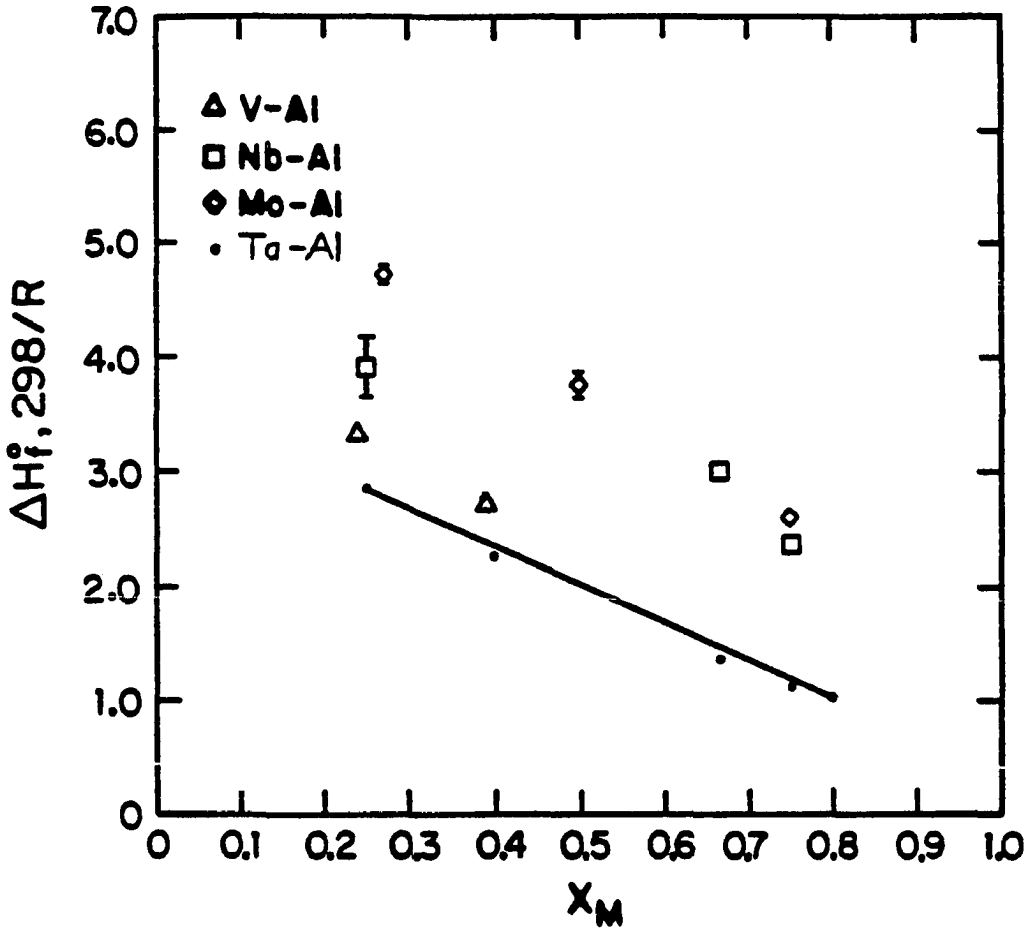

Figure 16. Normalized enthalpies of formation for phases in Ta-Al and related systems in 10^3 K

consistent with the previously mentioned lack of any noticeable drop in P_{Al} across the 2:3 composition. Numerous attempts to quench high temperature (as high as 1100°C) mixtures of Ta-Al phases repeatedly resulted in the presence of Ta_2Al_3 along with one of the other two phases. It cannot be concluded that Ta_2Al_3 is a stable phase relative to the neighboring phases since it is possible that the disproportionation quickly reversed upon cooling or that the transition temperature is >1100°C.

The values listed in Table 10 for $\Delta H^{\circ}_{at,298}$ for the various compounds result from combinations of $\Delta H^{\circ}_{f,298}$, $\Delta H^{\circ}_{at,298}(Al)$ and $\Delta H^{\circ}_{at,298}(Ta)$ and should, therefore, be regarded as having the same estimated uncertainty as corresponding $\Delta H^{\circ}_{f,298}$ values, i.e., about 0.7 kcal per mole of atoms.

Comparison of $\Delta H^{\circ}_{at,298}$ of Ta-Al phases with phases in related t-Al systems has the intent of assessing relative cohesive or bonding energies in the various systems. The similarities are evident in both Table 10 and Figure 17 although it is noticed that in each case $\Delta H^{\circ}_{at}/(x+y)/R$ is largest for Ta_xAl_y. Considering the relative sizes of $\Delta H^{\circ}_{at,298}(M)$ and $\Delta H^{\circ}_{at,298}(Ta)$ (cf. 123 kcal/mol atoms for V to 186.8 for Ta) and their comparable magnitudes of $\Delta H^{\circ}_{f,298}$ (cf. Figure 16) this trend may be related to the proposed idea, to be explored further in the next section, that bonding involving 5d or 6d orbitals of transition metals is more effective than that involving overlap of 4d orbitals. This idea assumes that factors involved in relative strengths of

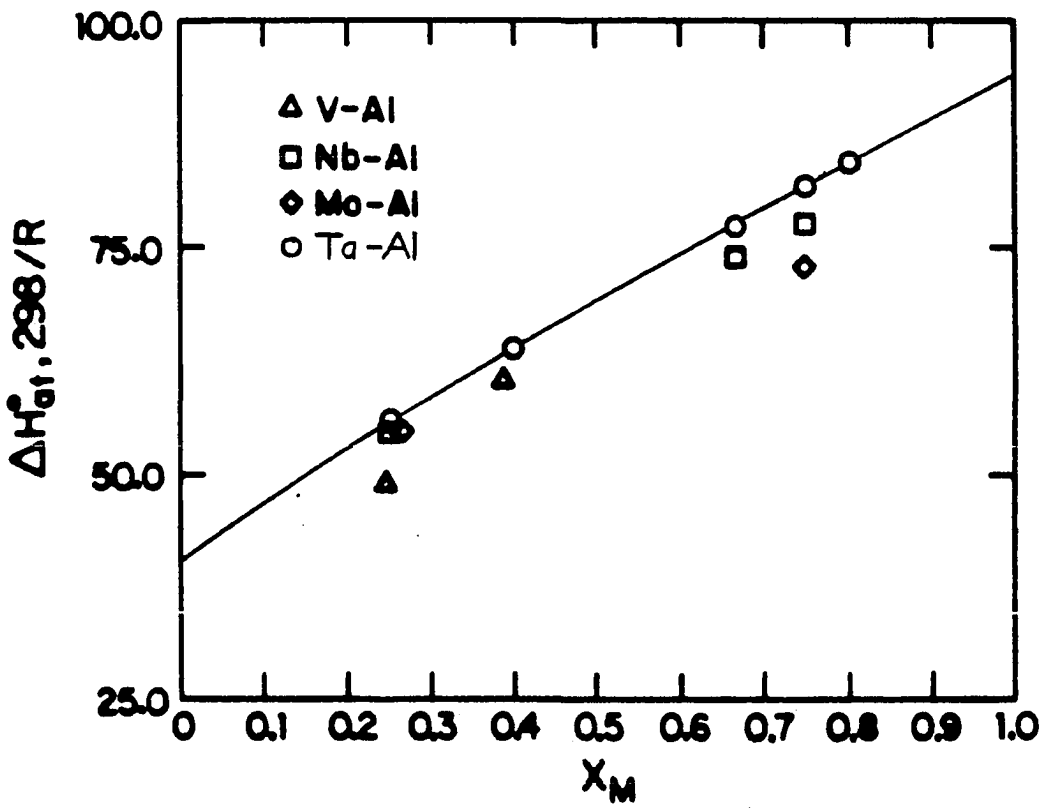

Figure 17. Comparison of normalized enthalpies of atomization in 10^3 K per mole of atoms for similar M-Al systems

transition metal-transition metal bonds are valid concepts when discussing bonding in transition metal-aluminum ("t-Al") compounds. As noted earlier in the discussion of Ta-S results, the most Ta-rich phases in the system most resemble Ta itself in cohesive energy because within the system these compounds involve the greatest amount of Ta-Ta bonding.

V. GENERAL INTERPRETATION

A. Introduction

Additional considerations of the significance of bonding enthalpies and enthalpies of formation as determined in this thesis were facilitated by the use of concepts from the two (arguably) most relevant treatments of the stability of intermetallics, the models of Brewer-Engel[49] and Miedema et al.[26] The validity of both these approaches in applications to the systems of interest is questionable for various reasons, but minimally each contains suggestions for starting points in understanding the relative magnitudes of ΔH°_{at} and ΔH°_{f} in intrasystem and intersystem comparisons.

B. Brewer-Engel Model

The essential feature of the Brewer-Engel ("B-E") treatment,[49] which is at best useful only for metallic elements and was not investigated here, proposes a correlation between the observed crystal structures (bcc, hcp and fcc) of most transition elements and the postulated number of s and p electrons involved in bonding. The correlation holds nearly without exception in that $d^{n-1}s$, $d^{n-2}sp$, and $d^{n-3}sp^2$ configurations are paired with bcc, hcp and fcc structures, respectively for series 4 through 6 of the periodic table. Even in this limited application the concept seems somewhat superficial since its valence-bond-like scheme, appropriate to gaseous atoms, is quite different from features of the band theory of metals. Extension of the B-E correlation to binary

intermetallic compounds of Al has even less basis because of the great variety of complex structure types not easily related to bcc, hcp and fcc.

Brewer also proposes, however, that while the number of s and p electrons involved in bonding directly determines structure, the total number of unpaired electrons in the valence state, which includes 3d, 4d, or 5d electrons as well, is among the determining factors of bond energy. On this assumption, he proceeds to apportion the bonding enthalpy of each transition metal into the contribution from s,p electrons vs that of d electrons. In doing so, a number of assumptions were made, the validity of which cannot conclusively be determined. Each of these assumptions will be introduced, in order of increasing detail in the model, for discussion of the validity of extending B-E concepts to intermetallics.

The least speculative way of calculating a property indicative of an element's capacity for bonding in a given binary system was employed first; the $\Delta H^{\circ}_{at,298}$ for each member of a series of compounds was related to the number of atoms of each type in its formula, e.g.:

$TaAl_3$:	A + 3B	=	445.6 kcal
Ta_2Al_3:	2A + 3B	=	632.3
Ta_2Al:	2A + B	=	460.5
Ta_3Al:	3A + B	=	648.0
Ta_4Al:	4A + B	=	836.3

A and B are (respectively) the putative contributions to the bond enthalpy from one Ta atom and one Al atom. A least squares minimization led to values of 187 kcal for A and 85.9 kcal for B. The fit of calculated to observed values of $\Delta H^{\circ}_{at,298}$ was excellent; the average

error per compound being ±0.40 kcal/mole. In comparing these results to 186.8 kcal/mole for Ta metal, and 78.7 kcal/mole for Al metal, one observes that the intermetallic bonding capacity of Al is increased over its intra-element bonding in a more significant way than that of Ta. This is an alternative way of stating the previously illustrated fact (Figure 16) that the largest $\Delta H^{\circ}_{f,298}$ (per mole of atoms) in the Ta-Al system are those of the most Al-rich compounds (and the smallest, those of the Ta-rich). Further speculation about this sort of trend for systems in general will be presented in the discussion of the Miedema model.

The least-squares fit described above was applied to available data on other t-Al systems and to t-S systems,[50] including Ta-S. The fits were typically very internally consistent, with the average deviation per compound less than 3 kcal for all but a small minority of systems. The results for Ta-S compounds were: 187.1 kcal/mole Ta atoms and 113.2 kcal/mole S atoms (cf. 66 in elemental S). Again, the main group element, S in this case, is stabilized more than is Ta in formation of the binary compounds.

The results from the entire t-Al and t-S series for ΔH°_{at}/S atom and ΔH°_{at}/Al atom are given in Table 11, while those of the transition elements in the same compounds are presented in Table 12.

The additional features of Brewer's assignment of bonding enthalpy per electron, namely its further division into (s,p) and d contributions and the inclusion of promotion energy to derive a valence state bonding enthalpy are mutually interdependent. Because the addition of a spectroscopically determined promotion energy[51] to the observed $\Delta H^{\circ}_{f,298}$

Table 11. Bonding (atomization) enthalpy per atom-mole and per e^--mole of Al or S in transition metal aluminides and sulfides (t-x) in kcal

x \ t	Sc	Ti	V	Cr
Al	—	88.9(29.6)	87.5(29.2)	82.3(27.4)
S	139(69.4)	100(50.0)	68.6(34.3)	—

	Y	Zr	Nb	Mo
Al	—	90.4(30.1)	88.0(29.3)	89.7(29.9)
S	150(75.0)	83.8(41.9)	101.8(50.9)	83.4(41.7)

	La	Hf	Ta	W
Al	81.7(27.2)	91.1(30.4)	85.9(28.6)	—
S	106(53.0)	—	113(56.6)	74.0(37.0)

cf. values for pure metals: Al 78.7(26.2)
S 66(33)

Mn	Fe	Co	Ni	Cu
81.6(27.2)	88.4(29.5)	82.2(27.4)	95.5(31.8)	80.1(26.7)
69.0(34.5)	83.0(41.5)	78.6(39.3)	76.6(38.3)	72.0(36.0)

Tc	Ru	Rh	Pd	Ag
—	—	—	103.3(34.4)	78.0(26.0)
—	—	77.1(38.5)	75.5(37.8)	—

Re	Os	Ir	Pt	Au
—	—	—	81.2(27.1)	90.6(30.2)
73.5(36.8)	—	78.0(39.0)	72.5(36.2)	—

Table 12. Bonding (atomization) enthalpy per atom-mole and per e^--mole for transition elements and their aluminides and sulfides in kcal

Type of Phase \ Element and no. electrons	Sc(3)	Ti(4)	V(5)	Cr(6)
metal	91(30.3)	113(28.2)	123(24.6)	95(15.8)
t-Al	-	117(29.4)	123(24.6)	97.9(6.3
t-S	117(29.4)	118(29.5)	183(36.7)	—
	Y	Zr	Nb	Mo
metal	102(34)	146(36.5)	172(34.4)	157(26.2)
t-Al	—	154(38.6)	176(35.2)	162(27.0)
t-S	125(41.8)	244(61.0)	187(37.4)	181(30.2)
	La	Hf	Ta	W
metal	104(34.7)	146(36.5)	187(37.4)	203(33.8)
t-Al	133(44.3)	156(39.1)	187(37.4)	—
t-S	184(61.3)	—	187(37.4)	249(41.5)

Mn(7)	Fe(6)	Co(5)	Ni(4)	Cu(3)
68(9.7)	99(16.5)	102(20.4)	103(25.8)	81.1(27.0)
78.2(11.2)	100(16.7)	126(25.3)	106(26.4)	88.2(29.4)
117(16.7)	106(17.8)	113(22.6)	113(28.2)	87.6(29.2)

Tc	Ru	Rh	Pd	Ag
158(22.6)	155(25.8)	133(26.6)	91(22.8)	68.4(22.8)
—	—	—	95.4(23.8)	70.1(23.4)
—	—	147(29.5)	92.9(23.2)	—

Re	Os	Ir	Pt	Au
187(26.7)	188(31.3)	160(32.0)	135(33.8)	87.3(29.1)
—	—	—	162(40.6)	93.8(31.3)
215(30.0)	—	167(33.5)	149(37.2)	—

requires the justification of a greater enthalpy difference between the two relevant electronic configurations (e.g., sd^6 and spd^5) in the solid than between the corresponding states in the gaseous atom, one must arrive at a self-consistent set of (s,p) and d bond enthalpy contributions. This was done by Brewer through assuming that the (s,p) contribution varies smoothly across a transition series and interpolating between the values known for Sr and Cd, (e.g.) which involve no d electrons in bonding. This rather flat curve was then subtracted from the trend in net valence state bonding enthalpy to give the d electron contribution.

Consideration was given to performing an analogous derivation of the bonding enthalpy due to (s,p) vs d electrons of the transition metal ("t") in t-Al and t-S systems, however, there was not sufficient information on such systems involving t-metals at the ends of each transition series to estimate the (s,p) contribution. Therefore, the division on the basis of assumed total number of electrons without regard for type (s,p, or d) is the furthest extension of Brewer's ideas to be attempted.

The second entry for each transition metal in Table 12 is based on the assumption that the total number of electrons involved in either elemental, intermetallic, or t-S bonding is incremented or decremented by one electron per element across the transition series and is independent of chemical composition within a given system. This number of electrons was assigned to be consistent with Brewer's treatment for purposes of comparison. Alternative ways of assigning this number are at least equally plausible, e.g., Pauling's metallic valences,[52] resulting in different normalized bonding enthalpies especially for the last few

members of a transition series. As may be seen in the numerical results, the trend in bonding enthalpies across the transition series is more pronounced in the 'per electron' than the 'per atom' form. No claims are made as to the greater significance of the trend as illustrated in the 'per electron' form; the values are presented for comparison without further justification, which would require better understanding of the meaning of 'valence' in a solid. Figures 18a and 18b show the results for 3d metals in t-Al phases along with Brewer's results for the pure 3d metals. The same general trend is evident, and if the s,p trend for the bonding in the compounds is similar to that for the pure metals, the trends for d electrons are probably quite similar also. The upper curve in Figure 18a is the trend for $\Delta H^{\circ}_{at,298}$/Al e^- which resembles the interpolated s,p curve in 18b.

It is quite reasonable, then, to suggest that the concept of a certain bonding enthalpy per electron in a given intermetallic system is valid. The slight variation across the transition series of $\Delta H^{\circ}_{at,298}$/Al atom may again be due to d electron terms in the net bond enthalpy. The considerable difference in the bond enthalpies of t-Al and t-S compounds for many t metals, and the lack of as smooth a trend in the sulfide results as in the aluminide results suggest that (i) bond enthalpy per atom is not strictly a property intrinsic to one atom type without regard for its environment and (ii) extension of the concept to compounds other than intermetallics has less validity than its application to intermetallics.

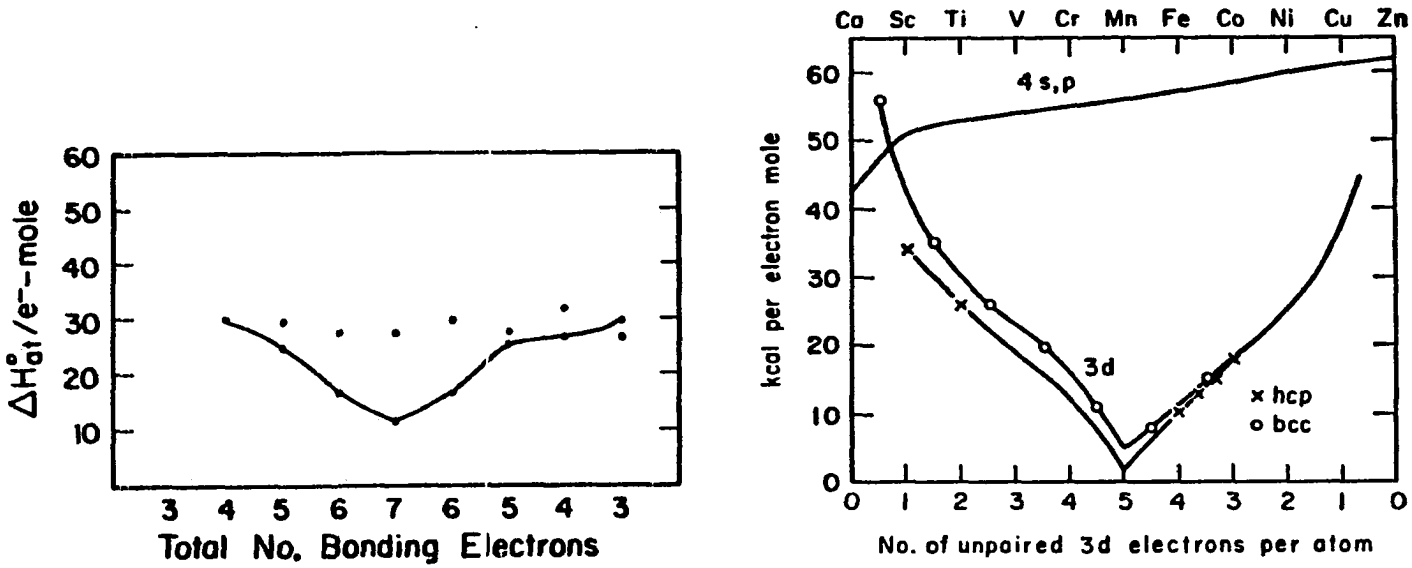

Figure 18. Comparison of bond enthalpy per 3d-transition metal electron in the aluminides (lower curve, left) as determined in this study with that in the pure metals as determined by Brewer

It should also be recognized, however, that the labeling of t-Al compounds as 'intermetallic' and thus distinct in character from t-S compounds is arbitrary and perhaps not useful in explaining the different properties of the two groups of compounds.

There is another trend in the bond enthalpies per atom, noticeable in the values derived for the transition metals as well as in those for Al and S. As a given group is descended the contribution rises markedly, a phenomenon commonly attributed to greater spatial extent of the d orbitals of the transition metal in rows 5 and 6 than in row 4. This would mean a corresponding improvement in both t-t and t-Al (or t-S) bonding capability, a factor which Brewer claims is compensated for by condensation of 3d elements into intermetallic structures having abnormally dense packing and thus shorter-than-average bond distances. A comparison of known structure types of t-Al and t-S compounds of row 4 transition metals with those of rows 5 and 6 provided no clear evidence that either coordination numbers or bond distances were consistently different from row to row, however.

Further examination of Table 12 reinforces the notion that there is little gain in bonding strength for most of the transition metals (most notably Ta) in forming compounds with Al or S as compared to intra-element bonding. Most exceptions to this generalization are sulfides, which in almost all cases have larger $\Delta H^{\circ}_{at,298}$ per t atom for t-S than for t-Al or pure t metals. Similarly, S contributes more to compound formation in terms of $\Delta H^{\circ}_{f,298}$ per atom than does Al in bonding to the same t-metal in most cases.

C. Tantalum-Sulfur vs Tantalum-Aluminum

In the most direct comparison possible between the binary systems studied here, Ta_2Al and Ta_2S may be contrasted. Their $\Delta H^{\circ}_{f,298}$ and $\Delta H^{\circ}_{at,298}$ which may be compared immediately (without normalization by x+y because they have equivalent stoichiometry) are:

Phase	$\lvert\Delta H^{\circ}_{f,298}\rvert$	$\Delta H^{\circ}_{at,298}$
Ta_2Al	8.2 kcal/mol	460.5
Ta_2S	41.8	482.0

In deducing chemical significance from this comparison, it is worthwhile to examine the relative effects of structure and composition. The average Ta-Ta bond distances in Ta_2Al and Ta_2S are 2.99 Å and 3.03 Å, respectively. The Ta substructures of these two phases (refer to Figures 3 and 10) are similar in essence, each possessing central rows of atoms, each member of which is sandwiched between two rings of atoms staggered relative to one another. The main differences are in terms of the placement of the non-Ta atoms. The Al-Al and S-S interactions are negligible in the two solids. These structural aspects combine to suggest that the larger enthalpy of atomization of Ta_2S reflects the greater cumulative bond strength of Ta-S interactions as compared to Ta-Al interactions in these binary solids. The average bond distance for the ten shortest Ta-S interactions in Ta_2S is 2.53 Å which corresponds to a Pauling bond order of 0.56 while the corresponding quantities for Ta-Al bonds in Ta_2Al are 2.92 Å and n = 0.29. Therefore, it is not a straightforward deduction to

conclude that Ta-S bonds are in general stronger than Ta-Al bonds since one is (in these compounds) probably not comparing bonds of the same order. It would be very helpful to obtain bond enthalpy information on gaseous Ta-S and Ta-Al species of known electronic configurations for further corroboration of this suggestion.

The derived enthalpies of formation exhibit an even larger difference than do the $\Delta H^{\circ}_{at,298}$ values since the atomization of Al(s) is more costly than that of S(s) by ~13 kcal/mol. For the majority of the other t-Al/t-S comparisons, both $\Delta H^{\circ}_{f,298}$ and $\Delta H^{\circ}_{at,298}$ are larger for the sulfide than for the aluminide of equivalent composition, but there are few, if any, other instances of t_xAl_y and t_xS_y compounds with the same t, x, and y whose structures are sufficiently similar to isolate the effects of relative bond strengths of S and Al with a given metal. In fact, there are examples of reversed orders in one or both of these comparisons for certain t-metals and therefore it is not safe to generalize about either trends or their causes in comparing stabilities of aluminides and sulfides. The complexity of the interactions in solids and the resultant idiosyncrasies of individual systems require as detailed an examination of each system as possible.

The Brewer-Engel model alone would not be particularly helpful in explaining why Ta-S interactions appear to be stronger than Ta-Al interactions since it would propose that Al employs three valence electrons (as sp^2) while S (s^2p^4) employs only two. Equally simplistic arguments based on the larger electronegativity difference between Ta and S (1.0 on Pauling's scale vs 0.0 for Ta-Al) at least predict the correct order but

are, like many chemical concepts, of more questionable validity when applied to solids rather than to gaseous molecules.

A more relevant and realistic approach is to compare charge density and density of states results derived from electronic band structure calculations. The only closely related systems thus examined are Zr-S and ZrAl; KKR method calculations having been performed at the Ames Laboratory in recent years on ZrS[53] and Zr_2Al.[54] The essential difference noted in the results is that the valence band bonding in ZrS involves p orbital contributions from sulfur, while the valence band in Zr_2Al has only s orbital contributions from Al, with the Al p states corresponding to the higher energy conduction band and are apparently nonbonding. One might propose by analogy that in Ta-S vs Ta-Al bonding in solids, Ta-S interactions are stronger because two electrons per S atom participate in bonding while only one electron per Al atom is involved. This is not necessarily in conflict with the B-E VB approach if the enthalpy gain in replacing one p electron by one s electron in the resultant bonding indeed outweighs the 83 kcal/mole required to promote Al from s^2p to sp^2.[51]

Verification of this is not achievable in any obvious way, and it is similarly difficult to relate the KKR results to the physical model implied by the concept of electronegativity differences.

D. Other Transition Metal-Aluminum Systems

Another comparison requiring less speculation and independent corroboration is that between $\Delta H^\circ_{at,298}$ values in the Nb-Al and

Ta-Al systems. Here, the unraveling of compositional, structural, and electronic factors which combine to determine relative cohesive energies is simpler because Nb_2Al and Ta_2Al have nearly identical structures ("σ", see Figure 10) as do $NbAl_3$ and $TaAl_3$ ($TiAl_3$-type). It can only be asserted that Ta-Ta and Ta-Al bonding have a combined strength greater than that of Nb-Nb and Nb-Al bonding as manifested in the larger $\Delta H^{\circ}_{at,298}$ of the Ta compounds. This may again be proposed as consistent with the belief, reinforced by Brewer, that 5d elements have greater d orbital spatial extent and therefore participate more effectively in bonding both with transition metals (including themselves in elemental form) and with (e.g.) s orbitals of Al.

It should be added that the visual comparison between $\Delta H^{\circ}_{f,298}$ values provided earlier in Figure 16, was intended only as qualitative evidence of the reasonableness of the Ta-Al results and not as a quantitative comparison suggesting underlying chemical differences or similarities with Nb-Al compounds. There is in fact no basis, generally for quantitative comparisons between ΔH°_{f} of compounds formed from different pairs of elements because ΔH°_{f} reflects qualities of both the compound and elements involved. Meaningful relationships between ΔH°_{f} values are best examined within a given binary system where only compositional and structural differences come into play.

E. Miedema Model

1. Description

Any attempt to predict or model ΔH_f^o behavior should include features dependent on both the elements and the compounds involved or on differences between the elements. The method due to Miedema et al.[26] attempts to account for ΔH_f^o of a wide variety of binary intermetallics using essentially a two parameter formula. This semi-empirical approach may be succinctly described as follows.

The enthalpy effects in formation of an alloy, whether a liquid, a solid solution, or an ordered compound, are attributed to the extent and quality of the surface contacts between 'macroscopic' atoms of the two component metals. The atoms are viewed as Wigner-Seitz cells which are, to first approximation, the same in shape and size whether situated in the alloy or in the respective metallic elements. Similar cellular models have been previously used with moderate success in theoretical attempts to account for the cohesive energies and valences of pure metals.[55]

For intermetallic phases in general, the model contains just two essential physical quantities:

$$\Delta H_f \approx -P(\Delta\phi^*)^2 + Q(\Delta n_{WS}^{1/3})^2 \quad . \tag{33}$$

The negative term depends on the contact potential difference between the two metals which in most instances varies negligibly from the difference in the work function ϕ. The positive term accounts for the difference in

the electron density at the boundary of the W-S cells. This discontinuity is presumed to be smoothed by charge transfer which also results in volume changes in the cells.

Determination of the more detailed forms of equation (33), which include the numerical values of P and Q appropriate to particular classes of intermetallics, was largely empirical. The ratio of Q to P was observed to be correlated to $\Delta\phi^*/\Delta n_{WS}^{1/3}$ and the critical ratio was chosen as that which correctly predicted the algebraic sign of ΔH_f° (taken from knowledge of the existence or nonexistence of phases in a given A-B system) for as many phases as possible. The best-fit value for P was found to differ for (i) solid or liquid alloys of two transition or noble metals, (ii) liquid alloys of two nontransition metals and (iii) solid or liquid alloys of a transition metal with a nontransition metal. For the latter category, of greatest interest here, an additional term -R was determined as necessary to bring calculated and observed signs of ΔH_f° into agreement.

The simple form of the Miedema model presented in equation 33 is adequate for disordered phases (i.e., solutions) in which the atoms are similar in size. The actual number of contacts between dissimilar atoms varies due to both the degree of order in the alloy and to the difference in volume of the types of atoms. Both of these variables are accounted for in the factor f_B^A which represents the fraction of the nearest neighbors to an A atom which are of element B. The empirically derived approximation is

$$f_B^A = (1-c_A^S)[1+8(c_A^S)^2(1-c_A^S)^2] \tag{34}$$

and in turn, the 'surface concentration' is given by

$$c_A^S = c_A V_A^{2/3} / (c_A V_A^{2/3} + c_B V_B^{2/3}) \tag{35}$$

to account for the size difference between atoms A and B.

The final expression for transition-nontransition metal intermetallics is

$$\Delta H^\circ_{f,298} = c_A f_B^A \left[\frac{2PV_A^{2/3}}{(n_{WS}^A)^{-1/3} + (n_{WS}^B)^{-1/3}} \right] \left[-(\Delta\phi^*)^2 + \left(\frac{Q}{P}\right)(\Delta n_{WS}^{1/3})^2 - \frac{R}{P} \right] \tag{36}$$

2. Comparison of predictions and measurements

Using this expression and Miedema's tabulated values for the coefficients P, Q, and R as well as the physical parameters n_{WS} and ϕ^*, the values represented by the parabolic curve in Figure 19 were calculated for comparison to the experimentally determined $\Delta H^\circ_{f,298}$ for Ta-Al compounds. An immediately obvious discrepancy is the model's failure to reproduce the concentration dependence; as in many other systems the observed maximum in formation enthalpy occurs at other than the 1:1 composition, while the Miedema equation results in a nearly symmetrical curve peaking at A:B = 1:1 for all binary systems. This point is to be returned to eventually. In addition, the magnitudes of the prediction exceed the observed values by approximately a factor of two,

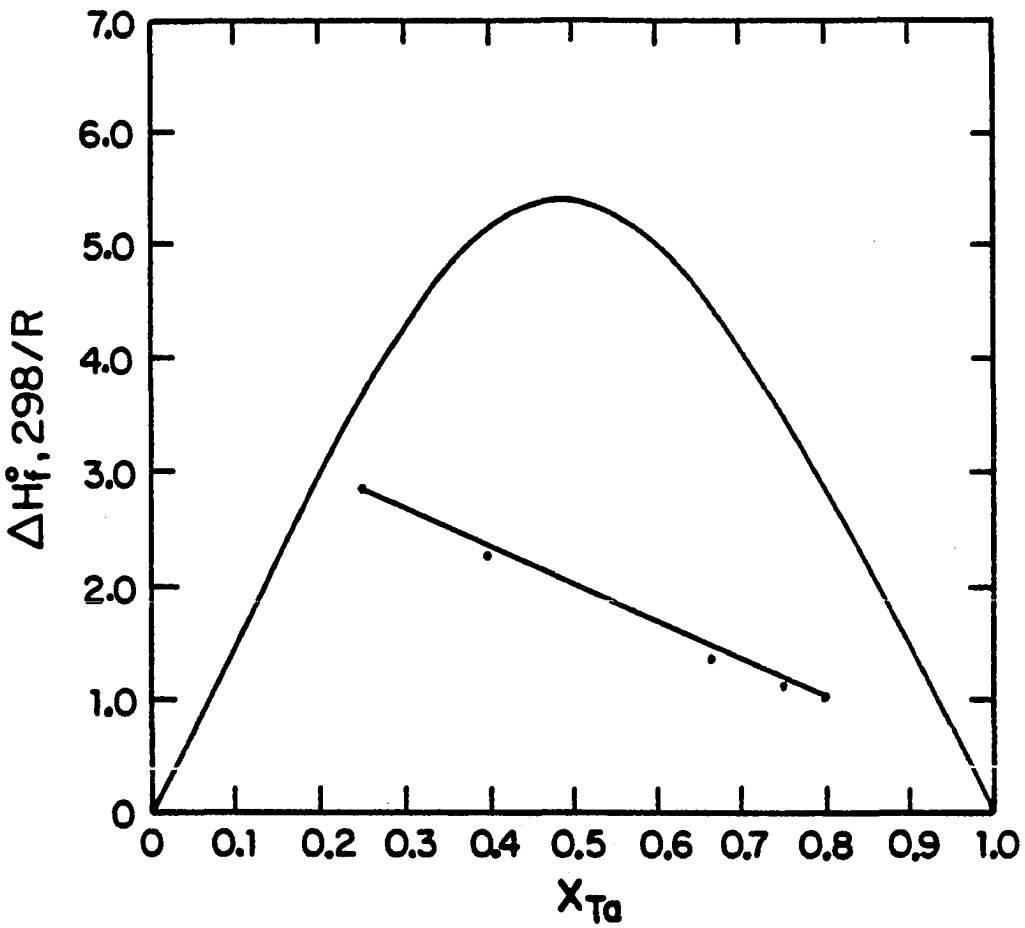

Figure 19. Comparison of $\Delta H^{\circ}_{f,298}/R$ in 10^3 K per mole atoms as measured (plotted points) and predicted by Miedema

and recalling that any systematic error in the P_{Al} is likely to be in the direction $P_{obs} < P_{equil.}$, if $\Delta H^{\circ}_{f,obs}$ is in error the discrepancy is probably larger than reported here.

Before proceeding with an assessment of the Miedema approach and its relationship to the results presented here it is appropriate to comment on the intent of what is to follow. It is difficult to fairly evaluate a model without first establishing what that model is expected to do and to what degree it is required to succeed. Although there is a variety of criteria one might apply in deciding whether or not a model is successful, most would seem to be concerned with either (i) accuracy in predicting measurable quantities or (ii) credibility of the model's physical features. Both of these criteria as applied to the Miedema model may be discussed at least qualitatively, with much greater difficulty in definitively establishing the latter.

In a first step, the available data[2] on enthalpies of formation of binary intermetallics containing Al and a transition metal or two transition metals were reviewed and compared to the values calculated using equation 36 (or its equivalent appropriate for the system in question). It was observed that of 18 t-Al phases with 1:1 stoichiometry the model overestimated the $|\Delta H^{\circ}_{f,298}|$ per mole of atoms in 10 cases, with an average discrepancy for all systems of ~3 kcal. Similar evidence of a systematic problem with the aluminides was provided by Miedema and coworkers[56] as reproduced in Figure 20. In accounting for the behavior of a range of types of compounds with essentially only two parameters,

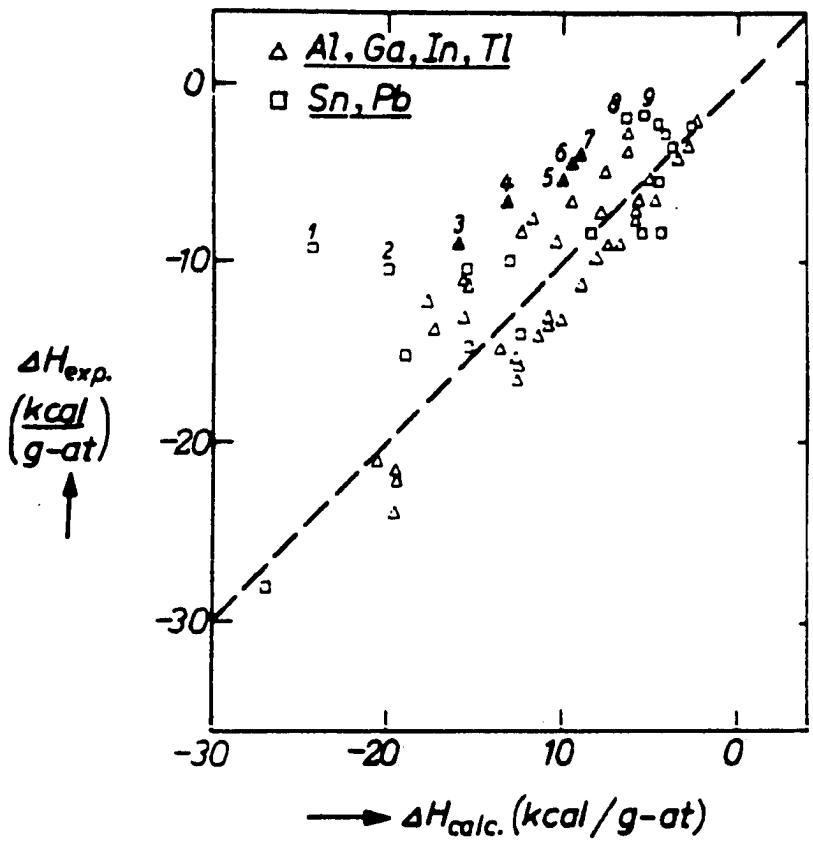

Figure 20. Reproduction from ref. 56 of predicted and observed $\Delta H^{\circ}_{f,298}$ for compounds of a transition metal with a nontransition metal. Darkened points represent aluminides

it is to be expected that both overestimates and underestimates of $|\Delta H_f^o|$ will result; the fact that for the aluminides the prediction is usually an overestimate suggests looking for some peculiarities of t-Al phases that distinguish them even from other intermetallics containing one nontransition metal.

The electrochemical parameter ϕ^* for Al has the same value, 4.0 V, as the experimental work function ϕ. Therefore, one probably cannot account for the consistent overestimate for t-Al phases as due to an unrealistically large electronegativity term. Among the transition elements for which both experimental ϕ and semi-empirical ϕ^* exist there are few instances of significant discrepancies, and the differences occur in both directions ($\phi-\phi^* > 0$ and $\phi-\phi^* < 0$). Examination of the electron density parameter n_{WS} for Al and the transition metals is similarly fruitless in accounting for the discrepancies; the comparison of n_{WS} with the ratio $(B/V_m)^{1/2}$ (where B = bulk modulus and V_m is molar volume) to which it is related shows very strong correlation for both types of metals.

The constant R which Miedema found necessary for modeling t-Al and similar systems is substantial, amounting to an additional negative term of approximately -9 kcal in the case of a 1:1 compound. This term is said to be due to d-p hybridization in bonding between transition metals and nontransition metals such as Al, Ga, Sn, Pb, Sb, and Bi, believed to be more effective than in pure transition metals. If such a concept has meaning, it is conceivable that t-Al compounds are not as well-accounted for as other t/non-t intermetallics because there are in fact not the

maximum number of Al p orbitals participating in this hydridization and thus the effect is smaller than -9 kcal/mole atoms. This idea was suggested but certainly not proven by the previously mentioned band calculations of Kematick.

The perusal of available data on compounds formed by two transition metals yields two conclusions: (i) there is a serious scarcity of data relative to the total number of possible compounds and (ii) the Miedema model is somewhat more successful in accounting for $\Delta H^{\circ}_{f,298}$ for these phases than for the aluminides. Of 23 1:1 compounds in this class, 11 had $|\Delta H^{\circ}_{f,298}|$ clearly smaller than predicted, only one clearly larger than predicted, and the remaining 11 (or approximately half the total) were within ±1 kcal/mole atoms or effectively correct.

In response to the question concerning the predictive capability of the Miedema model it can, therefore, be stated in summary that (i) predictions in general are only approximately correct, with both over- and underestimates as compared with measured values, and that (ii) predictions for transition metal aluminides seem to generally overestimate their stability in terms of $\Delta H^{\circ}_{f,298}$. The lack of sufficient data spanning the whole range of t-t possibilities and the use of primarily the sign rather than the magnitude of $\Delta H^{\circ}_{f,298}$ in deriving the predictive equation may account for (i), while (ii) is speculated to be due to some valence-related factor making aluminides an exception to Miedema's proposed d-p hybridization phenomenon and the corresponding term -R.

Some additional observations concerning the presence or absence of physically realistic features in the Miedema model may also be made. The electronegativity parameter $\Delta\phi^*$ is similar to parameters in other attempts[52] to model enthalpies of formation and certainly has intuitive appeal. However, the extension of this concept to solids may not be completely valid, as suggested by X-ray fluorescence results[57] on t-Al compounds pointing to electron transfer from the 'more electronegative' Al to the transition metal.

Atomic size differences are often invoked in attempts to account for relative stability of compounds. This factor is indirectly employed by Miedema in the positive term $\Delta n_{WS}^{1/3}$, which is dependent on volume differences and thus on Δr of the atoms, and in the surface concentration factors. It appears at first glance that the most important lack of specificity in the model may be that structural variation is not explicitly included. Miedema dismisses the need for this in claiming that the various structures of intermetallics do not result in contributions to stability which depart markedly from the corresponding structure-dependence of stability of the component metals. This seems to suggest both a relative lack of intra-system variety in structures of most intermetallics, with a resultant small curvature in the $\Delta H_{f,298}^{\circ}$ vs composition plot, and that the intent of the model is global approximation of enthalpies rather than specificity. The latter belief seems reinforced by aforementioned comparisons to measured quantities. The former idea would be more acceptable if the Ta-Al system's variation in

$\Delta H^\circ_{f,298}$ were typical; however, for certain other systems containing a larger maximum $|\Delta H^\circ_{f,298}|$ and exhibiting more stable phases it is not clear that structural factors are irrelevant in explaining relative stability. Admittedly, it is difficult to propose a way to incorporate more realistic structure dependence into a model without approaching the large time and monetary expense incurred in quantum mechanical calculations, which include the bond distances, coordination numbers and symmetry of a known structure.

3. Intrasystem trends in enthalpies of formation

It was noted earlier that the composition dependence of $|\Delta H^\circ_{f,298}|$ in many binary intermetallic systems differs from Miedema's prediction in that the maximum stability actually occurs at other than 1:1 stoichiometry. Speculation about the underlying factors for this asymmetry has led to further search for trends in and correlations between certain variables, mostly without producing a clear explanation. These attempts are summarized in what follows.

Difference in size of the component atoms can be imagined to result in optimum heteroatomic contact at a composition richer in the smaller atom. While recognizing that the radius of an atom is at best an ad hoc definition, both Pauling's metallic radii[52] and the radii of spheres equal in volume to WS cells (as used in the Miedema model) were compared for the components of various t-t and t-Al compounds. There appears to be no strong correlation between composition and radius ratio for the most stable compounds; there are instances such as $NiTi_3$ and $CrAl_4$ in which the minority atom is said to have the smaller radius. Such a

correlation may appear to exist for more ionic compounds where the postulated radii are more significantly different. The 'radius ratios' for intermetallics are mostly within ±10% of 1.0 and the effect of r_A/r_B may not be large enough to outweigh competing factors. One would expect any correlation of this sort to be manifested in a connection between maximum $\Delta H^{\circ}_{f,298}$ and coordination numbers as well, and there is conversely a lack of obvious coordination number effects in the data examined.

Another simplistic attempt compared the number of bonding electrons in the component atoms to test the assumption that the most stable compound has an optimum ratio (near 1:1) of valences such that heteroatomic bonding capacity is fully used. In a hypothetical system in which atom A has valence 3 and atom B has valence 2, one might expect the most stable compound to be A_2B_3. In examining t-Al, t-t, and t-S phases there is no indication of such a pattern.

One possible trend was noted when the stoichiometries of the most stable t-Al phases (with largest $|\Delta H^{\circ}_{f,298}|/(x+y)$) were compared across the transition series:

—	$TiAl$	VAl_3	$CrAl_4$	$MnAl_4$
—	$NbAl_3$	Mo_3Al_8	—	—
$LaAl_2$	$HfAl_2$	$TaAl_3$	—	—
$FeAl_3$	$CoAl$	$NiAl$	Cu_2Al	
—	—	$Pd_{1.13}Al$	$Ag_{0.77}Al_{0.23}$	
—	—	$PtAl$	$AuAl_2$	

The most aluminum-rich compositions seem to occur near the center of each series, although it is tenuous to claim a consistent pattern, given the gaps in knowledge about the 4d and 5d metals. This could, however, be yet another physical property whose extremum occurs at the Mn group where the maximum number of unpaired d electrons is said to occur.

Rules of thumb such as the ones explored above seem to hold more frequently for binary compounds formed by two elements from main groups at opposite ends of the periodic table whose bonding is designated as 'ionic'. By contrast, the pairs of atoms in the intermetallic systems considered here are mostly of similar size and electronegativity, and the resultant compounds are sometimes referred to as 'electron compounds'. Their bonding is apparently more covalent, if not metallic, in character.

4. Interpolative predictions

The Miedema model's usefulness as an accurate predictive tool has been seen to be quite limited. It is of some value in instances of binary systems for which no thermochemical data exist, in that at least rough estimates of $\Delta H^{\circ}_{f,298}$ can be obtained. Miedema et al.,[26] in fact, cite several previously unexamined systems in which measurements agreed well with earlier predictions.

For systems having existing $\Delta H^{\circ}_{f,298}$ data, it is possible to make interpolative predictions which can be trusted as quite accurate. These are based on the understanding that a given phase owes its existence at equilibrium not only to its stability relative to the elements

but relative to other intermediate compounds which bracket it in the phase diagram. Referring to Figure 19 it may be seen that Ta_2Al_3 is an example near the minimum limit for stability of a compound relative to its neighboring phases; in general the shape of the $|\Delta H^\circ_{f,298}|$ vs composition curve is clearly concave downward at all points. Any hypothetical phase whose optimum bonding enthalpy falls below the curve drawn through the stable phases does not form because its disproportionation into neighboring compounds is energetically favored. Likewise, a phase will not form with $|\Delta H^\circ_{f,298}|$ significantly larger than the existing trend because adjacent phases would disproportionate into combinations including this unusually stable phase. Therefore, the definition of a $|\Delta H^\circ_{f,298}|$ vs composition curve by measured values at both sides of the maximum allows the interpolation of $\Delta H^\circ_{f,298}$ values for those stable (= observed) compounds not yet studied thermodynamically. Table 13 lists such predictions for sulfides and aluminides; an obvious suggestion for future work is the experimental determination of these enthalpies.

Table 13. Predicted $\Delta H^{\circ}_{f,298}$ for selected transition metal aluminides and sulfides in kcal/mole

Phase	$\lvert\Delta H^{\circ}_{f,298}/(x+y)\rvert$	Phase	$\lvert\Delta H^{\circ}_{f,298}/(x+y)\rvert$
Ti_8S_3	13.0	Pd_5Al_3	12.0
Ti_2S	15.0	Pd_3S	3.9
V_3Al	2.2	Ag_3Al	1.1
Fe_2Al_5	7.2	$LaAl_3$	9.5
Fe_3S_4	13.0	$Ta_{17}Al_{12}$	3.0
Co_3Al	19.0	Pt_2Al_3	12.0
Co_4S_3	12.0	$PtAl_2$	11.0
Ni_3Al_2	4.5	Au_4Al	7.6
Cu_2Al_3	3.7		
$Nb_{14}S_5$	21.0		
$Nb_{21}S_8$	21.0		
Nb_2S	22.0		

VI. FINAL SUMMARY AND CONCLUSIONS

The enthalpies of formation and atomization of Ta-S and Ta-Al compounds are comparable to those of phases with similar chemical composition. The atomization enthalpies may be taken as indication of cohesive strength or bonding capacity that is consistent with extensive Ta-Ta bonding in the most Ta rich compounds Ta_2S, Ta_6S, 'Ta_2Al' and 'Ta_4Al'. Within each binary system the trends in enthalpy of formation suggest certain phases to be nearly unstable with respect to disproportionation at 298 K. The transition temperatures for disproportionation are not known, and only in the case of Ta_6S was such a reaction observed.

Comparison of $\Delta H^{\circ}_{at,298}$ and $\Delta H^{\circ}_{f,298}$ between the systems Ta-S and Ta-Al show that net tantalum-sulfur bonding interactions are stronger than tantalum-aluminum interactions. This is proposed as due to different numbers of participating bonding orbitals and electrons as suggested by previous band structure calculations.

The investigation of t-S and t-Al systems as classes of compounds reveals trends in bonding capacity of each component which seem to be related to the number of unpaired d-electrons of the transition metals. Trends within a group in the periodic table indicate improved bonding effectiveness as the atomic number of the transition metal increases. Both trends as well as other hypotheses are limited in supporting evidence because of the lack of thermochemical data for some systems.

The enthalpies of formation of aluminides appear to be somewhat anomalous; $\Delta H^{\circ}_{f,298}$ values of t-t and other t-non-t compounds are more easily accounted for by Miedema's semi-empirical formula. The effectiveness of the d-p hybridization proposed as the explanation for enhanced stability of t-non-t compounds may be reduced for aluminides by the apparent contribution to bonding from only s rather than both s and p electrons.

More empirically-based predictions for the enthalpies of formation of t-S and t-Al compounds may be derived from existing data and an understanding of the reasons for the general shape of $\Delta H^{\circ}_{f,298}$ vs X curves. Specific details such as the direction of asymmetry of the curves are not predictable on the basis of simple factors such as atomic size ratios or valence.

The bonding interactions in solids may be considered represented in their complexity and resultant structural and electronic structural variety by the transition metal sulfides and aluminides studied here. Overriding principles that account for thermodynamic properties in a consistent and plausible way are not yet available. Further experimentation on related systems and theoretical exploration aimed at bridging the gap between concepts of chemical bonding and features of solid state physics are greatly needed.

VII. REFERENCES

1. Stull, D. R.; Prophet, H., eds, "JANAF Thermochemical Tables", 2nd edition, U. S. Government Printing Office: Washington, DC, 1971.

2. Hultgren, R.; Desai, P. D.; Hawkins, D. T.; Gleiser, M.; Kelley, K. K., eds., "Selected Values of the Thermodynamic Properties of Binary Alloys", Amer. Soc. for Metals: Metals Park, OH, 1973.

3. Gilles, P. W. J. Nuc. Materials 1974, 51, 12.

4. Schiffman, R. A.; Franzen, H. F.; Ziegler, R. J. High Temp. Sci. 1982, 15, 69.

5. Shilo, I.; Franzen, H. F.; Schiffman, R. A. J. Electrochem. Soc. 1982, 129(7), 1608.

6. Shilo, I.; Franzen, H. F. J. Electrochem. Soc. 1982, 129(11), 2613.

7. Kematick, R. J.; Franzen, H. F. J. Solid State Chem. 1984, 54, 226.

8. Cater, E. D. "The Effusion Method at Age 69: Current State of the Art", Nat'l. Bur. Stand., Special Publication, No. 561, 1979.

9. Biltz, W.; Köcher, A. Z. Anorg. Allg. Chem. 1938, 238, 81.

10. Kubashewski, D.; Evans, E. U.; Alcock, C. B. in "Metallurgical Thermochemistry", 4th ed.; Pergamon Press: Oxford, 1967, 220.

11. Larson, H. R.; Elliott, J. F. Trans. A.I.M.E. 1967, 239, 1713.

12. Smeggil, J. G. Ph.D. Dissertation, Iowa State University, Ames, IA, 1969.

13. Tuenge, R. Ph.D. Dissertation, Iowa State University, Ames, IA, 1975.

14. Franzen, H. F.; Hariharan, A. V. J. Chem. Phys. 1979, 70(11), 4907.

15. Amonenko, V. M.; Vasjutinskij, B. M.; Kartmazov, G. N.; Smirnov, Ju. N.; Finkel, V. A. Phys. Metals Metallogr. 1963, 15(3), 102.

16. Jellinek, F. J. Less-Common Metals 1962, 4, 9.

17. Hultgren, R.; Desai, P. D.; Hawkins, D. T.; Gleiser, M.; Kelley, K. K.; Wagman, D., eds., "Selected Values of the Thermodynamic Properties of the Elements", Amer. Soc. for Metals: Metals Park, OH, 1973.

18. Niwa, K.; Yokokawa, T.; Isoya, T. Bull. Chem. Soc., Japan 1962, 35, 1543.

19. Nakahara, J. F. Ph.D. Dissertation, Iowa State University, Ames, IA, 1984.

20. Edwards, J. G.; Franzen, H. F.; Gilles, P. W. J. Chem. Phys. 1971, 54, 545.

21. Owzarski, T. P.; Franzen, H. F. J. Chem. Phys. 1974, 60, 1113.

22. Karsten, K. Pogg. Ann. 1839, 46(2), 160.

23. Baker, T. J. Phil. Trans. 1901, 196A, 529.

24. Brewer, L.; Wengert, P. R. Met. Trans. 1973, 4, 83.

25. Kubaschewski, O. "The Physical Chemistry of Metallic Solutions and Intermetallic Compounds", N.P.L. Symposium, H.M.S.D., London, 1959, 1(9), 2.

26. Miedema, A. R.; de Chatel, P. F.; deBoer, F. R. Physica 1980, 100B, 1.

27. Kubaschewski, O., Dench, W. A. Acta Met. 1955, 3, 339.

28. Neckel, A.; Nowotny, H. "Fünfte Internat. Leicht Metallagung", Leoben, 1969, 72.

29. Kubaschewski, O.; Heymer, G. Trans. Far. Soc. 1960, 56, 473.

30. Schauer, A.; Roschy, M.; Juergens, W. Thin Solid Films, 1975, 27(1), 111.

31. Beaver, W. W.; Stonehouse, A. J.; Paine, R. M., Plansee Proc. 5th Seminar, Reutte/Tyrol, 1965, 682/700, 684.

32. Glazov, V. M.; Lazarov, G. P.; Korolkov, G. A. Metal Sci. Heat Treat. Metals (USSR), 1959, 10, 51.

33. Paine, R. M., WADC-TR-59-29 (Pt. II), 2960, 1(119), 70.

34. Marignac, L. Compt. Rend. 1868, 66, 180.

35. Brauer, G. Naturwiss. 1938, 26, 710.

36. Edshammar, L.-E.; Holmberg, B. Acta Chem. Scand. 1960, 14(5), 1219.

37. McKinsey, C. R.; Faulring, G. M. Acta Cryst. 1959, 12, 701.

38. Nowotny, H.; Brukl, C.; Benesovsky, F. Monatsh. Chem. 1961, 92, 116.

39. Wilhelm, H. A.; Witte, J. H. U. S. At. Energy Comm. 1962, IS 500, M48.

40. Glazov, V. M.; Mal'tsev, M. V.; Chistyakov, Y. D. Izv. Akad. Nauk SSSR Otd. Tekhn. Nauk 1956, 4, 131.

41. Spengler, H. F. Metall. 1957, 11, 384.

42. Wilhelm, H. A.; Cowgill, D. S. U. S. At. Energy Comm. 1959, IS17, 96.

43. Gupta, K. P. Trans. A.I.M.E. 1961, 221, 1047.

44. Schubert, K. Naturwiss. 1964, 51, 287.

45. Raman, A. Aluminium 1965, 41, 318.

46. Magneli, A; Edshammar, L.; Dagerhamn, T., Final Technical Report on Contract DA-91-591-EUC-2734 (AO426927), 1963, 1, 40.

47. Girgis, K.; Harnik, A. B. Naturwiss. 1970, 57, 242.

48. Kematick, R. J., private communication, Department of Chemistry, Iowa State University, 1984.

49. Brewer, L. Science 1968, 161, 115.

50. Mills, K. C. "Thermodynamic Data for Inorganic Sulphides, Selenides, and Tellurides", Butterworths: London, 1974.

51. Moore, C. E. "Atomic Energy Levels from Optical Spectra", U. S. Government Printing Office: Washington, DC, 1948-1958.

52. Pauling, L. "The Chemical Bond", 1st ed.; Cornell University Press: Ithaca, New York, 1967.

53. Nguyen, T. H. Ph.D. Dissertation, Iowa State University, Ames, IA, 1980.

54. Kematick, R. J. Ph.D. Dissertation, Iowa State University, Ames, IA, 1984.

55. Rundle, R. E. in "Intermetallic Compounds", Westbrook, J. H., ed.; Wiley and Sons: New York, 1967, Chapter 2.

56. Miedema, A. R.; de Boer, F. R.; Boom, R. J. Less-Common Metals 1976, 46, 67.

57. Wenger, A.; Bürri, G.; Steinemann, S. Solid State Commun. 1971, 9, 1125.

VIII. ACKNOWLEDGEMENTS

The author recognizes his dependence on the technical and theoretical expertise of a number of individuals during the preparation of this dissertation and the performance of the work reported herein. In particular, Bernd Harbrecht, Robert Kematick, and James Anderegg were especially helpful in terms of experimental know-how and timely advice. The theoretical understanding and philosophical attitudes imparted during numerous discussions with Professor H. F. Franzen have been important in the author's scientific development as well as very enjoyable. The patience and skill exhibited by Shirley Standley during seemingly endless alterations of the manuscript have been invaluable.

The love, support, understanding and patience of my wife Zsuzsanna under rather difficult circumstances have provided emotional sustenance that has been too frequently taken for granted. Occasional boosting of confidence and goal-directedness from my parents and siblings has often come at critical times as well. To all of the above I extend my most heartfelt gratitude.

IX. APPENDIX A: THERMOCHEMICAL DATA

TABLE A1. RAW DATA AND DERIVED P_S VALUES FROM Ta-S EXPERIMENTS

Reaction (3)

EXPT.	T in K	DEL m in mg	DEL t in min	P(S) in atm	P'S)corr in atm
2	1576.2	0.580	2520	0.132 E-7	0.353 E-7
2	1585.8	0.540	2100	0.153 E-7	0.398 E-7
2	1595.4	0.560	1620	0.198 E-7	0.523 E-7
2	1605.0	0.530	1500	0.218 E-7	0.566 E-7
2	1614.6	0.420	780	0.303 E-7	0.796 E-7
2	1614.6	0.590	1560	0.331 E-7	0.678 E-7
2	1624.2	0.510	980	0.322 E-7	0.798 E-7
2	1624.2	0.330	720	0.402 E-7	0.817 E-7
1	1633.8	0.410	1080	0.953 E-7	0.129 E-6
1	1633.8	0.130	390	0.899 E-7	0.119 E-6
2	1633.8	0.570	720	0.446 E-7	0.115 E-6
2	1633.8	0.400	720	0.488 E-7	0.984 E-7
1	1643.4	0.730	1980	0.101 E-6	0.135 E-6
2	1643.4	0.590	690	0.506 E-7	0.126 E-6
2	1643.4	0.430	660	0.581 E-7	0.115 E-6
1	1653.0	0.330	780	0.120 E-6	0.157 E-6
2	1653.0	0.630	600	0.618 E-7	0.153 E-6
2	1653.0	0.600	720	0.725 E-7	0.145 E-6
1	1662.6	0.410	960	0.132 E-6	0.168 E-6
2	1662.6	0.360	672	0.149 E-6	0.195 E-6
2	1662.6	0.460	380	0.726 E-7	0.176 E-6
3	1662.6	0.760	830	0.830 E-7	0.161 E-6
1	1672.2	0.430	720	0.172 E-6	0.228 E-6
1	1672.2	0.480	780	0.175 E-6	0.227 E-6
2	1672.2	0.520	330	0.919 E-7	0.225 E-6
3	1672.2	0.430	340	0.108 E-6	0.218 E-6
1	1681.8	0.750	960	0.217 E-6	0.282 E-6
2	1681.8	0.740	420	0.109 E-6	0.252 E-6
1	1691.4	0.800	756	0.277 E-6	0.360 E-6
1	1691.4	0.680	900	0.231 E-6	0.293 E-6
2	1691.4	0.760	330	0.133 E-6	0.322 E-6
3	1691.4	0.620	345	0.331 E-7	0.302 E-6
1	1701.0	0.480	510	0.281 E-6	0.359 E-6
2	1701.0	0.810	300	0.157 E-6	0.376 E-6
3	1701.0	0.520	240	0.186 E-6	0.361 E-6
3	1701.0	0.370	180	0.180 E-6	0.347 E-6
1	1710.5	0.360	316	0.340 E-6	0.431 E-6
1	1710.5	0.700	520	0.372 E-6	0.431 E-6
2	1710.5	0.850	260	0.189 E-6	0.450 E-6
2	1710.5	0.720	225	0.187 E-6	0.447 E-6
2	1710.5	0.420	155	0.170 E-6	0.386 E-6
3	1710.5	0.500	180	0.231 E-6	0.452 E-6
3	1710.5	0.310	120	0.221 E-6	0.428 E-6
1	1720.1	0.480	300	0.443 E-6	0.428 E-6
3	1720.1	0.320	100	0.270 E-6	0.521 E-6
1	1729.7	0.670	372	0.511 E-6	0.651 E-6
2	1729.7	0.580	123	0.271 E-6	0.636 E-6
1	1739.3	0.500	270	0.561 E-6	0.702 E-6

Reaction (4)

EXPT.	T in K	DEL m in mg	DEL t in min	P(S) in atm	P'S)corr in atm
2	1614.6	0.510	3480	0.138 E-7	0.327 E-7
2	1633.8	0.460	2040	0.209 E-7	0.497 E-7
2	1653.0	0.380	960	0.344 E-7	0.844 E-7
3	1653.0	0.510	2040	0.355 E-7	0.671 E-7
3	1672.2	0.370	840	0.581 E-7	0.113 E-6
2	1672.2	0.550	960	0.499 E-7	0.123 E-6
3	1681.8	0.540	1200	0.632 E-7	0.119 E-6
2	1691.4	0.850	1080	0.698 E-7	0.143 E-6
3	1691.4	0.490	840	0.796 E-7	0.152 E-6
1	1710.5	0.460	1176	0.187 E-6	0.235 E-6
2	1710.5	0.720	600	0.104 E-6	0.251 E-6
3	1710.5	0.520	540	0.124 E-6	0.242 E-6
1	1729.7	0.440	708	0.283 E-6	0.356 E-6
2	1729.7	0.230	135	0.148 E-6	0.353 E-6
3	1729.7	0.400	300	0.174 E-6	0.335 E-6
1	1748.9	0.600	660	0.407 E-7	0.516 E-6
1	1748.9	0.670	810	0.386 E-6	0.486 E-6
1	1748.9	0.740	930	0.377 E-6	0.472 E-6
2	1748.9	0.510	180	0.231 E-6	0.589 E-6
2	1748.9	0.590	240	0.211 E-6	0.505 E-6
2	1748.9	0.400	180	0.198 E-6	0.464 E-6
3	1748.9	0.510	270	0.246 E-6	0.471 E-6
1	1768.1	0.420	348	0.552 E-6	0.695 E-6
2	1768.1	0.490	135	0.306 E-6	0.734 E-6
3	1768.1	0.660	240	0.352 E-6	0.677 E-6
1	1787.3	0.500	240	0.867 E-6	0.111 E-5
1	1787.3	0.700	360	0.834 E-6	0.168 E-5
1	1787.3	0.480	270	0.793 E-6	0.100 E-5
2	1787.3	0.650	124	0.435 E-6	0.105 E-5
3	1787.3	0.450	100	0.540 E-6	0.167 E-5
1	1806.5	0.510	198	0.112 E-5	0.142 E-5
2	1806.5	0.850	112	0.618 E-6	0.149 E-5
3	1806.5	0.800	150	0.680 E-6	0.130 E-5
1	1825.7	0.600	150	0.165 E-5	0.211 E-5
1	1825.7	0.690	180	0.161 E-5	0.205 E-5
1	1825.7	0.760	198	0.161 E-5	0.205 E-5
1	1825.7	0.390	135	0.137 E-5	0.176 E-5
1	1825.7	0.370	120	0.143 E-5	0.177 E-5
2	1825.7	0.500	43	0.906 E-6	0.223 E-5
2	1825.7	0.700	66	0.857 E-6	0.207 E-5
1	1844.9	0.510	104	0.212 E-5	0.267 E-5
2	1844.9	0.620	40	0.122 E-5	0.297 E-5
3	1844.9	0.580	50	0.139 E-5	0.278 E-5
1	1864.1	0.610	75	0.321 E-5	0.413 E-5
2	1864.1	0.650	31	0.165 E-5	0.398 E-5
3	1864.1	0.500	30	0.195 E-5	0.381 E-5
3	1873.7	0.420	25	0.208 E-5	0.394 E-5
2	1883.3	0.650	22	0.228 E-5	0.553 E-5
3	1883.3	0.350	18	0.241 E-5	0.455 E-5
3	1892.8	0.290	12	0.291 E-5	0.555 E-5
2	1902.4	0.670	17	0.304 E-5	0.733 E-5
3	1902.4	0.540	16	0.375 E-5	0.743 E-5

1	1748.9	0.410	180	0.679 E-6	0.850 E-6
1	1748.9	0.710	312	0.678 E-6	0.849 E-6
1	1748.9	0.510	216	0.692 E-6	0.869 E-6
1	1748.9	0.600	276	0.661 E-6	0.825 E-6
1	1748.9	0.850	450	0.612 E-6	0.755 E-6
2	1748.9	0.820	110	0.408 E-6	0.968 E-6
2	1748.9	0.710	120	0.357 E-6	0.802 E-6
2	1748.9	0.670	116	0.352 E-6	0.786 E-6
3	1748.9	0.510	9[illegible]	0.466 E-6	0.892 E-6
3	1748.9	0.850	150	0.466 E-6	0.892 E-6
1	1758.5	0.520	189	0.812 E-6	0.102 E-5
3	1758.5	0.510	90	0.502 E-6	0.921 E-6
1	1768.1	0.580	170	0.984 E-6	0.123 E-5
2	1768.1	0.470	50	0.537 E-6	0.122 E-5
3	1768.1	0.550	70	0.649 E-6	0.122 E-5
1	1777.7	0.720	170	0.119 E-5	0.150 E-5
3	1777.7	0.360	45	0.704 E-6	0.128 E-5
1	1787.3	0.620	120	0.143 E-5	0.180 E-5
1	1787.3	0.640	134	0.137 E-5	0.171 E-5
1	1787.3	0.610	138	0.132 E-5	0.163 E-5
1	1787.3	0.560	111	0.141 E-5	0.177 E-5
1	1787.3	0.630	150	0.128 E-5	0.158 E-5
2	1787.3	0.500	37	0.761 E-6	0.172 E-5
2	1787.3	0.710	55	0.741 E-6	0.165 E-5
3	1787.3	0.770	70	0.904 E-6	0.168 E-5
3	1787.3	0.480	47	0.867 E-6	0.159 E-5
1	1796.9	0.550	97	0.162 E-5	0.201 E-5
3	1796.9	0.920	80	0.995 E-6	0.179 E-5
1	1806.5	0.680	104	0.188 E-5	0.233 E-5
3	1806.5	0.440	30	0.122 E-5	0.223 E-5
2	1811.3	0.410	2[illegible]	0.101 E-5	0.212 E-5
1	1816.1	0.540	66	0.229 E-5	0.284 E-5
2	1820.9	0.500	26	0.118 E-5	0.246 E-5
1	1825.7	0.730	80	0.260 E-5	0.321 E-5
1	1825.7	0.630	74	0.251 E-5	0.307 E-5
1	1825.7	0.820	102	0.243 E-5	0.296 E-5
2	1825.7	0.340	14	0.140 E-5	0.300 E-5
2	1825.7	0.590	25	0.137 E-5	0.293 E-5
3	1825.7	0.850	4[illegible]	0.162 E-5	0.287 E-5
3	1825.7	0.880	45	0.165 E-5	0.294 E-5
3	1825.7	0.260	10	0.139 E-5	0.234 E-5
2	1830.5	0.370	16	0.140 E-5	0.292 E-5
1	1835.3	0.560	54	0.300 E-5	0.367 E-5
2	1840.1	0.680	24	0.168 E-5	0.351 E-5
1	1844.9	0.590	50	0.344 E-5	0.420 E-5
2	1844.9	0.760	25	0.181 E-5	0.375 E-5
3	1844.9	0.520	18	0.235 E-5	0.419 E-5
2	1849.7	0.450	14	0.193 E-5	0.396 E-5
3	1854.5	0.530	16	0.271 E-5	0.479 E-5
3	1864.1	0.510	14	0.305 E-5	0.530 E-5

TABLE A2. P_{Al} vs T DATA FROM $TaAl_3/Ta_2Al_3$ REGION

T	P(Al)	T	P(Al)	T	P(Al)
1386	0.164E-06	1492	0.150E-05	1571	0.671E-05
1386	0.179E-06	1492	0.159E-05	1571	0.701E-05
1396	0.136E-06	1492	0.165E-05	1580	0.805E-05
1414	0.302E-06	1492	0.125E-05	1580	0.737E-05
1414	0.314E-06	1502	0.196E-05	1581	0.825E-05
1425	0.387E-06	1502	0.181E-05	1581	0.775E-05
1425	0.412E-06	1502	0.209E-05	1581	0.794E-05
1425	0 385E-06	1503	0.187E-05	1581	0.871E-05
1425	0.325E-06	1510	0.220E-05	1587	0.902E-05
1434	0.356E-06	1510	0.247E-05	1587	0.860E-05
1435	0.426E-06	1512	0.172E-05	1591	0.670E-05
1435	0.512E-06	1512	0.143E-05	1591	0.570E-05
1435	0 318E-06	1512	0.175E-05	1591	0.671E-05
1435	0.541E-06	1513	0.152E-05	1591	0.565E-05
1435	0.204E-06	1519	0.170E-05	1596	0.692E-05
1435	0.351E-06	1529	0.341E-05	1606	0.118E-04
1435	0.364E-06	1529	0.307E-05	1606	0.122E-04
1453	0.722E-06	1531	0.313E-05	1610	0.111E-04
1453	0.803E-06	1531	0.340E-05	1610	0.134E-04
1453	0.694E-06	1531	0.270E-05	1610	0.129E-04
1453	0.739E-06	1531	0.353E-05	1610	0.108E-04
1453	0.703E-06	1532	0.317E-05	1620	0.150E-04
1454	0.564E-06	1532	0.343E-05	1620	0.154E-04
1463	0.898E-06	1541	0.417E-05	1621	0.164E-04
1464	0.855E-06	1542	0.385E-05	1621	0.157E-04
1464	0.868E-06	1542	0.437E-05	1625	0.164E-04
1464	0.951E-06	1542	0.399E-05	1625	0.164E-04
1472	0.108E-05	1548	0.434E-05	1629	0.169E-04
1473	0.119E-05	1548	0.480E-05	1630	0.107E-04
1473	0.787E-06	1551	0.299E-05	1630	0.122E-04
1473	0.641E-06	1551	0.356E-05	1634	0.115E-04
1473	0.709E-06	1551	0.350E-05	1645	0.221E-04
1473	0.801E-06	1551	0.291E-05	1649	0.202E-04
1481	0.770E-06	1558	0.349E-05	1650	0.240E-04
1482	0.123E-05	1568	0.666E-05	1660	0.301E-04
1482	0.137E-05	1568	0.614E-05	1661	0.290E-04
1491	0.167E-05	1571	0.553E-05	1673	0.187E-04
1491	0.158E-05	1571	0.601E-05	1713	0.326E-04

TABLE A3. P_{Al} vs T DATA FROM $Ta_2/Al_3/Ta_2Al$ REGION

T	P(Al)	T	P(Al)	T	P(Al)
1386	0.191E-06	1483	0.172E-05	1568	0.531E-05
1386	0.197E-06	1483	0.146E-05	1568	0.610E-05
1386	0.190E-06	1483	0.153E-05	1568	0.628E-05
1387	0.184E-06	1490	0.162E-05	1568	0.512E-05
1387	0.200E-06	1491	0.160E-05	1568	0.581E-05
1425	0.424E-06	1491	0.135E-05	1577	0.752E-05
1425	0.413E-06	1491	0.143E-05	1577	0.759E-05
1435	0.549E-06	1491	0.155E-05	1577	0.651E-05
1435	0.584E-06	1491	0.159E-05	1578	0.714E-05
1435	0.560E-06	1491	0.908E-06	1578	0.688E-05
1435	0.294E-06	1491	0.131E-05	1578	0.735E-05
1435	0.537E-06	1500	0.195E-05	1580	0.927E-05
1435	0.650E-06	1500	0.191E-05	1580	0.908E-05
1435	0.507E-06	1501	0.191E-05	1580	0.882E-05
1435	0.565E-06	1501	0.187E-05	1580	0.867E-05
1435	0.604E-06	1501	0.187E-05	1580	0.952E-05
1435	0.623E-06	1501	0.167E-05	1580	0.930E-05
1435	0.515E-06	1510	0.225E-05	1580	0.899E-05
1435	0.546E-06	1510	0.237E-05	1580	0.952E-05
1435	0.507E-06	1510	0.230E-05	1580	0.940E-05
1435	0.519E-06	1510	0.222E-05	1580	0.857E-05
1435	0.450E-06	1510	0.225E-05	1580	0.922E-05
1435	0.619E-06	1511	0.200E-05	1580	0.911E-05
1435	0.574E-06	1511	0.195E-05	1580	0.979E-05
1435	0.394E-06	1511	0.191E-05	1580	0.993E-05
1435	0.440E-06	1519	0.278E-05	1587	0.771E-05
1435	0.530E-06	1519	0.274E-05	1587	0.880E-05
1435	0.569E-06	1520	0.238E-05	1587	0.877E-05
1435	0.655E-06	1520	0.271E-05	1587	0.830E-05
1444	0.614E-06	1520	0.266E-05	1587	0.861E-05
1444	0.638E-06	1520	0.251E-05	1587	0.725E-05
1444	0.627E-06	1528	0.326E-05	1587	0.693E-05
1444	0.561E-06	1529	0.331E-05	1587	0.805E-05
1444	0.642E-06	1529	0.315E-05	1596	0.995E-05
1444	0.361E-06	1529	0.282E-05	1596	0.103E-04
1444	0.608E-06	1529	0.264E-05	1596	0.102E-04
1453	0.771E-06	1529	0.290E-05	1596	0.896E-05
1453	0.767E-06	1529	0.322E-05	1597	0.975E-05
1453	0.778E-06	1529	0.269E-05	1597	0.894E-05
1453	0.621E-06	1531	0.385E-05	1597	0.949E-05
1453	0.743E-06	1531	0.358E-05	1605	0.113E-04
1454	0.779E-06	1531	0.368E-05	1606	0.104E-04
1454	0.684E-06	1531	0.395E-05	1606	0.104E-04
1454	0.642E-06	1531	0.379E-05	1606	0.114E-04
1454	0.441E-06	1531	0.375E-05	1606	0.119E-04
1462	0.951E-06	1531	0.407E-05	1606	0.117E-04
1463	0.852E-06	1531	0.389E-05	1606	0.975E-05
1463	0.939E-06	1531	0.385E-05	1606	0.933E-05
1463	0.904E-06	1531	0.430E-05	1606	0.110E-04
1463	0.947E-06	1532	0.369E-05	1615	0.131E-04
1463	0.545E-06	1532	0.382E-05	1615	0.123E-04
1472	0.114E-05	1532	0.429E-05	1616	0.120E-04
1472	0.111E-05	1532	0.389E-05	1616	0.131E-04
1472	0.937E-06	1538	0.338E-05	1616	0.138E-04
1472	0.112E-05	1539	0.392E-05	1616	0.139E-04
1472	0.102E-05	1539	0.397E-05	1616	0.128E-04
1473	0.644E-06	1539	0.376E-05	1624	0.150E-04
1473	0.108E-05	1539	0.385E-05	1625	0.147E-04
1473	0.922E-06	1539	0.351E-05	1625	0.143E-04
1481	0.134E-05	1548	0.471E-05	1625	0.161E-04
1482	0.129E-05	1548	0.383E-05	1626	0.139E-04
1482	0.133E-05	1548	0.369E-05	1629	0.208E-04
1482	0.782E-06	1548	0.399E-05	1629	0.199E-04
1482	0.147E-05	1548	0.453E-05	1629	0.209E-04
1482	0.152E-05	1549	0.412E-05	1629	0.213E-04
1482	0.157E-05	1558	0.542E-05	1629	0.188E-04
1482	0.164E-05	1558	0.473E-05	1629	0.205E-04
1482	0.146E-05	1558	0.559E-05	1629	0.215E-04
1482	0.149E-05	1558	0.522E-05	1634	0.171E-04
1482	0.158E-05	1558	0.488E-05	1635	0.178E-04
1482	0.155E-05	1558	0.537E-05	1635	0.167E-04
1482	0.164E-05	1567	0.553E-05	1635	0.176E-04
1483	0.174E-05	1568	0.638E-05	1645	0.197E-04

TABLE A4. P_{Al} vs T DATA FROM σ-PHASE REGION

T	P(Al)	T	P(Al)	T	P(Al)
1321	0.108E-07	1398	0.113E-06	1548	0.161E-05
1321	0.149E-07	1398	0.907E-07	1548	0.173E-05
1321	0.116E-07	1398	0.119E-06	1548	0.175E-05
1321	0.143E-07	1398	0.916E-07	1548	0.171E-05
1321	0.141E-07	1398	0.874E-07	1548	0.166E-05
1321	0.149E-07	1398	0.706E-07	1548	0.159E-05
1321	0.117E-07	1398	0.687E-07	1548	0.170E-05
1321	0.108E-07	1398	0.119E-06	1548	0.176E-05
1321	0.122E-07	1398	0.149E-06	1548	0.176E-05
1321	0.186E-07	1398	0.722E-07	1548	0.160E-05
1322	0.181E-07	1398	0.704E-07	1548	0.154E-05
1322	0.147E-07	1398	0.708E-07	1548	0.154E-05
1322	0.199E-07	1398	0.800E-07	1548	0.153E-05
1322	0.176E-07	1471	0.373E-06	1548	0.169E-05
1322	0.194E-07	1471	0.332E-06	1548	0.166E-05
1322	0.158E-07	1471	0.359E-06	1548	0.171E-05
1322	0.162E-07	1471	0.342E-06	1548	0.167E-05
1322	0.155E-07	1471	0.361E-06	1548	0.162E-05
1322	0.165E-07	1471	0.371E-06	1549	0.164E-05
1323	0.224E-07	1471	0.381E-06	1549	0.187E-05
1323	0.193E-07	1471	0.356E-06	1549	0.169E-05
1323	0.148E-07	1472	0.379E-06	1549	0.165E-05
1323	0.267E-07	1472	0.319E-06	1549	0.191E-05
1323	0.184E-07	1472	0.377E-06	1549	0.183E-05
1323	0.166E-07	1472	0.376E-06	1549	0.190E-05
1323	0.174E-07	1472	0.383E-06	1549	0.193E-05
1323	0.137E-07	1472	0.364E-06	1549	0.181E-05
1323	0.126E-07	1472	0.382E-06	1549	0.185E-05
1323	0.278E-07	1472	0.358E-06	1549	0.189E-05
1395	0.585E-07	1472	0.387E-06	1549	0.194E-05
1396	0.715E-07	1472	0.365E-06	1549	0.192E-05
1396	0.702E-07	1472	0.377E-06	1550	0.205E-05
1396	0.597E-07	1472	0.406E-06	1550	0.212E-05
1396	0.632E-07	1472	0.349E-06	1550	0.203E-05
1396	0.724E-07	1472	0.321E-06	1550	0.232E-05
1396	0.640E-07	1472	0.351E-06	1550	0.206E-05
1396	0.665E-07	1472	0.366E-06	1550	0.227E-05
1396	0.752E-07	1472	0.381E-06	1550	0.237E-05
1396	0.633E-07	1472	0.348E-06	1550	0.198E-05
1396	0.671E-07	1472	0.410E-06	1550	0.244E-05
1396	0.701E-07	1472	0.293E-06	1550	0.211E-05
1396	0.737E-07	1472	0.271E-06	1550	0.207E-05
1396	0.723E-07	1472	0.409E-06	1550	0.237E-05
1396	0.711E-07	1472	0.427E-06	1550	0.243E-05
1396	0.680E-07	1472	0.344E-06	1550	0.241E-05
1396	0.784E-07	1472	0.419E-06	1550	0.201E-05
1396	0.632E-07	1473	0.255E-06	1550	0.180E-05
1396	0.733E-07	1473	0.284E-06	1550	0.210E-05
1396	0.689E-07	1473	0.389E-06	1550	0.180E-05
1396	0.116E-06	1473	0.403E-06	1550	0.180E-05
1396	0.658E-07	1473	0.386E-06	1550	0.183E-05
1396	0.725E-07	1473	0.410E-06	1550	0.236E-05
1396	0.736E-07	1473	0.421E-06	1550	0.237E-05
1396	0.677E-07	1473	0.357E-06	1550	0.179E-05
1396	0.871E-07	1473	0.421E-06	1625	0.598E-05
1396	0.429E-07	1473	0.435E-06	1625	0.621E-05
1397	0.729E-07	1473	0.461E-06	1626	0.691E-05
1397	0.795E-07	1473	0.426E-06	1626	0.625E-05
1397	0.892E-07	1473	0.530E-06	1626	0.649E-05
1397	0.850E-07	1473	0.450E-06	1626	0.677E-05
1398	0.851E-07	1473	0.457E-06	1627	0.733E-05
1398	0.101E-06	1473	0.384E-06	1628	0.815E-05
1398	0.857E-07	1473	0.541E-06	1628	0.880E-05
1398	0.123E-06	1473	0.465E-06	1628	0.796E-05
1398	0.122E-06	1473	0.368E-06	1628	0.876E-05
1398	0.119E-06	1473	0.380E-06	1628	0.868E-05
1398	0.104E-06	1474	0.432E-06	1628	0.738E-05
1398	0.934E-07	1474	0.380E-06	1628	0.806E-05
1398	0.108E-06	1474	0.378E-06	1628	0.813E-05
1398	0.899E-07	1474	0.548E-06	1628	0.808E-05
1398	0.823E-07	1548	0.157E-05	1628	0.724E-05
1398	0.886E-07	1548	0.155E-05	1628	0.866E-05
1398	0.124E-06	1548	0.160E-05	1628	0.707E-05

TABLE A5. P_{Al} vs T DATA FROM Ta_4Al/Ta REGION

T	P(Al)	T	P(Al)	T	P(Al)
1321	0.864E-08	1471	0.278E-06	1547	0.101E-05
1321	0.116E-07	1471	0.290E-06	1548	0.130E-05
1321	0.911E-08	1471	0.268E-06	1548	0.137E-05
1396	0.526E-07	1471	0.281E-06	1548	0.137E-05
1396	0.503E-07	1471	0.274E-06	1548	0.136E-05
1396	0.460E-07	1471	0.301E-06	1548	0.136E-05
1396	0.493E-07	1472	0.297E-06	1548	0.137E-05
1396	0.481E-07	1472	0.303E-06	1548	0.133E-05
1396	0.644E-07	1472	0.189E-06	1548	0.134E-05
1396	0.469E-07	1473	0.169E-06	1549	0.872E-06
1396	0.519E-07	1473	0.171E-06	1550	0.825E-06
1396	0.560E-07	1489	0.270E-06	1566	0.133E-05
1417	0.477E-07	1489	0.316E-06	1567	0.149E-05
1432	0.701E-07	1489	0.303E-06	1567	0.147E-05
1432	0.732E-07	1489	0.324E-06	1567	0.145E-05
1433	0.891E-07	1491	0.272E-06	1569	0.125E-05
1433	0.839E-07	1492	0.257E-06	1569	0.121E-05
1433	0.847E-07	1492	0.253E-06	1585	0.190E-05
1434	0.793E-07	1508	0.407E-06	1585	0.212E-05
1435	0.730E-07	1509	0.462E-06	1585	0.202E-05
1435	0.552E-07	1509	0.478E-07	1586	0.207E-05
1435	0.698E-07	1509	0.473E-06	1588	0.179E-05
1451	0.110E-06	1511	0.410E-06	1589	0.172E-05
1451	0.115E-06	1511	0.388E-06	1604	0.273E-05
1452	0.131E-06	1512	0.381E-06	1605	0.298E-05
1452	0.136E-06	1527	0.611E-06	1605	0.299E-05
1452	0.144E-06	1528	0.703E-06	1605	0.286E-05
1453	0.122E-06	1528	0.701E-06	1607	0.248E-05
1454	0.113E-06	1528	0.705E-06	1607	0.245E-05
1454	0.115E-06	1530	0.595E-06	1624	0.422E-05
1469	0.171E-06	1531	0.574E-06	1624	0.396E-05
1470	0.202E-06	1531	0.570E-06	1625	0.531E-05
1470	0.176E-06	1547	0.900E-06	1625	0.538E-05
1470	0.219E-06	1547	0.102E-05	1626	0.532E-05
1470	0.208E-06	1547	0.100E-05	1626	0.530E-05

X. APPENDIX B: PHASE TRANSITIONS IN MANGANESE ARSENIDE

A. Introduction

Much of what may be regarded as creative or original in scientific endeavors is essentially the unprecedented pairing of existing techniques or paradigms with problems which also have a history. Whether or not the tests of time and subsequent study prove that such initial attempts were insightful or merely clever and unusual, attacking old problems with tools not previously recognized as most appropriate for their solution has both probable and potential, (but not guaranteed) value. Specifically, it most likely will result, at the very least, in (i) a greater appreciation of the strengths and limitations in application of the technique in question. In addition, it can (ii) reveal additional facets of the problem or system being studied and suggest paths to their resolution, if not actually solving them. And finally, if an investigator is fortunate, his/her viewing the situation from an uncommon angle can lead to open-mindedness conducive to (iii) a discovery that was not the original aim of the project.

The author's reinvestigation of the phase transitions in manganese arsenide (MnAs) using the Rietveld, or total profile analysis method was (at the outset) recognized as an example of the sort of undertaking just described. It is regarded in retrospect as having paid dividends in the sense of (i) and (ii) above, and intermediate developments briefly inspired hope that a revelation as in (iii) would occur. When the latter did not come about and the significance of the results was weighed vs

those of the Ta-Al and Ta-S studies, it was decided to feature the thermochemistry while reporting the Rietveld analysis here in a separate appendix. While admittedly the order and format of this reporting were arbitrarily chosen, their intended purpose is to clearly distinguish this section as unrelated and subordinate to the thermodynamics results of the main text while still paying due attention to a piece of work believed to be worthwhile in its own right. The exposition here was approached in proportion to this project's relative significance and is therefore less detailed, especially in terms of discussion of results, than in the main body of the dissertation.

B. Phase Behavior of MnAs and Phase Transitions in General

Phase transitions, taken in the broadest sense, are probably as frequently observed by the general public as well as by physical scientists as any type of natural phenomenon. As one limits focus to consider more specific kinds of phase transitions, however, one encounters less common events which are not as easily detected as the dramatic and familiar melting of ice or boiling of liquid water. The latter are examples of 1st-order phase changes, in which the molar volume and entropy of a substance, both first derivatives of its chemical potential, jump discontinuously at some point in thermodynamic space. First order transitions are not limited to changes in 'states of aggregation' (solid ⇔ liquid, solid ⇔ gas, liquid ⇔ gas), but also include transformations from one solid form to another, as in the equilibrium between rhombic and monoclinic sulfur at ~95°C. An additional category, 2nd-order

transitions, includes other solid-solid transformations in which the associated observable effects are even more subtle. Here, the discontinuities with respect to T and P occur in second-and higher-order derivatives of the chemical potential such as heat capacity (e.g., the lambda point in β-brass) or isothermal compressibility, but not in $\bar{V}$ and S. Other criteria distinguishing 1st-order from 2nd-order processes are that (i) two phases coexist in equilibrium in a 1st-order transition but not in the 2nd-order type and (ii) no measurable variable "anticipates" the abrupt property increments about to occur as a 1st-order transition point is neared, while for 2nd order processes it is possible at least in principle to observe continuous variations in certain quantities in that region of thermo space. In certain cases, one observes changes in (i) crystal structure, which changes culminate in the gain (or loss) of symmetry elements at the transition point, or in (ii) C_p^o which has a gradual rise close to the transition point.

In addition to the aforementioned observations via which one may characterize continuous or 2nd-order processes (a few relevant examples will be cited later), there exist theoretical treatments, the most noteworthy of which, by Landau[1] clearly spells out criteria that must be met if a process is to be labeled '2nd-order'. In the discussion of Landau's theory by Franzen,[2] there is an emphasis on its relevance to chemistry, and the ways in which the theory relates thermodynamics to symmetry properties are illustrated both schematically and through examples. One salient aspect of this treatment is its expression of the Gibbs free

energy of a solid in terms of a disorder parameter, η. It was recognized that this is usually a quantity whose functional form is only qualitatively known. A desire to accurately determine the η parameter for a known 2nd-order transition was the initial motivation for this study and for some time that remained the sole purpose.

The aspects of the phase behavior of MnAs which are immediately relevant to this effort will be summarized first, with more detailed exposition of these and other known properties to come later. MnAs is found to exhibit two closely related crystalline modifications: a hexagonal ($P6_3/mmc$) form of NiAs-type structure (Figure B1) and an orthorhombic (Pnma) form of MnP-type. What is unusual is that the more symmetrical hexagonal structure occurs <u>below</u> as well as above the temperature range (39°-125°C) in which the distorted orthorhombic structure is stable, while ordinarily one expects the higher symmetry form to exist at higher temperature. While a phase transition between these structures meets the Landau criteria alluded to above (e.g., group-subgroup relationship between $P6_3/mmc$ and Pnma), only the transition at ~125°C was considered to be of 2nd order while surprisingly, a clearly 1st order transition occurs at ~39°C. That is an interesting point in itself and one on which much study on MnAs has been centered. The focus here, however, was on characterization of the second order change as T approaches ~125°C. To accomplish this, the broad objective was to measure and analyze X-ray powder diffraction profiles for precise determination of both lattice parameters and atomic positions.

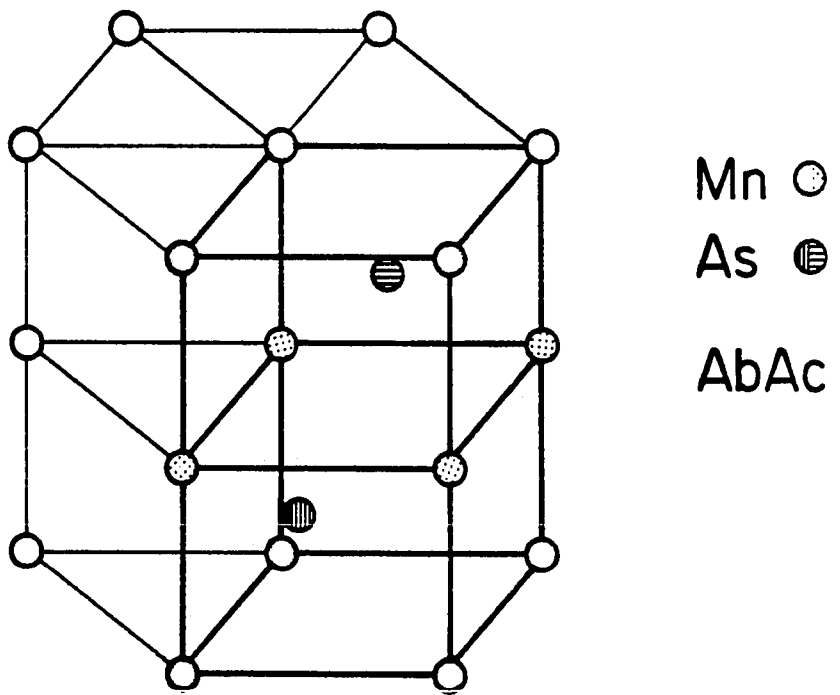

Figure B1. NiAs-type (hexagonal) structure of MnAs emphasizing a single unit cell and the AbAc stacking of hcp layers. Mn atoms are at z = 0 and $^1/_2$, As atoms at $^1/_4$ and $^3/_4$

C. Experimental Approach

The choice of specific experimental and data analysis techniques was not difficult. For most continuous transitions the obvious method for achieving our aims would be temperature-dependent Guinier camera measurements, then carefully analysis of the pattern's line positions for lattice parameter determination, as done by Franzen and Wiegers[3] for the transition by VS, and then determination of the relative intensities of appropriately chosen lines for calculation of atomic coordinates (as in the study of β-SnS and β-SnSe by von Schnering and Wiedemeier[4]). However, because there are, due to the relatively high symmetries involved for MnAs, many 2θ regions in the powder data with overlap of multiple lines, and because the even more important information contained in nonoverlapped superstructure lines could be beyond the sensitivity of film techniques due to the small extent of structural distortion,[5] Guinier analysis was deemed inadequate. The alternative of the Rietveld or total-profile method was chosen because it can in principle overcome both of these difficulties, as will be explained in a section describing the technique.

D. Historical Background on MnAs

The perceived importance of MnAs as a subject of study is clear to a reviewer of the literature; an unfolding of its history will convey that as well as setting the stage for presenting the potential implications of the Rietveld analysis and its supporting experiments.

The earliest reported experiments by Bates[6] (1929), Serres[7] (1947), and Guillaud[8] (1951) focused on the magnetic ordering behavior of MnAs, which was undisputedly of ferromagnetic character below the transition at 39°C. These first three experimenters all performed temperature-dependent susceptibility measurements, which they interpreted as indicative of antiferromagnetic ordering above T_1 (39°C) because of the characteristic rise in χ with T. Cursory neutron diffraction experiments on powdered MnAs by Bacon and Street[9] (1955) failed to confirm any magnetic ordering in this intermediate region. In the meantime, Willis and Rooksby[10] (1954) did the only systematic determination of lattice parameter dependence on T, but claimed the symmetry was hexagonal both below and above T_1, and also rationalized the discontinuity in unit cell volume at T_1 as consistent with a ferromagnetic → antiferromagnetic (F→A) change. Kornelson[11] (1961) was the first to show that the MnP-type orthorhombic symmetry existed above T_1, concluding this from line splittings in well-resolved X-ray powder diffraction profiles. Other studies returned to the antiferromagnetic ordering controversy and attempted to reconcile the susceptibility and neutron diffraction results, which argue respectively for and against A ordering. Kittel,[12] in a theoretical treatment and Basinski, Kornelson and Pearson[13] (1961) and Frazer and Brown[14] (1961) with χ vs T measurements supported the claim for A-ordering. Bean and Rodbell[15] (1962), with a theory and deBlois and Rodbell[16] (1963) with supporting experiments showed that a first-order or discontinuous volume change at T_1 was not inconsistent with an F→P (paramagnetic) transition

and adopted the view that the latter is a correct description of the magnetic behavior above T_1. This view remained the general consensus for some time. It is internally consistent in accounting for most of the observations of the phase behavior of MnAs, and is not refuted by the observation of a λ-point in C_p vs T at T_2 (~120°C) by Grønvold, Snildal and Westrum[17] (1970). That feature can be attributed to a continuous structural change (but not necessarily a concomitant change in magnetic order) between the intermediate and high-T regions, but the rise in χ with T for 39°C < T < 125°C remained unexplained. Goodenough and Kafalas[18] (1967) proposed a theoretical explanation invoking a high spin → low spin change in Mn atoms at T_1, but this was discredited by Schwartz, Hall, and Felcher (1971)[19] whose neutron scattering experiments showed no such spin change.

Probably the most relevant or similarly motivated study for this work was that by Wilson and Kasper[5] (1964) on single crystal MnAs. In that investigation intensity data were taken from a twinned crystal of MnAs at 55°C, at which temperature the distortion from hexagonal symmetry should be near its maximum extent since the structure is believed to revert continuously to NiAs form as T_2 is approached. Their relevant findings were (i) the smallness of the distortion in the atomic coordinates Z_{Mn} and X_{As} (relative to that in the structure of MnP, e.g.) and (ii) qualitative verification that superstructure lines of type hkl, k + l = 2n + 1 diminish in intensity as T nears T_2, although refinement of the structure from this latter information was not attempted. That was the unfinished task taken on by the current work.

After over a decade during which no further enlightening work on MnAs was reported, a theoretical explanation of its phase behavior was published by Kato et al.[20] (1983). Their model arguably accounts for the antiferromagnetic-like susceptibility vs temperature curves without the need for magnetic ordering. Awareness of this explanation did not occur until the Rietveld analysis was well underway and an additional experiment (neutron diffraction) had been arranged. Comparison of current findings with those of Kato et al. and additional comments on their contribution to the problem's resolution is contained in the discussion section.

E. The Rietveld Method

As mentioned earlier, it is often impossible to make use of all the structural information in a powder pattern if integrated intensities of peaks in the pattern are used, because regions where peaks overlap strongly are not easily resolved into their individual contributing reflections. The Rietveld method, named for its inventor,[21] takes the alternative approach of fitting a structural model to the entire diffraction profile and thereby dealing with the complex shape of the overlapped regions. In fitting to the whole pattern, this approach also makes use of the presence or absence of peaks in addition to those likely to be observed and indexed by visual inspection of film, and so truly obtains the maximum information available from powder diffraction data. As pointed out by Werner[22] (1981) the Rietveld technique has its ultimate importance and power in refinement of structures for which a reasonable

guess already exists, and is augmented by use of the most accurate relative intensity data, achieved by step scanning with a powder diffractometer.

While the method was developed by Rietveld for analysis of neutron diffraction data originally, it has been modified numerous times to deal with X-ray profiles as well. A major obstacle to this adaptation was acquiring a function to accurately describe the shape of an X-ray powder diffraction peak. As discussed by Wiles and Young[23] (1981) and by Santoro and Prince[24] this seems to be best accomplished by various contrived functions, e.g., 'pseudo-Voigt' or 'Pearson VII' functions which are intermediate in form between Lorentzian and Gaussian lineshapes (see Figure B2).

Specifically, the Rietveld method, as implemented in the FORTRAN program used here, due to Wiles and Young minimizes a weighted nonlinear sum-of-squares residual:

$$R = \sum_i W_i |Y_{i,o} - Y_{i,c}|^2$$

in which the weights W_i are defined as $1/\sigma_i^2$, σ_i being the estimated standard deviation in the measured intensity $Y_{i,o}$ at a given angle $2\Theta_i$ in the profile. $Y_{i,c}$ is calculated from an equation of the form

$$Y_{i,c} = A \sum_k L_k |F_k|^2 \phi (2\Theta_i - 2\Theta_k) P_k + Y_{bi}$$

in which parameters have the following meaning:

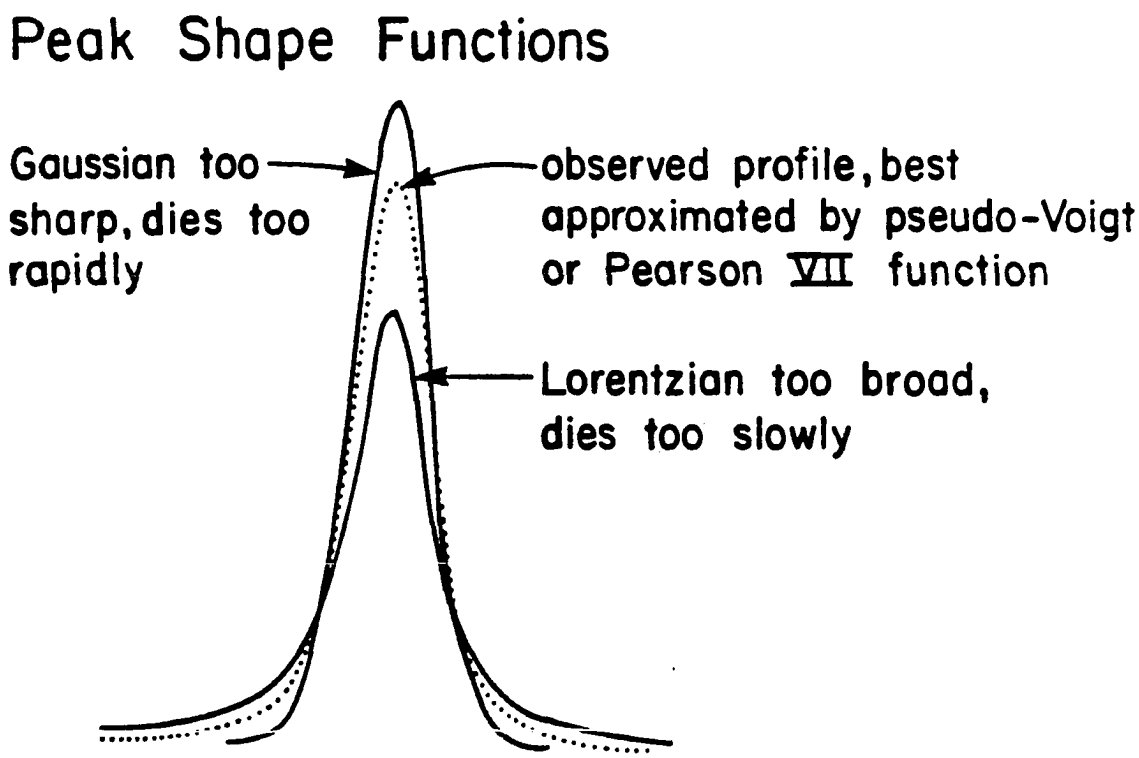

Figure B2. Comparison of peak shape functions used in attempts to fit X-ray diffraction profiles. All peaks have the same total area and FWHM

A	scale factor
L_k	combined Lorentz, polarization, and multiplicity factors
F_k	structure factor
P_k	preferred orientation function
ϕ	profile function, including asymmetry
Y_{bi}	background intensity

The background intensity is approximated by a polynominal with terms to fifth order in 2Θ. The $Y_{i,c}$ at a given step may contain contributions from the "tails" of several nearby peaks.

The actual minimization uses the matrix method known as the Newton-Raphson algorithm. Ordinarily, the criterion for goodness of fit is the weighted profile R factor:

$$R_{pw} = \frac{\sum W_i[Y_{i,o}-Y_{i,c}]^2}{\sum W_i[Y_{i,o}]^2}$$

of which the numerator is the minimized quantity. Although this is the most meaningful measure of accuracy of a refinement, it is not useful in comparisons with fits to data from other diffractometers or unrelated compounds because fit quality is affected by undeterminable instrumental factors and by variation in sample quality. In addition, $R_{p,w}$ is not relevant for comparison with single crystal R-factors (which are defined differently) and therefore it is desirable to derive from a

Rietveld fit some quantity that makes such comparisons possible. That quantity is

$$R_B \equiv \frac{\sum_k |'I_{k,o}' - I_{k,c}|}{\sum_k 'I_{k,o}'}$$

in which $I_{k,c}$ and $'I_{k,o}'$ are integrated intensities for given reflections K which come, respectively, from the area under an idealized calculated peak and from contributions to the net observed peak area assumed to be allocated in the same proportions as those in the model. R_B is flawed in that this proportional allocation of intensities biases the fit in favor of the starting model, and must be used with that caveat in mind. Interestingly, R_B can be impressively small (e.g., ~5%) even when visual comparison of the calculated and observed fits shows relatively severe discrepancies in fitting individual peaks, because it relies on peak area, not peak shape. It is therefore best regarded as an indicator of correctness of the structural parameters in the model (as opposed to those factors affecting peak shape or those due to crystallite orientation).

In summary, one employs the method by making a starting guess of both structural variables (lattice parameters, temperature factors, and atomic positions, etc.) and instrument- and sample-dependent variables (peak shape parameters, preferred orientation, 2Θ zero point correction, etc.) and allowing refinement to proceed until some predetermined iteration-terminating criterion is met.

F. Experimental

1. Sample preparation

Single phase MnAs samples were made using a typical high temperature synthetic technique in which the reactants are sealed in an evacuated fused silica ('quartz glass') tube, heated until initial stage reaction stops, cooled to room temperature, then homogenized by fine grinding and repeated high temperature annealings similar to the first heating step. In detail, this was accomplished as follows: amounts of elemental As (lump form, Puratronic, m 99.9999%) and Mn (granular, m 99.9%) corresponding to a 5-10 atomic % excess of As and totaling up to 15 g in mass were melted together at temperatures up to 900°C. Early trials in which the silica container cracked while cooling led to the precaution of sealing one such tube inside another for an extra layer of protection from oxidizing environments. After this first step, a large solid mass resulted, the pulverization of which, using a mortar and pestle, usually required considerable effort. The second step was usually performed at about 850°C-900°C for 3-4 days with one end of the reaction tube extending slightly out of the hot zone of a horizontal tube furnace to allow condensation of unreacted arsenic. It was expected that this would result in nearly stoichiometric MnAs, as the compound's homogeneity range had been reported as $MnAs_{0.98}$ to $MnAs_{1.00}$,[17] and indeed a chemical analysis performed by Ames Laboratory analyst M. Tschetter yielded $MnAs_{1.002}$. This same sample exhibited NiAs-type structure in a Guinier

powder diagram (Table B1) and yielded a_0 = 3.7190(2) Å, c_0 = 5.705(1) Å, c_0/a_0 = 1.534 . Previously reported values (see Table B2) in the literature ranged from 3.72 to 3.725 for a_0 and 5.702 to 5.713 for c_0. Separation of the product from bulk contaminants such as fragments of glass from the reaction tube was easily achieved by using a strong magnet since MnAs is ferromagnetic at room temperature.

2. Data collection

As compared with a routine powder diffractometer scan, only minor adaptations were necessary for these measurements. A schematic diagram of the sample holder is seen in Figure B3. At the outset, heating of the aluminum sample holder was accomplished using only an Acra-Watt resistive patch heater of 10 Watt rating attached to the bottom of the holder. To achieve higher temperatures and to minimize temperature gradients in the sample, the holder was also heated radiatively from above using a 250 Watt infrared lamp. Power inputs from both the patch heater and the IR lamp were controlled using a Variac to continuously adjust the applied voltage. Temperature of the sample was monitored both from below and above using identical chromel-alumel thermocouples attached to AD 2050 digital meters. In this manner, a desired temperature could be achieved manually; adjusting the two power inputs in a roughly proportional fashion was attempted to avoid thermal gradients. The latter were seen to consistently be 2°C or less from top to bottom of the sample holder,

Table B1. Guinier X-ray diffraction data on polycrystalline MnAs at room temperature. Indexing corresponds to $P6_3/mmc$. CuKα radiation was used

2θ	d(Å)	h k ℓ
27.666	3.222	1 0 0
31.311	2.854	0 0 2
31.882	2.805	1 0 1
42.284	2.136	1 0 2
49.938	1.860	1 1 0
59.601	1.550	2 0 1
65.392	1.4260	0 0 4
66.628	1.4025	2 0 2
77.620	1.2290	2 0 3
80.644	1.1904	2 1 1
85.788	1.1317	1 1 4
86.922	1.1198	2 1 2

Table B2. Lattice constants (in Å) of hexagonal ($P6_3/mmc$) MnAs at room temperature

a_0	c_0	References
3.7185(3)	5.7037(6)	this work, sample #4
3.7190(2)	5.705(1)	this work, sample #3
3.720(1)	5.710(2)	25
3.72	5.71	26
3.722	5.702	27
3.725	5.713	28
3.724	5.706	10

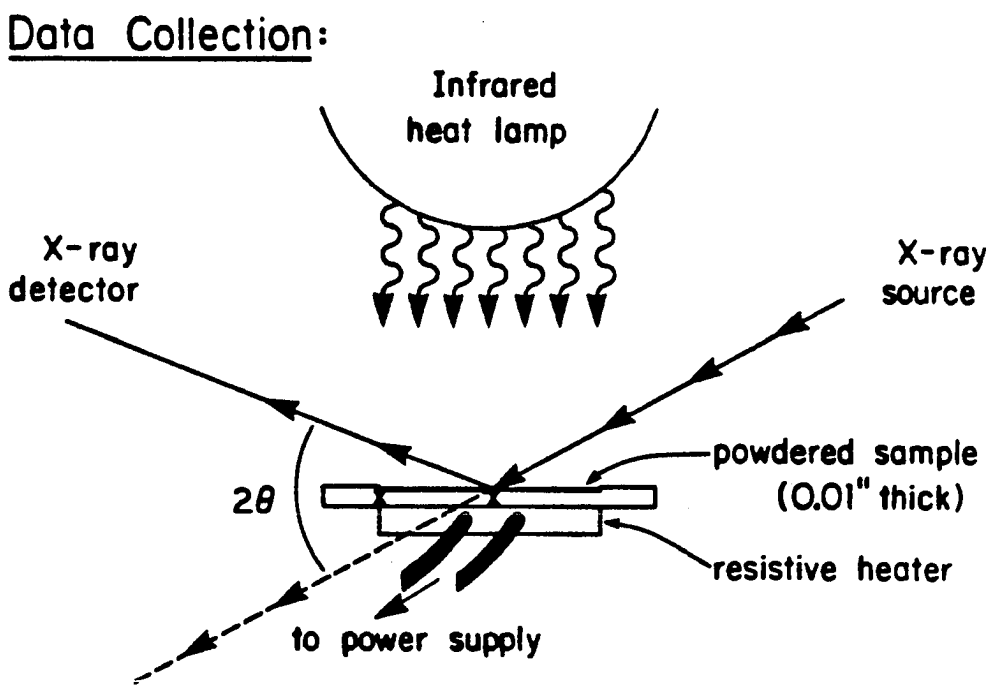

Figure B3. Schematic diagram of the powder diffractometer as adapted for use at elevated temperatures. "X" indicates positions of thermocouples

and stability of a temperature for a fixed power input was approximately ±2°C for as long as 12 hrs even though no feedback control was employed.

Because intensity data of excellent and reproducible quality were desired, various tests of sample and scanning characteristics were done to determine their effectiveness in improving the profile. By trial and error it was first determined that a step size of 0.02° to 0.03° in 2θ was optimum. This proved to be the angular increment below which no real improvement in detail of a profile could be attained.

Three common sources of intensity errors and suggested practices for their elimination are described by Klug and Alexander.[29] For each type of error, short scans of the (101) peak in the MnAs room temperature profile were repeated with varying scan-time and sample characteristics to determine amounts of correction necessary to achieve acceptable reproducibility in the intensities. The first type of error is random statistical fluctuation in the X-ray photon rate as counted by the detector, presumed due to instability in either the intensity of the incident X-ray beam or in the detector response. This fluctuation is a type of high frequency noise, which is expected to average to zero given sufficient time, and therefore longer counting times at each 2θ should result in greater reproducibility in I_{obs}. A second source of error, caused by too large an average particle size, is the random nonrepresentative distribution of Bragg scattering planes; i.e., even in the absence of preferred orientation the crystallites will not necessarily lie in an arrangement which exposes Bragg planes to the incident beam in proportion to their relative multiplicities, because there are too few crystallites

in the effective volume "seen" by the beam. Thus, the heights of diffraction peaks relative to each other will be different with each deposition of a sample, and a meaningful test would be to observe what scatter resulted in the step-by-step average of intensities measured for several different samples, and how that scatter would be reduced by using finer particles. Unfortunately, the depth and smoothness of the sample layer also affect overall and relative intensities and are difficult to reproduce exactly from one sample deposition to the next, so reproducibility of relative intensities was instead gauged by the size of $R_{p,w}$, the Rietveld fit criterion for an entire diffraction pattern, for particle sizes differing by roughly a factor of 10. The ~10 μ particle size finally used was achieved by prolonged grinding of the MnAs powder suspended in isopropanol in a ceramic ball mill. Contamination incurred at this stage was removed by flotation and decantation.

The results of the scan time and particle size tests are summarized in Table B3, along with the characteristics of actual experimental scans. A third problem, preferred orientation, was thoroughly tested for and never conclusively found. No particular crystallite morphology that would be expected to allow for orientation in any given direction could be observed using an optical microscope. The prolonged grinding of the sample likely reduced whatever degree of distinct crystallite shape existed originally. As preferred orientation is not a well-understood concept, and was probably not a factor in this work, it will not be discussed further here.

Table B3. Data collection parameters: (i) scan time, (ii) and (iii) sample quality

(i) Dependence of random counting errors on dwell time for scan of (1 0 0) peak centered at 2θ = 12.64 (Mo radiation)

Time (sec)	Avg. std. dev./step
2	9.1%
4	7.7%
6	5.5%

(ii) Dependence of profile reproducibility (assessed in terms of goodness-of-fit) on average particle size in sample

Avg. size (microns)	$R_{p,w}$
>100 μ	18.5%
10 μ	13.0%

(iii) Relationship of required sample thickness t[a] to linear absorption coefficient μ

	Mo Kα	Fe Kα
μ[b]	340 cm^{-1}	750 cm^{-1}
required t[b]	0.005 cm	0.002 cm

actual thickness: ~0.01 in or ~0.015 cm

[a]Minimum t for maximum diffracted intensity, calculated from $t \geq \frac{3.2}{340\ cm^{-1}} \frac{\rho}{\rho'} \sin\theta$ (source: Stout and Jensen).[30]

[b]Calculated from $\mu = \frac{n}{V_c} \sum_i (\mu_a)_i$ (source: International Tables for X-ray Cryst., v 3).[31]

The diffractometer merits a brief description. It is a Picker instrument provided and maintained by J. E. Benson of the Ames Lab X-ray diffraction group headed by R. A. Jacobson. It has the common flat-plate sample holder and a geometrical arrangement in which the beam source and detector move synchronously while the sample position is fixed. The X-ray beam is monochromatized at the detector using a graphite (111) crystal; K α_1 and K α_2 components remain in the beam. Ordinarily for Fe target radiation, the accelerating voltage and current are 50 kV and 14 mA, respectively, and for Mo radiation the values are 50 kV, 16 mA. The entire apparatus is controlled by interfacing to a Motorola 6802 and then to a VAX 11/730 computer, and the intensity vs 2Θ data are digitally recorded on the disk of the VAX 11/730.

Scans were done at a variety of temperatures bracketing both the 1st-order and 2nd-order transition temperatures reported in earlier studies. Typical profiles collected below (23°C) and above (56°C) T_1 are shown in Figures B4a and B4b. As can be seen by comparing these figures, the new features appearing in the pattern corresponding to the MnP-type or distorted structure are (i) small superstructure peaks for hkℓ, k + ℓ = odd type reflections and (ii) line splittings, such as that at 2$\Theta \approx$ 37°. The superstructure peaks are not present in the hexagonal or undistorted form, in which Z_{Mn} = 0.250 and X_{As} = 0.250 (as described in Pnma) correspond to special positions (in mirror planes) making the reflections in question extinct. The line splittings for pairs of reflections such that h = h', $3k^2 + \ell^2 = 3k'^2 + \ell'^2$ (e.g., (131)

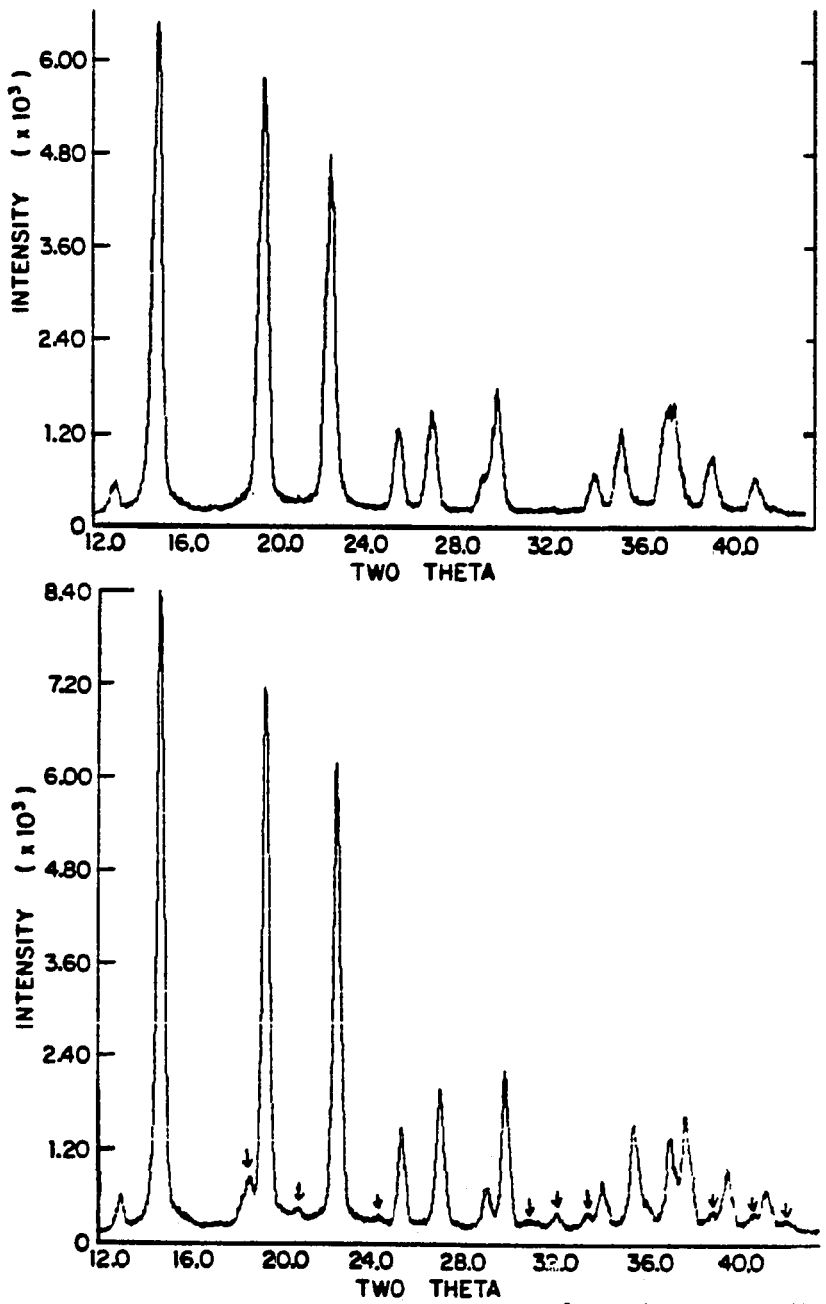

Figure B4a. Diffraction profile of MnAs at 23°C using Mo Kα X-rays. Intensity in arbitrary units, 2θ in degrees

Figure B4b. Diffraction profile of MnAs at 56°C; all other features as in Figure B4a. Arrows indicate superstructure peaks due to distortion from hexagonal symmetry

= $hk\ell$, (115) = $h'k'\ell'$) are nonexistent in the hexagonal form where c_o = $\sqrt{3}\ b_o$ (again, described in Pnma).

As the upper limit of the distorted-phase range (~130°C) was approached the differences between the distorted and undistorted patterns could no longer be clearly seen by mere visual inspection and the results of Rietveld analysis became the necessary data in determining whether the structural parameters had reverted to $\sqrt{3}\ b_o = c_o$ and $X_{As} = Z_{Mn} = 0.250$. As will be accounted for in the discussion section, the lattice parameter ratio c_o/b_o did not prove to be a valid criterion for distinguishing the distorted from the undistorted structure due to correlations between fit parameters. Emphasis was therefore placed mainly on accurately determining the extent of deviation from 0.250 in X_{As} and Z_{Mn}. (The other coordinates are either invariant, $Y_{As} = 0.2500$, $Y_{Mn} = 0.2500$ or vary to a much smaller degree than X_{As} or Z_{Mn}, as shown by Wilson and Kasper.[5])

One may look ahead to the graphical representation of the main result (Figure B11) to see that the coordinates determined in Rietveld refinements on data from Mo X-rays ($\lambda\ K\alpha_1$ = 0.7093 Å) do not approach the limit of 0.250 even at 50°C or more above the reported T_2 of ~125°. With only this result obtained at that point in the study, two decisions regarding subsequent experiments were made: (i) to repeat the X-ray diffractometer scans using Fe X-rays ($\lambda\ (K\alpha_1)$ = 1.9360 Å) and (ii) to do a careful reinvestigation of the region 40°C < T < 130°C using neutron diffraction and to look for evidence of magnetic ordering. The switch to a new X-ray source of longer wavelength was made on the speculation that

the greater angular dispersion in the resulting pattern would provide better resolution. If insufficient resolution had been the problem in the Mo-radiation case this switch could verify that the structure indeed reverted to NiAs-type as expected. Alternatively, if the Mo results were meaningful and no structural second-order transition actually occurred at ~130°C, some magnetic structure would be expected in the phase region below that temperature (since some type of continuous change occurred, being completed at T_2 as evidenced by the λ-pt in C_p[17]).

Scans using Fe radiation required longer times (16 sec) than these using Mo radiation due to the much weaker incident intensity of the former. Only a few points in the dubious temperature region were remeasured. The resulting patterns were much smoother with less background (see Figure B5) scatter than the Mo radiation patterns. This seems to have been the only visible improvement, as the increased angular dispersion still did not separate strongly overlapped groups of reflections, the splittings simply being too small for the choice of X-ray wavelength to matter.

The neutron diffraction experiments were performed March 23-26, 1984 at the IPNS facility at Argonne National Laboratory. The results contained no new information and neither the methods nor results will be reported here.

G. Data Analysis

Rietveld refinements of the MnAs structure from diffraction patterns were accomplished using the FORTRAN program DBW3.2 provided by R. A. .

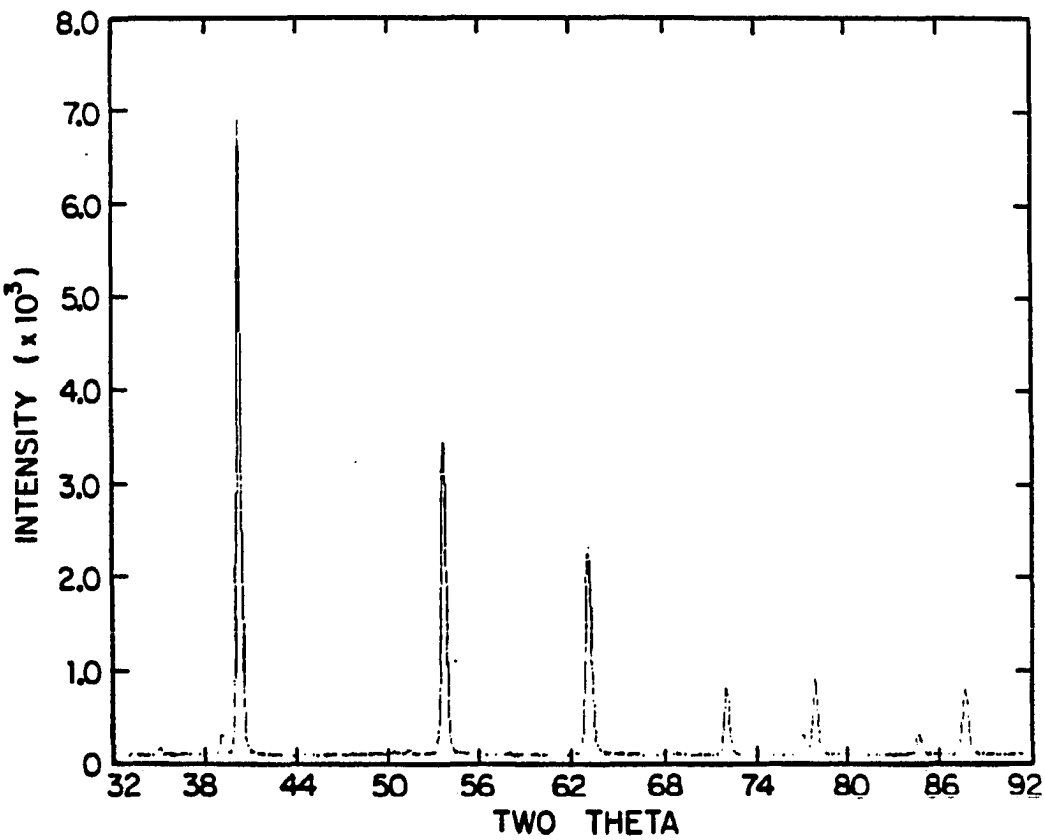

Figure B5. Diffraction profile of MnAs at 23°C using Fe Kα X-rays

Young and D. B. Wiles of Georgia Institute of Technology. The program was modified by the author for compatibility with the VAX11 computer system available at Iowa State University. This mainly entailed conversion of various IBM-system-specific functions and commands to their equivalents in the VAX system.

In general, the refinements required approximately two to four minutes per cycle and required from 10 to 15 cycles to converge or to reach near-constancy in the structural parameters. In many cases, small oscillations about an apparent midpoint would appear in certain fit parameters, perhaps due to correlations with other parameters. As these oscillations did not occur in the more important atomic coordinates or lattice constants, a refinement was often arbitrarily terminated without actual convergence so as to avoid needless expense of time and funds. In test cases in which refinements were allowed to continue beyond the usual termination point, the trends in certain nonstructural variables became asymptotic to a constant, as did the goodness-of-fit indicator $R_{p,w}$, i.e., the fit improved extremely slowly with increasing number of cycles. Convergence occurred more often in fits to the smoother Fe-radiation patterns, so it is speculated that the main cause of nonconvergence was noise in the Mo-source profiles, which diminished the ability of the model to fit lineshapes and background exactly but did not cause fluctuations in the structural part of the model.

Although analysis of each sequence of temperature-dependent patterns seemed to require a slightly new approach, certain systematic methods were developed in terms of the order in which various parameters were

refined in the model. DBW3.2 allows the user to fix any number of parameters in a refinement while varying others. The procedure generally used was the following:

(i) refine only scale factor and lattice constants, a_0, b_0, c_0.

(ii) next add background coefficients as variables.

(iii) include atomic coordinates.

(iv) include all parameters affecting peak shape.

(v) lastly refine anisotropic thermal parameters Bij.

This order of refinement usually succeeded by first finding the positions of peak centers and then gradually approximating their shape and the 2Θ dependence of their height and asymmetry. Figure B6 shows a comparison of observed and calculated profiles.

Two systematic difficulties were encountered which required additional care in the refinements, namely (i) correlations of the 2Θ zero-point with the lattice constants a_0, b_0, and c_0, and (ii) refining to a negative (and therefore physically unreasonable) value for the overall temperature factor $B_{iso} = (B_{Mn,iso} + B_{As,iso})/2$. Each of these difficulties proved to be related to the positioning of the sample holder (see Figure B3) in the diffractometer housing. This positioning is rather crudely achieved by the use of a spring-loaded clamp to restrict lateral movement and by manual adjustment of set screws which control height. The latter was done so as to optimize the intensity of some known diffraction peak but resulted in a slightly different effective zeropoint (usually within ±0.2° 2Θ of true zero) with each replacement of the holder. There also was evidently a nonreproducible amount of tilt

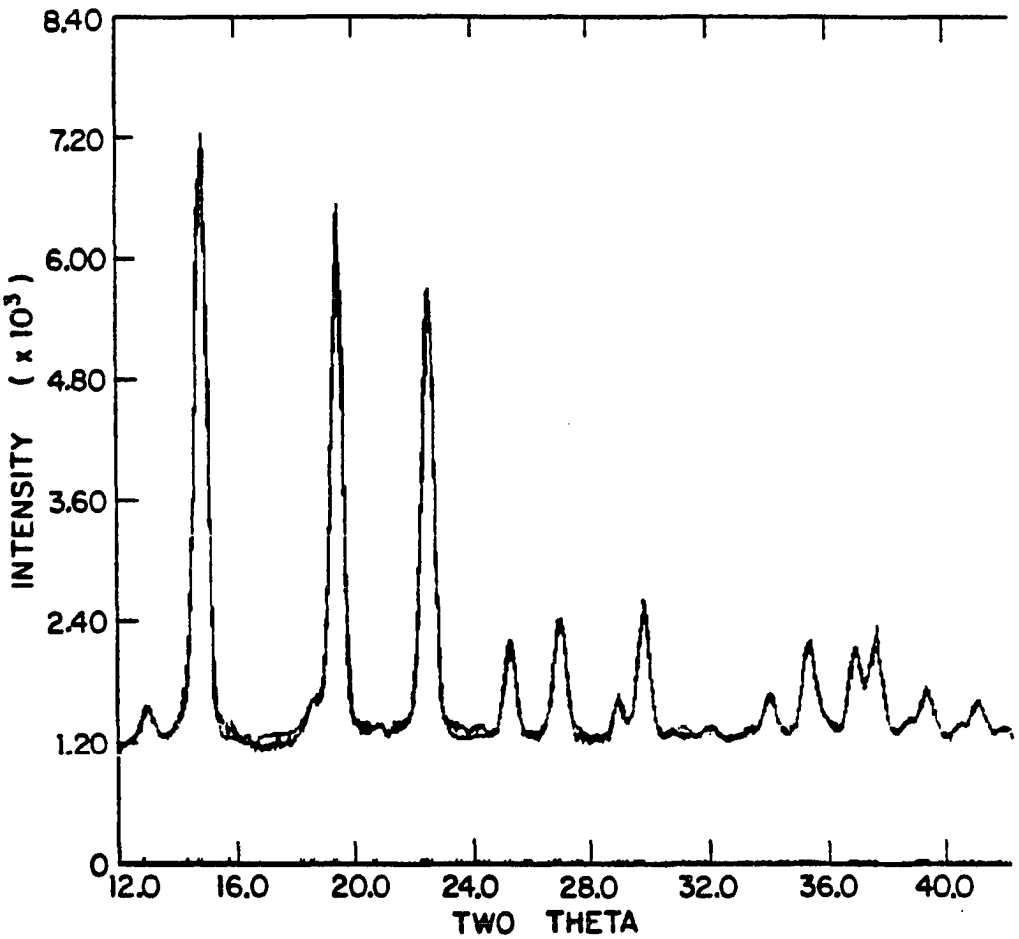

Figure B6. Comparison of observed and calculated profiles resulting from a Rietveld refinement at 45°C

in the sample holder relative to the X-ray beam such that as 2θ was varied there was a contribution to the trend in total diffracted intensity in the pattern, and hence the negative B_{iso}. Both of these systematic errors could be corrected by calibration. In the case of the zeropoint problem allowing both the lattice parameters and zeropoint to vary in a refinement resulted in false minima in parameter space, as detected by starting with guesses for the parameters in various places and seeing different refined values result, and by noting inconsistencies in the trends of individual lattice parameters vs temperature. A room temperature Guinier camera pattern of the sample used for the diffractometer scans yielded lattice parameters (see Table B2), which could be fixed in determining the zeropoint for room-temperature diffractometer scan. Once this zeropoint was known, it could be fixed in refinements for all patterns which had been scanned before again moving the sample holder. In a similar way, the amount of B_{iso} correction necessary to account for tilt of the holder was found by fixing $B_{Mn,iso}$ and $B_{As,iso}$ to agree with values reported in Wilson and Kaspers single-crystal study and allowing B_{iso} to vary. This correction term, once found, could again be applied to all data sets taken with a fixed sample holder position. Corrections of both types (ϕ-point and B_{iso}) were subsequently determined for other experimental runs by interpolation of lattice parameters or $B_{atom,iso}$ from previously determined trends. In at least the case of B values, it is therefore the trends with temperature, and not necessarily absolute values which have been determined in this work.

H. Results and Discussion

Table B4 lists the structural parameters as determined in Rietveld refinements. In the case of Mo-radiation scans at temperatures above 100°C, the atomic coordinates (in parentheses) were shown to be indeterminable due to the lack of resolution described in the experimental section. Lattice parameters for these scans are not believed to be any less reliable than those from Fe-radiation scans, as the positions of peaks are mostly unambiguous. One type of ambiguity, however, does result in the relatively large uncertainties in b_o and especially c_o, regardless of the X-ray wavelength employed. This is the near-coincidence of pairs of lines $(h_1k_1\ell_1)$, $(h_2k_2\ell_2)$ such that $3k_1^2 + \ell_1^2 = 3k_2^2 + \ell_2^2$. For such pairs there is little effect on the goodness-of-fit if the wrong indices are assigned to both lines. There are resultant broad minima in the fit residuals vs b_o and c_o and also a strong negative correlation between the two axis lengths (-0.96, reduced to -0.50 by Fe-radiation). Thus, where a b_o value appears to be somewhat lower than the trend with temperature predicts (see Figures B7 to B9), there is usually a higher than expected result for the corresponding c_o. Aside from this difficulty, which is inherent in the compound and thus unavoidable, the lattice parameter results are qualitatively useful. The slight discrepancies between the findings of Willis and Rooksby and those of this author are presumed due to differences in sample purity. The odd slope discontinuity at ~80°C in a_o was alluded to as "typical" by these previous workers but is not presently recognized as having any theoretical basis and is more likely the result of a systematic error in

Table B4. Structural parameters of MnAs as determined by Rietveld analysis

T(C)	#	R'n	X(Mn)	Z(Mn)	X(As)	Z(As)	a	b	c	V(cell)
21	11	Fe	1.000	0.250	0.250	0.917	5.6989	3.7195	6.4378	136.4±
36	4	Mo	1.000	0.250	0.250	0.917	5.706	3.697	6.403	136.0
43	4	Mo	0.995	0.226	0.274	0.919	5.717	3.668	6.359	133.4
45	2	Mo	0.997	0.226	0.273	0.921	5.719	3.666	6.364	133.4
46	9	Mo	0.997	0.227	0.273	0.921	5.717	3.664	6.368	133.4
48	1	Mo	0.996	0.227	0.273	0.920	5.716	3.666	6.363	133.3
55	2	Mo	1.005	0.229	0.273	0.923	5.731	3.676	6.378	134.4
56	9	Mo	1.001	0.229	0.271	0.913	5.721	3.668	6.369	133.6
65	9	Mo	0.993	0.229	0.274	0.928	5.726	3.677	6.365	134.0
71	4	Mo	1.005	0.228	0.272	0.913	5.726	3.681	6.351	133.9
79	8	Mo	1.009	0.234	0.267	0.918	5.731	3.668	6.396	134.4
80	11	Fe	0.998	0.238	0.264	0.919	5.7389	3.6872	6.3778	134.9±
86	10	Mo	0.984	0.223	0.270	0.907	5.733	3.685	6.367	134.5
89	8	Mo	1.003	0.234	0.266	0.916	5.736	3.672	6.399	134.8
92	4	Mo	0.999	0.230	0.272	0.910	5.735	3.689	6.361	134.6
94	8	Mo	1.005	0.235	0.267	0.918	5.735	3.675	6.395	134.8
95	8	Mo	0.998	0.233	0.265	0.913	5.730	3.680	6.374	134.4
98	9	Mo	1.000	0.233	0.265	0.909	5.737	3.677	6.395	134.9
99	11	Fe	0.997	0.237	0.262	0.920	5.7380	3.6809	6.3939	135.05
100	5	Mo	(0.999	0.235	0.265	0.911)	5.739	3.685	6.381	134.9
102	6	Mo	(1.001	0.234	0.263	0.911)	5.744	3.682	6.404	135.4
103	8	Mo	(1.002	0.234	0.263	0.911)	5.751	3.687	6.410	135.9
105	8	Mo	(1.002	0.236	0.264	0.916)	5.740	3.678	6.407	135.3
107	11	Fe	0.997	0.240	0.259	0.922	5.7392	3.6814	6.3917	135.05
108	4	Mo	(1.004	0.238	0.266	0.924)	5.743	3.682	6.393	135.2
116	8	Mo	(1.003	0.242	0.263	0.915)	5.745	3.678	6.412	135.5
117	11	Fe	0.995	0.245	0.255	0.922	5.7427	3.6833	6.3983	135.34
119	9	Mo	(0.998	0.238	0.260	0.911)	5.747	3.692	6.387	135.5
122	9	Mo	(0.999	0.237	0.259	0.912)	5.748	3.692	6.388	135.6
126	4	Mo	(1.004	0.238	0.263	0.909)	5.751	3.693	6.383	135.5
127	11	Fe	0.998	0.246	0.253	0.920	5.7458	3.6852	6.3980	135.47
133	4	Mo	(0.997	0.238	0.262	0.912)	5.754	3.695	6.380	135.6
138	5	Mo	(0.999	0.239	0.261	0.909)	5.753	3.687	6.400	135.8
139	11	Fe	1.000	0.249	0.252	0.917	5.7496	3.6916	6.3854	135.53
141	5	Mo	(1.000	0.240	0.260	0.910)	5.754	3.690	6.394	135.8
146	10	Mo	(0.995	0.239	0.261	0.910)	5.757	3.695	6.394	136.0
149	6	Mo	(1.002	0.241	0.257	0.910)	5.754	3.688	6.415	136.1
150		Mo	(0.997	0.242	0.260	0.911)	5.749	3.687	6.401	135.7
152	10	Mo	(0.993	0.238	0.260	0.910)	5.758	3.695	6.395	136.1
158	9	Mo	(0.999	0.240	0.260	0.912)	5.758	3.696	6.393	136.0
179	7	Mo	(0.999	0.238	0.258	0.909)	5.761	3.696	6.396	136.2
191	7	Mo	(1.006	0.236	0.259	0.909)	5.764	3.694	6.403	136.3

Uncertainties

	Mo	Fe
Z(Mn)	0.001	0.001
X(As)	0.002	0.001
a	0.001	0.0002
b	0.002	0.0001
c	0.003	0.0006

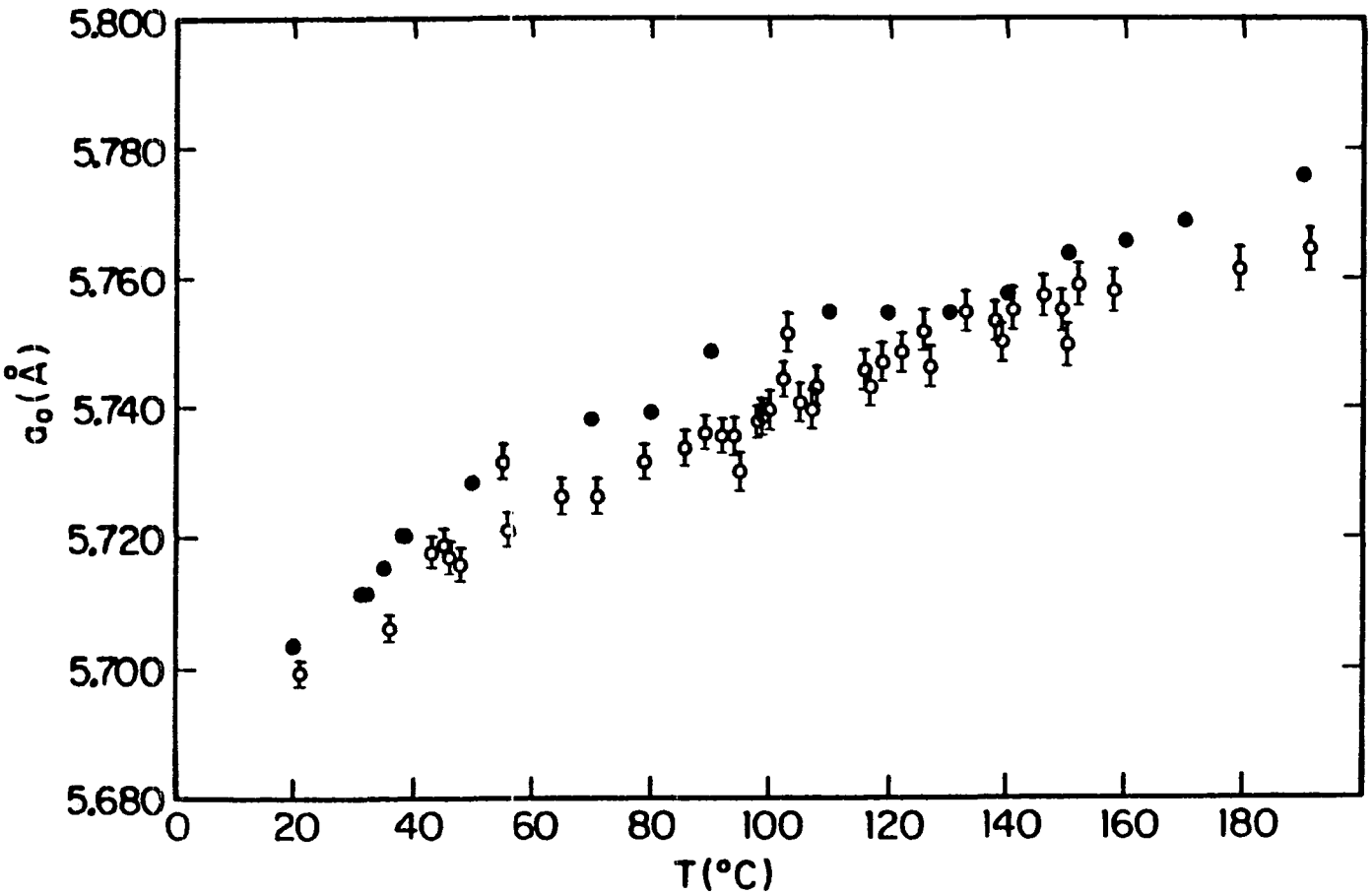

Figure B7. a_0 lattice parameter of MnAs as determined by Rietveld refinements and by Willis and Rooksby's powder camera study (darkened points) as a function of temperature

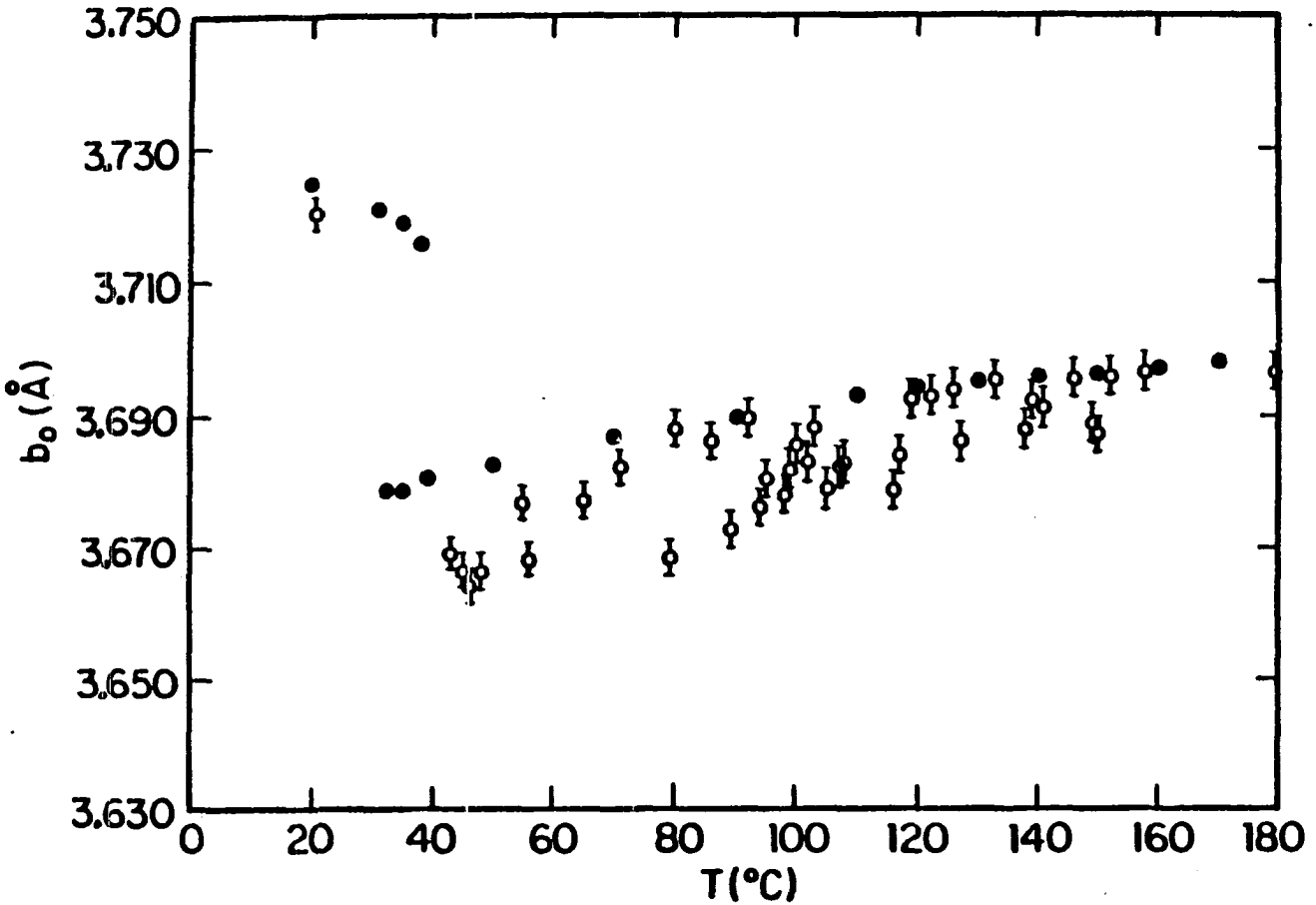

Figure B8. b_o lattice parameter of MnAs as determined by Rietveld refinements and by Willis and Rooksby's powder camera study (darkened points) as a function of temperature

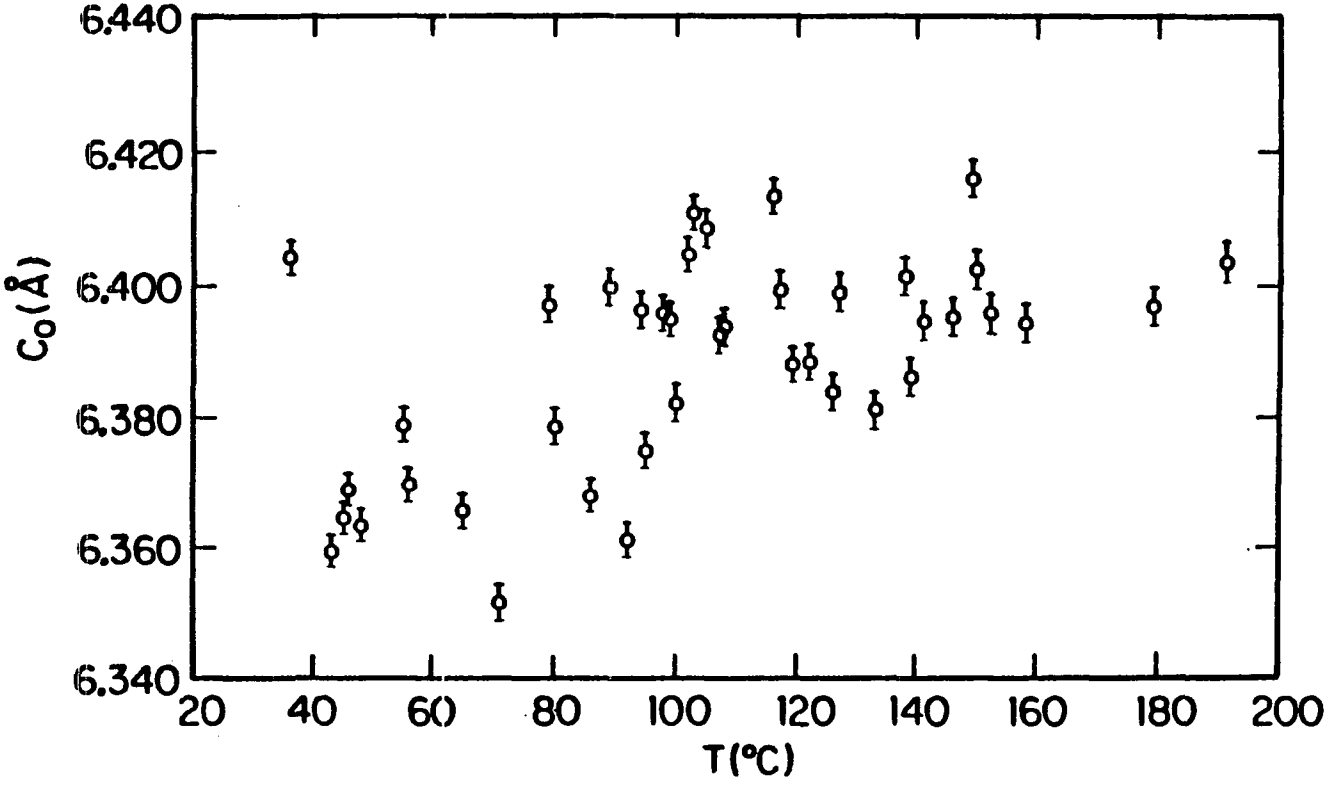

Figure B9. c_o lattice parameter of MnAs as a function of temperature as determined by Rietveld refinements

measurement. As may be clearly seen in Figure B10, there is a discontinuity in the slope of unit-cell volume vs T. The quantity $\alpha' = \left(\frac{\delta V}{\alpha T} \right)_p$ is an example of a second derivative of the chemical potential ($\left(\frac{\delta \mu}{\delta P} \right)_T = V$) in which such a discontinuity is expected in a 2nd-order phase transition, and was determined above and below 125°C by a least squares fit to the V_{cell} data. The results were 2.1×10^{-4}/deg at $T < T_2$ and 8.0×10^{-5}/deg at $T > T_2$. The latter value does not strongly disagree with the value of (6.9×10^{-5}) determined by Grazhdankina and Burkhanov[31] in a study of elasticity constants of MnAs. It can also be added that the uncertainties in the Fe-X-ray cell constants of 1×10^{-4} Å to 6×10^{-4} Å are in the same range as those of the most precise values to be found in the literature.

Little really needs to be said in conclusions based on the atomic coordinate results. A second-order phase transition of structural nature occurs at ~125°C as expected (see Figure B11). From these coordinates, the quantity $\Delta \equiv 4|(Z_{Mn} - 0.250)|$ was derived for comparison with the model-based prediction by Kato et al. Figure B12 illustrates the general correctness of their prediction. Figure B13 shows a final summary of the relationships between atomic positions in the distorted and undistorted structure.

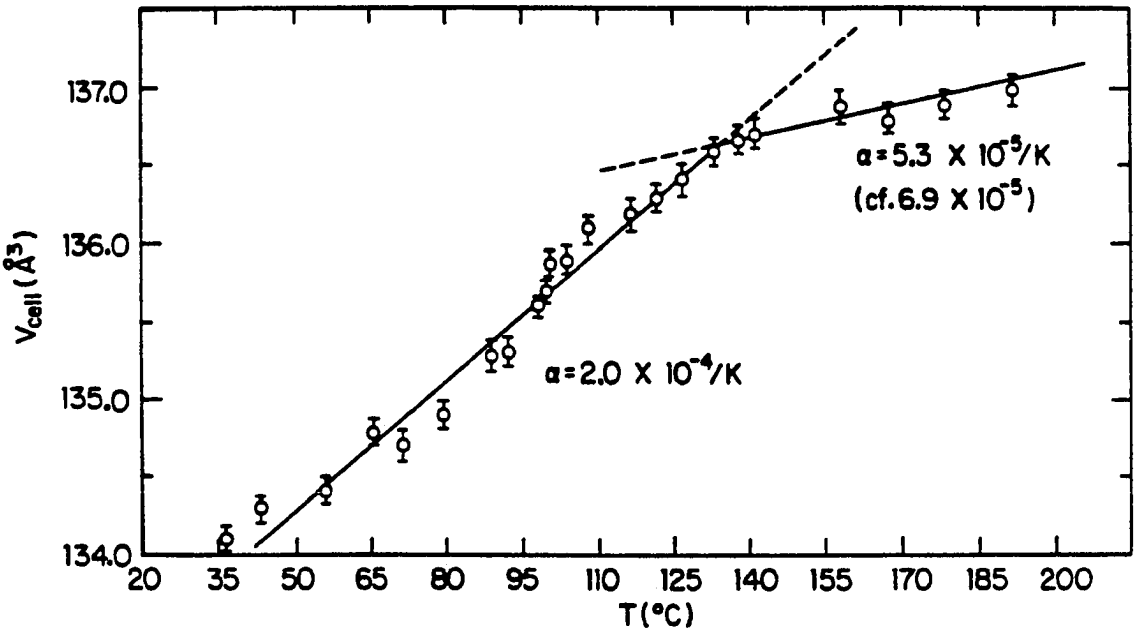

Figure B10. Plot of orthorhombic unit cell volume of MnAs vs temperature, showing discontinuity in slope

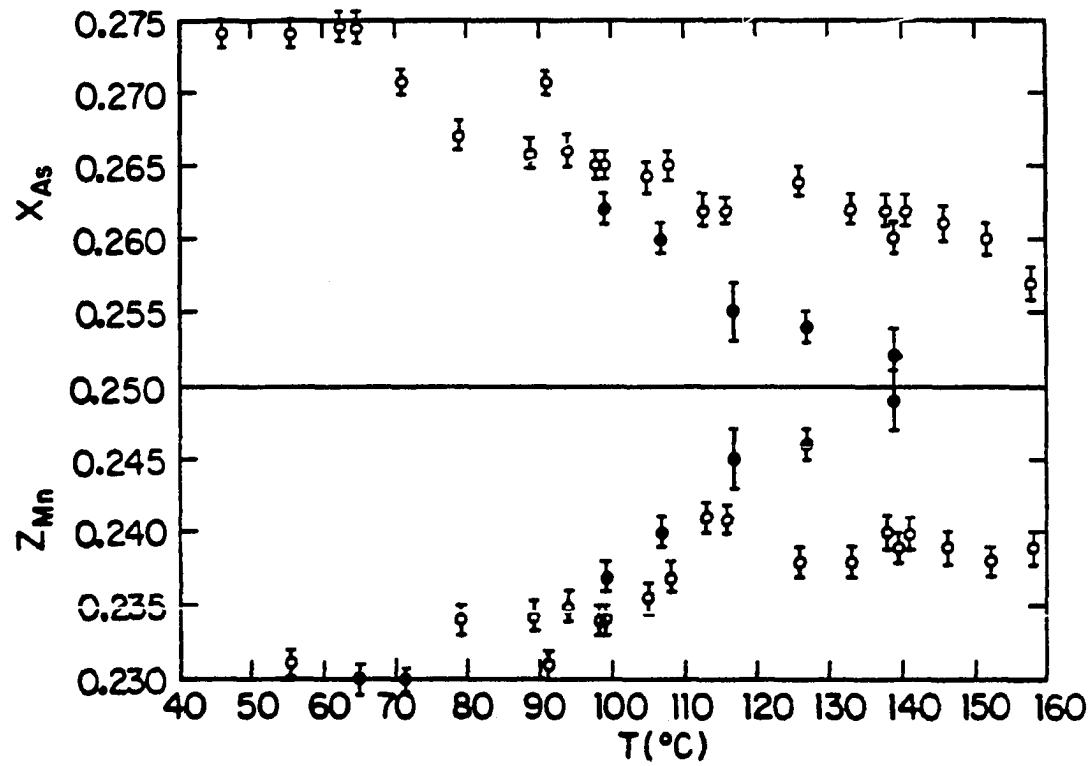

Figure 811. Trends in atomic coordinates of MnAs as a function of temperature. Darkened points indicate values refined from Fe Kα data; others are from Mo Kα data

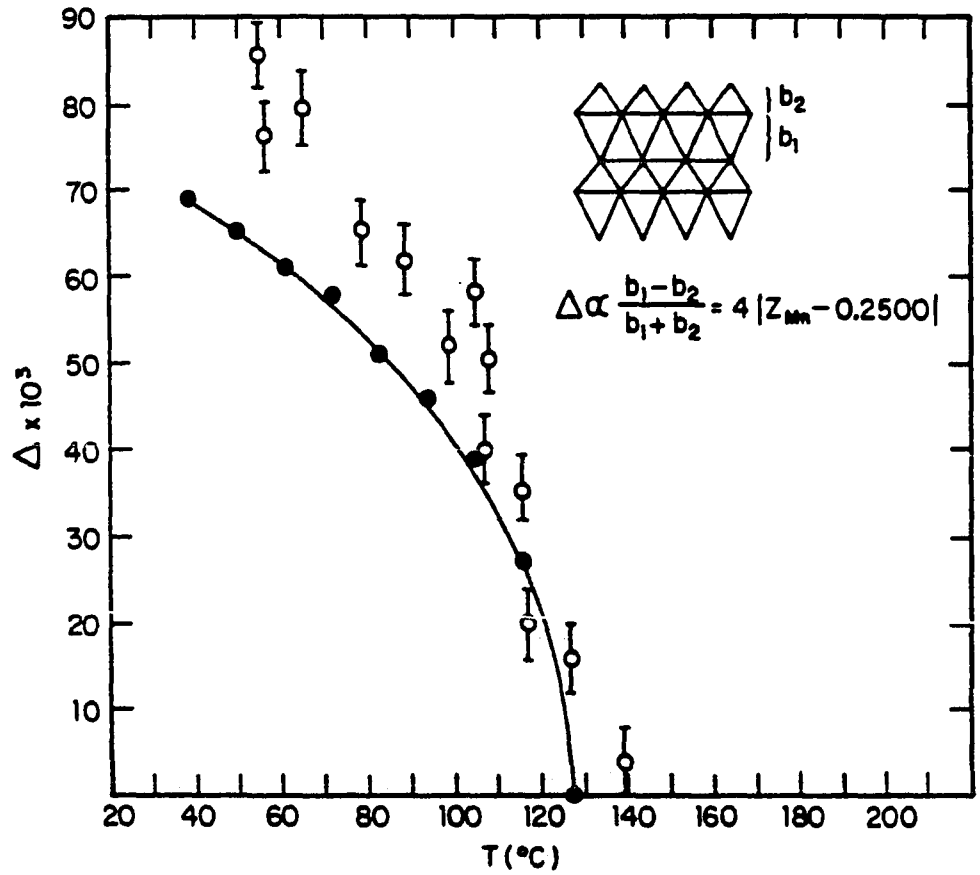

Figure B12. Definition of disordered parameter Δ as defined by Kato et al.[20] and comparison of calculated values (darkened points on curve) with experimental values from this study

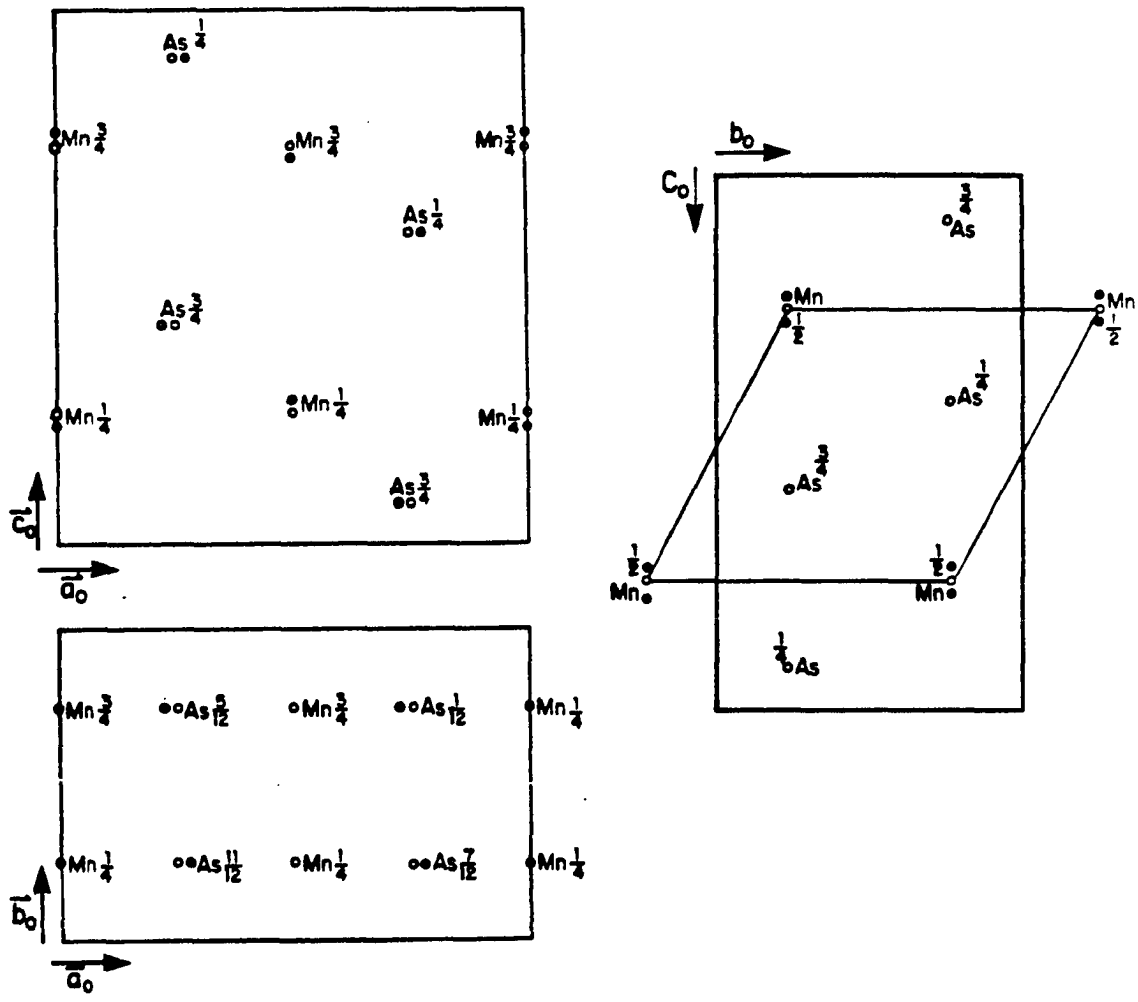

Figure B13. Projections of the most distorted (darkened points) and undistorted (empty points) atomic positions in MnAs on various planes of the orthorhombic unit cell. Coordinates labeling points indicate heights above plane of projection

The general concluding comments yet to be made are of two types: (i) assessment of the Rietveld technique and its appropriateness in application to this problem and (ii) reconciliation of the now more complete body of data on the MnAs phase transitions. The Rietveld method has great power if one uses it with awareness of the aforementioned actual or potential limitations: the need for a good starting guess of the structure and for high quality data, the dependence of resolution on choice of X-ray wavelength, and the possible systematic errors in 2θ zeropoint and thermal parameters. There are also several ways in which the technique could be made even more powerful, including development of a more accurate shape function to describe X-ray peaks and of a function to more meaningfully account for preferred orientation. Work is reportedly underway[32] in attempts to derive a statistical test akin to that of Hamilton[33] for determining whether a Rietveld fit with an N-parameter model is statistically more meaningful than one using M parameters ($M < N$ and the former are a subset of the latter). This can be accomplished if it is possible to circumvent or solve the problem presented by the unequal weighting of residuals in a Rietveld minimization.

As for the application of the technique to the MnAs problem, Rietveld analysis is evaluated in retrospect as having been perhaps more powerful than was necessary, given the discouragingly small amount of new information obtained; probably conventional integrated intensity data analysis was as accurate a method as could be justified by the result. On balance, the Rietveld method was certainly not a bad choice. However, a preferable approach might be to attack any similar future problems

using Fe (or longer λ) X-rays, scanning at fewer and more widely spaced temperatures so that both flawed and redundant data are avoided.

An evaluation of the current state of understanding of the findings on MnAs is really beyond the scope of this effort, but it is worthwhile to note that the one new finding, namely the actual extent of structural distortion in MnAs as a function of temperature, fits nicely into the most current explanation, that proposed by Kato. His effort (like most other relevant theoretical treatments) focuses on the nature of the first order transition at about 40°C but he also accounts for the 2nd order transition as well, in a hypothesis that seems plausible to those much more familiar with critical phenomena than this author.[34] The significance of the current study, as seen in contrast to previous work, is perhaps that it has been the first to carefully examine the 2nd order transition in a quantitative manner.

XI. REFERENCES

1. Landau, L.; Lifshitz, E. "Statistical Physics", Pergamon Press: New York, 1959, pp. 430-456.

2. Franzen, H. F. "Lecture Notes in Chemistry", Springer-Verlag: New York, 1982, p. 32.

3. Franzen, H. F.; Wiegers, G. A. J. Solid State Chem. 1975, 13, 114.

4. von Schnering, H. G.; Wiedemeier, H. Z. Krist. 1981, 156, 143.

5. Wilson, R. H.; Kasper, J. S. Acta Cryst. 1964, 17, 95.

6. Bates, F. Phil. Mag. 1929, 8, 714.

7. Serres, A. J. Phys. Radium 1947, 8, 146.

8. Guillaud, C. J. Phys. Radium 1951, 12, 223.

9. Bacon, G. E.; Street, R. Nature 1955, 175, 518.

10. Willis, B. T. M.; Rooksby, H. P. Proc. Phys. Soc. (London) 1954, B67, 290.

11. Kornelson, R. O. Can. J. Phys. 1961, 39, 1728.

12. Kittel, C. Phys. Rev. 1960, 120, 335.

13. Basinski, Z. S.; Kornelson, R. O.; Pearson, W. B. Trans. Ind. Inst. Met. 1960, 120, 335.

14. Frazer, B. C.; Brown, B. J. Phys. Rev. Lett. 1961, 7(12), 273.

15. Bean, C. P.; Rodbell, D. S. Phys. Rev. 1962, 126(1), 104.

16. deBlois, R. W.; Rodbell, D. S. Phys. Rev. 1963, 130(4), 1347.

17. Grønvold, F.; Snildal, S.; Westrum, E. F. Acta Chem. Scand. 1970, 24, 285.

18. Goodenough, J. B.; Kafalas, J. A. Phys. Rev. 1967, 157, 389.

19. Schwartz, L. H.; Hall, E. L.; Felcher, G. P. J. App. Phys. 1970, 41(3), 939.

20. Kato, I.; Nagai, K.; Aiska, T. J. Phys. Chem. 1983, 16, 3183.

21. Rietveld, H. M. J. Appl. Cryst. 1969, 2, 65.

22. Werner, P.-E. "Chemical Communications", University of Stockholm, 1981, 6, 4.

23. Wiles, D. B.; Young, R. A. J. Appl. Cryst. 1981, 14, 149.

24. Santoro, A.; Prince, E. "Reactor Radiation Division Programs", NBS: Washington, DC., 1980.

25. Powder Diffraction File, JCPDS Int'l Centre for Diffraction Data, Swarthmore, PA, 1982.

26. Nowotny, H.; Funk, R.; Pesl, J. Monatsh. Chem. 1951, 82, 513.

27. Zieba, A.; Selte, K.; Kjekshus, A.; Andresen, A. F. Acta Chem. Scand. 1978, A32, 173.

28. Guillaud, C.; Wyart, J. Compt. Rend. 1944, 219, 393.

29. Klug, H. P.; Alexander, L. E. "X-Ray Diffraction Procedures", 2nd ed.; J. Wiley: New York, 1974, p. 635.

30. Stout, G. H.; Jensen, L. H. "X-Ray Structure Determination", Macmillan: Toronto, 1970.

31. MacGillavry, C. H.; Rieck, G. D., eds. "International Tables for X-Ray Crystallography", 2nd ed., Vol. 3; Kynoch Press, Birmingham: England, 1968.

32. Grazhdankina, N. P.; Burkhanov, A. M. Soviet Phys. JETP 1966, 23(6), 1013.

33. Young, R. A., private communication, School of Physics, Georgia Institute of Technology, March 1984.

34. Hamilton, W. C. Acta Cryst. 1965, 18(3), 502.

35. Lindgard, P.-A., private communication, Department of Physics, Iowa State University, March 1984.